DOCTORAATSPROEFSCHRIFT

2009 | Faculteit Wetenschappen

Development of biosensors for the detection of histamine for intestinal application

Proefschrift voorgelegd tot het behalen van de graad van Doctor in de Wetenschappen, richting natuurkunde, te verdedigen door:

Ir. Evi Bongaers

Promotor: Prof. dr. Patrick Wagner

Copromotor: dr. Freddy Troost

Table of Contents

Acknowledgements

Abstract

In recent health care is a growing need for bio- and chemosensors for the rapid and accurate detection of molecules. A biosensor uses a recognition element of biological origin. Immunosensors in particular are biosensors that use antibodies or immunoglobulines as their biological recognition element. Sensing systems based on biological recognition elements have some restrictions, limiting their use. Replacing the biological recognition element by a chemical receptor is therefore becoming of increasing interest. As opposed to the sensors containing biological recognition elements, biomimetic sensors, containing artificial receptors, are chemically and physically inert. Using Molecularly Imprinted Polymers (MIPs) the specificity and affinity of biological receptors can be mimicked. In addition, a MIP-based sensor can measure in harsh environments. This is beneficial for the use of sensors in vivo, in bodily fluids or in the intestines, for example in research for the Irritable Bowel Syndrome (IBS).

The IBS is characterized by visceral hypersensitivity. The pathogenesis is poorly understood, but there is evidence that mast cells are involved in this process. Mast cells degranulate upon activation, and release histamine, tryptase and other compounds. The accessibility of the intestine makes it difficult to measure this intestinal mast cell activation *in vivo*. Therefore a biosensor for the detection of histamine and tryptase *in vivo* in the intestine is developed.

Firstly, prototype immunosensors for the rapid and accurate detection of histamine and tryptase are constructed. The different building blocks of this biosensor are under investigation: AFM and contact angle measurements confirm the electrode functionalization with biological receptors. Antibodies against tryptase and histamine were successfully immobilized on polymer-based electrodes, incubation of 100 pmol/ml antibodies result in saturated surfaces. It is shown that physical adsorption is a fast and easy way to build a recognition layer. The sensor detects the antigen impedimetrically. For tryptase (135 kDa) coplanar electrodes are coated with the polymer MDMO-PPV and antibodies are immobilized on the polymer surface using physical adsorption. Binding of these

antibodies with their specific antigen will result in a measurable change in capacitive properties at the interface. The immunosensor shows a 10% response to 100 pmol/ml tryptase. Low-molecular weight molecules can for the first time also be impedimetrically detected with a direct assay by using IDE's. For the detection of the antigen histamine (111 Da) IDE's functionalized with antibodies against histamine are used to detect 50 nmol/ml histamine with a 10% change in the impedimetric signal. IDE's are proven to be beneficial for use in future electronic sensing of tryptase and histamine.

Biomimetic sensors based on molecular imprinted polymers (MIPs) can be an alternative to sensors with chemically and physically instable biological receptors. Molecular imprinting leads to the formation of inert polymer particles with nanocavities, which mimick the selectivity and specificity of biological receptors such as natural antibodies. Histamine occurs in harsh environments in food and bodily fluids. MIPs can withstand such harsh environments. It is demonstrated that MIPs can be readily incorporated into a biomimetic sensor for the detection of histamine in aqueous media. Using electrochemical impedance spectroscopy, histamine is successfully detected in the nanomolar range. In pH neutral environments the sensitivity is 45% to 10nM histamine. Typical physiological conditions in i.e. mast cells are around 200 nM. A dose response curve is measured in the 0-12 nM range. Sensor saturation begins at 9.3 nmol/l. Using the analogous molecule histidine, it is demonstrated that the impedimetric sensor is specific for the detection of histamine.

When a sensor for the detection of histamine in bodily fluids or in the intestines is developed the pH of the environment is an important factor to consider. Although the MIP can withstand a wide range of pH values, the pH of the electrolyte affects protonation or deprotonation of target molecule and MIP. The sensor is tested under various pH environments between pH 5 and pH 11. These measurements have shown that this pH dependent degree of protonation of both the MIP and histamine has a substantial impact on the formation of hydrogen bonds, which are needed for binding of the target molecule to the nanocavity in the MIP. Hence, the detection of histamine by a MIP-based sensor is affected by the pH of the solution. A novel model has been established to verify the impedimetric results. This model is useful for adapting the MIP to allow for the

formation of hydrogen bonds at lower pH values. This makes it possible for histamine to be impedimetrically detected at low pH conditions by means of synthetic receptors.

Nederlandse samenvatting

In de moderne gezondheidszorg is er een groeiende nood aan bio- en chemosensoren voor de snelle en accurate detectie van moleculen. Een dergelijke voorbeeld is het onderzoek naar het prikkelbare darm syndroom. Bij het prikkelbare darm syndroom leidt een emotioneel stressvolle situatie, via een verstoorde hersen/darm interactie tot het vrijzetten van histamine, tryptase en andere moleculen door de mestcellen in de darmen. Gezien de moeilijke toegankelijkheid van de darmen is het moeilijk om veel informatie in te winnen over de precieze werking van dit syndroom. Dat bemoeilijkt het vinden van een gepaste behandeling. In dit doctoraat is een sensor onder ontwikkeling om stoffen zoals tryptase en histamine te detecteren met het oog op een toepassing rechtstreeks in de ingewanden. Een impedimetrische uitlezing is wenselijk gezien via deze methode elektronische data aangeleverd wordt. Dit gaat gepaard met eenvoudige opslag van data en snelle verwerving en verwerking van grote hoeveelheden data.

Als eerste biosensoren werden prototype immunosensoren ontwikkeld voor de doelmoleculen tryptase en histamine. Deze biosensoren gebruiken antilichamen of immunoglobulines als biologisch herkenningselement. Antilichamen voor tryptase en histamine werden succesvol geïmmobiliseerd op polymeer-gebaseerde elektrodes. Fysische adsorptie van 100 pmol/ml leidde tot een verzadigd mono-moleculair oppervlak. Hogere concentraties leidden niet tot een betere bezetting van het oppervlak. Fysische adsorptie is een snelle en eenvoudige methode om een herkenningslaag te creëren. Deze immunosensor toonde een impedimetrische reactie van 10% op de aanwezigheid van 100 pmol/ml tryptase. Histamine heeft een laag moleculair gewicht, hetgeen een rechtstreekse impedimetrische detectie bemoeilijkte. Echter, door het gebruik van kleine interdigitale elektrodes (IDE's) is het voor het eerst gelukt om ook dergelijke kleine moleculen direct impedimetrisch te detecteren. De detectie van 50 nmol/ml doelmolecules veroorzaakte een impedantiestijging van 10%. Het is aangetoond dat het gebruik van IDE's nuttig is voor het toekomstig elektronisch detecteren van histamine en tryptase. Er doken reproduceerbaarheidsproblemen

op door een slechte hechting van de antilichamen aan de polymeren transducerlaag.

In een tweede stap werd de instabiele biologische herkenningslaag vervangen door een stabieler chemisch herkenningselement gebaseerd op moleculair geïmprinte polymeren (MIPs). MIPs met een hoge affiniteit en specificiteit voor histamine werden succesvol gesynthetiseerd door de scheikundige groep. Hun batch rebinding experimenten karakteriseerden het bindingsfenomeen tussen doelmolecule en de verscheidene aangemaakte MIPs om op die manier de meest optimale MIP te selecteren. Hierbij werkt ook de corresponderende NIP, het niet-geïmprinte polymeer, mee getest als referentie. Een weinig binding van histamine aan de MIP wordt waargenomen omwille van de aspecifieke binding van het histamine aan de polymeermatrix. De geoptimaliseerde MIP bindt significant meer histamine in vergelijking met de corresponderende NIP en deze werd uitgekozen voor integratie in sensorsystemen.

De geoptimaliseerde MIP en corresponderende NIP warden vervolgens beiden succesvol gebruikt als synthetisch herkenningselement. De impedimetrische MIP-gebaseerde sensoren vertoonden een selectieve reactie op histamine. Impedimetrische detectie is een snelle en specifieke techniek voor het opsporen van lage concentraties in de nanomolaire range. Typische concentraties in de mastcellen variëren rond de 200 nM. De sensor karakteristieken zijn bepaald, met een detectielimiet van 2 nM. De sensitiviteit is 45% impedantie stijging op een concentratie van 10 nM, hoewel dit resultaat varieert van sample tot sample. Een dosis-responsie curve is gemeten in een range van 0 tot 12 nM. Verzadiging treedt op rond 9.3 nmol/l. Specificiteit is bevestigd door middel van testen met histidine, een gelijkend molecule, waarop de sensor geen significante reactie vertoonde. Door het modelleren van het bindingsmechanisme in de sensor met een equivalent elektrisch circuit, blijft het echter onbepaald wat deze impedantie stijging veroorzaakt, maar er wordt verondersteld dat het effect tweeledig is. Enerzijds kan de weerstand van de interface laag stijgen. Anderzijds stijgt de impedantie omwille van een daling van de capaciteit van de dubbele laag die zich gevormd heeft aan deze interface. Deze daling kan te wijten zijn aan een verminderde oppervlakte of een daling in permittiviteit. Het halfgeleidende polymeer MDMO-PPV, gebruikt als transducerlaag bemoeilijkt de

reproduceerbaarheid van het modelleren en het verwerven van gedetailleerde kennis over de bindingsprocessen die plaatsvinden in de sensor. Een substituut transducer materiaal zou hier oplossingen kunnen bieden.

Wanneer een sensor voor de detectie van histamine in lichaamsvloeistoffen of in de ingewanden ontwikkeld wordt, is de pH van de omgeving een belangrijke factor. Hoewel MIPs een brede range van pH waardes kunnen doorstaan, wordt hun functionaliteit wel aangetast door de pH van het elektrolyt. Deze pH beïnvloedt de protonering of deprotonering van zowel het doelmolecule als de MIP zelf. Dit heeft een aanzienlijke invloed op de vorming van waterstofbruggen, die nodig zijn voor de binding van het doelmolecule aan de MIP. Daarom is de sensor getest onder verschillende pH condities, variërend van pH 5 tot pH 12. De sensor werkt optimaal bij pH 9, maar vertoont geen reactie in zuurdere milieus (pH 5). Een vereenvoudigd model is opgesteld dat deze impedimetrische metingen verklaart. Aan de hand van dit model kan dit type van MIP-gebaseerde sensor aangepast worden voor gebruik bij lagere pH waardes. Met een vast pKa-waarde, is het op te sporen histamine een vast gegeven en kan de protonering ervan niet beïnvloed worden. Toch kan aan de hand van het model de pKa van de MIP aangepast worden, om een situatie te creëren waarin de vorming van waterstofbruggen alsnog mogelijk is onder lagere pH waardes. Het ontwikkelen van dergelijke MIP zou de impedimetrische detectie van histamine in zure omgevingen mogelijk maken.

1 Introduction

The development of novel biosensors is a rapidly growing field. This chapter first gives an introduction on biosensors in general. In recent health care there is a growing need for bio- and chemosensors for rapid and accurate detection of molecules. One such demand comes from gastroenterological world, where research for irritable bowel syndrome (IBS) takes place. This chapter then explains what IBS is. The impact of IBS is pointed out and how IBS research would benefit from a new type of sensor for relevant molecules in IBS. The goal of this project is to make such a sensor. Therefore the chapter continues with a third and fourth section about two types of sensors that have been developed for this purpose and the materials needed to build these sensors.

1.1 Biosensors

Not many people are aware of the fact that we all are in the possession of two biosensors ourselves, being the nose and the tongue. With the nose it is possible to detect small amounts of chemicals. It can distinguish qualitatively between different chemical substances at very low concentrations. Our nose is an extremely selective instrument that is not easily being built artificially. The tongue works in a similar way to taste substances and distinguish in flavors. The interest in sensors for detection of molecules rapidly expanded over the last decade, due to a high interest from modern health care, food industry and environment. Nowadays biosensors are a hot topic in research. In this section biosensors are introduced in a conceptual way.

1.1.1 Introduction to biosensors

Sensors are commonly known as devices which can detect light, mass, movement, smoke and other occurring events. A biosensor is a sensing device that is able to trace down molecules using biological receptors. Although not

very well known by most people, they are an interesting topic in research and more related to every-day life than one would suspect.

Biosensors have various purposes. One of them is the determination of the presence of a certain molecule in the human body. The most commonly known example is the glucose sensor used by diabetes patients. It is shown in Figure 1-1. A droplet of blood is put on a test strip. When the strip is placed in the glucose sensor, this sensor determines the amount of glucose present in the blood droplet. Depending on the result the patient himself can administer the appropriate insulin levels. This biosensor uses an enzyme as recognition element and the glucose sensor measures the product of the enzymatic reaction, which is a measure of the present glucose concentration. The quality of life of diabetes patients is tremendously increased by these types of biosensors.

Another commonly known example of the biosensor is the pregnancy test (Figure 1-1), which is widely available at the pharmacist. This test detects biomolecules in urine related to the increased level of the hormone HCG (human chorionic gonadotropin) in the morning urine of a pregnant woman. When it successfully detects the desired molecules it will give an optical feedback to the user through a color changing strip.

Figure 1-1: The home pregnancy test (left) and the glucose sensor for diabetes patients [OneTouch® Ultra® 2 from LifeScan] (right) are both examples of successful, commercially available biosensor.

In modern health care early detection of certain disease marking molecules is becoming of increasing importance. A rapid diagnose can prevent or slow down

the illness. For instance, C-Reactive Protein (CRP) is a marker for heart and vascular conditions. It is assumed that increased levels of CRP are already present in young adulthood. Early detection of elevated levels of CRP may avoid hart infarcts. Biosensors for this purpose are already made [1, 2]. Biosensors have also been created for the detection of low concentrations of toxic substances, before the toxicity reaches levels that cause damage, for instance the monitoring of the quality of water [3] and the detection of biological warfare agents [4].

Biosensors are a hot topic in research, as is illustrated by Figure 1-2. The number of publications per year has increased tremendously over the past few years. At the time of writing only seven months of 2009 had passed. Biosensors represent a rapidly expanding field, mainly stimulated and financed by the health-care industry with assistance from other areas such as food quality control and environmental monitoring. An estimated 13 billion EUR are annually spent in the market of analytical tests (such as on patient samples, environmental samples) while only 0.1 % of this budget is used for biosensors. Although this presents a budget of 13 million EUR, tremendous commercial opportunities still lie ahead in this market section. This is not the only reason of interest. Researchers from a wide range of backgrounds are drawn to the field of biosensors, as research and development in this field is wide and multidisciplinary.

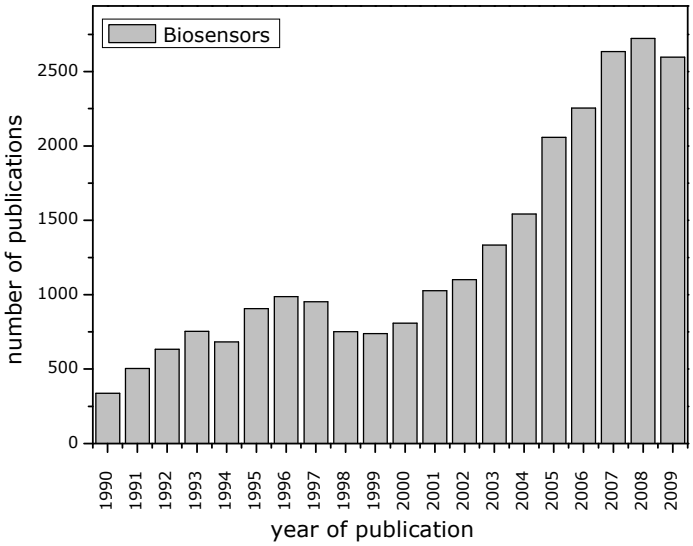

Figure 1-2: Growing number of publications on the topic 'biosensors' on Science Direct (www.ScienceDirect.com).

1.1.2 Description of a biosensor

A biosensor is defined as a compact analytical device consisting of a recognition element of biological origin, associated with a transducer element. The aim is to produce a signal that is proportional to a single analyte or a related group of analytes. A schematic representation of the biosensor can be seen in Figure 1-3. Biomimetic sensors use a chemical recognition element.

The recognition element can specifically detect its analyte. This recognition layer can be all sorts of biological material, e.g. tissue, enzymes, antibodies, nucleic acids, but in modern developments it can also be synthetic material such as artificial receptors.

The recognition layer is connected with a transducer layer. This layer will convert the chemical or physical binding event into a measurable signal, which may be optical, electrochemical, piezoelectric or magnetic. A digital electronic signal is desirable as this method can be combined with easy data storage, easy

data analyses and possible wireless data transfer applications for sensing with remote devices. The type of transducer applied in the sensor usually depends on the recognition element that is used to detect the desired analyte. The recognition element must be compatible because it needs to be immobilized onto the transducer element.

The transducer layer then sends out a signal which is processed by means of the signal processor. Which type of recognition layer, transducer or read-out is being used, depends mainly on the envisaged sensor. The analyte to detect and under which circumstances the process is executed, influences the choice of the different components. A major merit of biosensors is the combination of the specificity of a biological system and the sensitivity, combined with the power of a microprocessor.

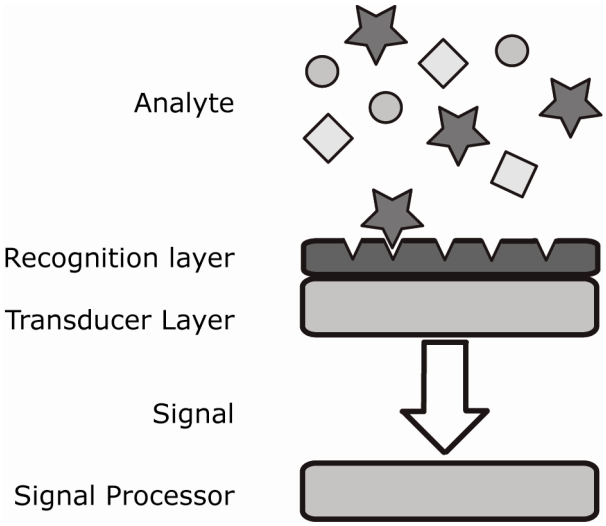

Figure 1-3: Schematic layout of a biosensor.

1.2 Irritable Bowel Syndrome (IBS)

The most recognized example of IBS is also known as 'exam nerves', where an emotionally stressful event causes an increased motility of the bowel system, better known as "pre-exam diarrhea". But which processes are involved in this reaction? How many people are affected by this syndrome? How much do we know about this syndrome nowadays? And why do we call it a syndrome? Is it

really necessary to invest in research about this syndrome? After all, what's the harm in some exam nerves?

1.2.1 What is IBS exactly?

Irritable Bowel Syndrome (IBS) is defined as "a functional bowel disorder in which abdominal pain is associated with defecation or a change in bowel habits, with features of disordered defecation and distention" [5]. In 1966 the condition had been called its name 'irritable bowel syndrome´ for the very first time by DeLor [6]. IBS is a functional disorder, meaning the bowel does not function properly. IBS mainly affects the colon or the large bowel. This is the part where the stool takes place. A malfunctioning colon can cause not only discomfort but even severe pain. As IBS patients suffer from a group of symptoms, the condition is called a syndrome.

On the mucosal tissue of the large bowel mast cells are present. This type of cells is especially prominent in places where the internal environment and the outside world are close to meet, like skin, mouth, nose, and also the mucosa of the lungs and digestive tract. Mast cells contain a lot of granules with various mediators. Histamine is a small molecule stored within mast cells, and so are neutral proteases like tryptase.

For a lot of people an exam can cause quite a lot of stress. With IBS such a psychologically or emotionally stressful situation causes the release of a hormone in the hypothalamus which is named corticotrophin release hormone. This hormone can interact with the bowel system via the brain/bowel interaction. Through this interaction the hormone can cause activation and destabilization of mast cells in the intestinal mucosal tissue [7, 8]. Upon activation, they release histamine, tryptase and other compounds. Histamine and tryptase also play an important role in allergies [9], asthma [10], rheumatoid arthritis [11], and related diseases. Histamine will cause redness and warmth and it can also attract other inflammatory substances to the site of release, adding up to the allergic reaction. It can also cause irritation at nerve endings causing itching or pain.

These compounds negatively affect the integrity of the mucosal tissue in the bowel system, leading to an increased motility of the bowel system. This symptom is more commonly known as "pre-exam diarrhea" when relating back to our given example. However, there are many more severe cases of IBS. Possible complaints are abdominal pain, problems with diarrhea and constipation and other intestinal problems, such as bloating and gas. Complaints apart from the stomach-bowel system can be headaches, lower back ache, tiredness, irregular menstrual cycle, pain during or after sexual intercourse, painful urination,…

1.2.2 Prevalence of IBS

Data about IBS patients are not easy to obtain as it is very hard to diagnose patients. In the USA a lot of studies about the prevalence of IBS have been performed. Some of the most important findings are summarized here. IBS is one of the most common large bowel disorders [12]. Up to 20% of the US population reports symptoms corresponding to IBS symptoms [13]. IBS mainly affects women, approximately 70% [14]. It is in the top 10 list of reasons to consult an emergency department. [5]. Typical syndromes for IBS patients are diarrhea, constipation or a continuous alteration of both. 5-10 % of the American population suffers from a type of IBS controlled by diarrhea. This group is approximately 50% of all IBS patients [15]. Despite the large prevalence of the syndrome only 5% of all IBS patients suffer severe complaints [16].

However these prevalence numbers may vary greatly from one study to the next. An important aspect of this is the method of diagnose. In general there are three ways of diagnosing a functional gastrointestinal disorder like IBS, starting with the Manning criteria [17] in 1978 (Figure 1-4).

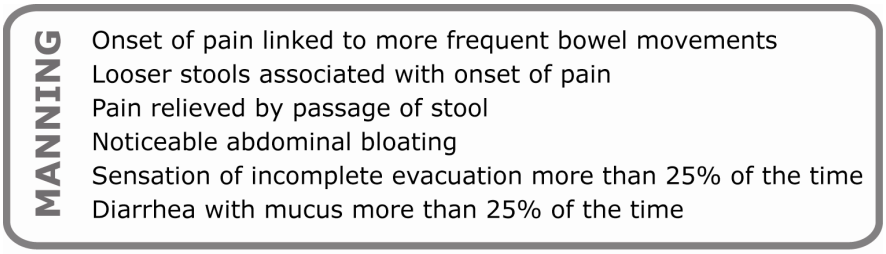

Figure 1-4: Manning criteria for IBS.

Further refinements of the Manning criteria were established, known as Rome I in 1992, Rome II in 1998 and recently Rome III in 2006. One of the refinements of the Rome criteria is the use of 'red flag symptoms', symptoms that are not typical of IBS (Figure 1-5). Blood in the stool, for instance, is a red flag symbol, meaning the patient suffers from a functional gastrointestinal disorder other then IBS. The Rome criteria made it easier for physicians to diagnose a patient. An Australian study showed that Rome II criteria for IBS patients did not lead to a different population than Rome I criteria [18]. However an epidemiologic study about IBS in Korea reported a 2.2-6.6 % prevalence of IBS according to Rome II criteria and a 22.3% prevalence following the Manning criteria. [19]. Diagnose method needs to be taken into consideration when discussing epidemiology of IBS.

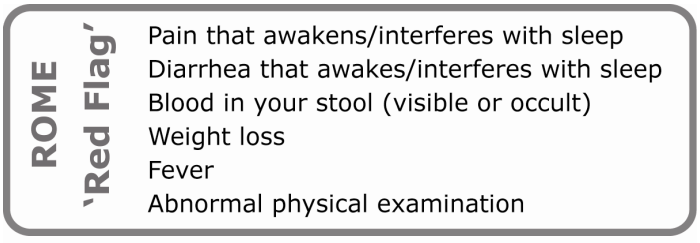

Figure 1-5: 'Red flag' symptoms, described in the Rome criteria for IBS.

Nevertheless the difference in prevalence numbers, this brief discussion shows that IBS is a very common problem. In 2008, Belgian authorities organized a national campaign for awareness of IBS amongst its population, resulting in an advertisement in the news paper 'Metro' (Figure 1-6) explaining the symptoms, side effects, prevalence and possible treatments of IBS.

Figure 1-6: Belgian campaign about IBS, published in Metro in 2008.

An estimated 20 % of the Belgian population suffers from some form of IBS and an IBS patient is very costly for an employer due to absence by illness and for the health care system regarding medicine and treatments. Several studies on the costs of IBS have been reported in the UK and USA, but due to the difference in diagnose and treatment costs, accounting studies can not be compared [20]. However, let's focus on one study that addressed the healthcare resources involved in IBS patients [21]. To make clear what we are talking about, some numbers from the combined US/UK based study are stated. Direct costs per patient per year vary between USD 348 en USD 8750. Indirect costs, such as absenteeism (time lost from work) and presenteeism (reduced productivity at work) are between USD 355 and USD 3344. The average number of sick leave days for an IBS patient is between 8.5 and 21.6 annually. These high numbers desperately call for a solution for IBS.

1.2.3 Current techniques in IBS understanding

Throughout the world a lot of effort is put into a better understanding of IBS and into techniques leading to better diagnoses. An accurate understanding of IBS is the first step into developing efficient treatment of IBS. Current state-of-the-art techniques used for understanding IBS however are less effective. First the intestines are rinsed. The rinsing liquid is then condensed for obtaining a more concentrated sample of molecules one wishes to detect. Volumes are usually reduced by a factor 40 to 100. In this concentrated liquid, histamine concentrations can now be determined [22].

Until date the following techniques have been reported in literature for the analysis of histamine in biological fluids. Fluorometric assay, which measures the difference in fluorescence between the product and the substrate, was widely used in tissue [23] and in whole blood and plasma [24,25,26]. The measurement of a large number of samples is complicated by the extraction steps that are needed. High-speed liquid chromatography overcame some disadvantages of the fluorometric assay but was time consuming. [27]. Radioisotopic enzymatic assay is a sensitive method and it is specific in biological fluids [28]. However the presence of other compounds inhibits the enzymatic reaction necessary for this method of detection, making it difficult to

determine histamine levels. Gas chromatography-mass spectroscopy [29] meets a lot of sensitivity, specificity and accuracy demands, while sample manipulation is very complex and instrumentation very expensive. Other techniques are High-Performance Liquid Chromatography (HPLC) [30] and Capillary Electrophoresis (CE) [31], which are both suitable for separating molecules in liquids. However, HPLC is very costly in equipment. The technique requires a whole column of materials, so HPLC also has a high material cost. CE seperates molecules in fluids in capillaries, hence it uses only microliters of fluid. It is hence cheaper, but the sensitivity of CE is very low.

For routine determination of histamine an immunoassay is suitable for the rapid analysis of large quantities of samples. In an immunoassay histamine is detected by binding specifically with its antibody. Preparation of such an antibody has only been made possible in 1984 [32]. The binding of histamine with its antibody can be detected with a radioimmunoassay (RIA). The binding of the antigen with its antibody is detected by measuring radioactivity. This technique is often used for the detection of a wide range of biologically important molecules. Successful RIA's for the detection of histamine started to develop ever since [33,34,35,36]. The antibody-antigen binding can also be detected enzymatic by means of Enzyme-Linked Immunosorbent Assay (ELISA) [37]. Here the antigen can be labeled with an enzyme. After the binding if the antigen to the antibodies an enzymatic reaction will occur, usually resulting in a color change. But these techniques remain time consuming and none of them make it possible to measure histamine concentrations directly in the intestine.

Tryptase as also a mediator stored in the granules of the mast cells.. Upon allergic reaction the granule will degranulate. Tryptase is released and this protein can now negatively affect the mucosa of the bowel, disrupting the normal functionality of the bowel system. Several immunoassays have been developed for the detection of tryptase [38,39,40]. The fluoroimmunoassay UniCap Tryptase from Pharmacia & Upjohn [41] is the most commonly used method in research and analytical laboratories nowadays.

In vivo measurements as such are not yet possible. Accurate data of release of histamine directly at the mucosa in the intestines can only be obtained by

performing biopsies on voluntary patients. As this is a rather painful procedure, voluntary patients are hard to find and acquiring data on histamine release in the intestines is greatly slowed down by this circumstantial procedure.

1.2.4 Aim of this thesis

Although IBS is not a life threatening condition, IBS can seriously impair overall quality of life. The importance of IBS research has been pointed out in previous sections. For verification of the effectiveness of an adjusted diet with respect to mast cell stabilization, histamine measurements need to be performed in double blind tests. This involves a test group supplied with placebos. This kind of research would definitely benefit from a measurement device for measuring released levels of histamine, tryptase and other compounds directly in the intestines. To obtain information about the release of histamine and tryptase as function of dietary programs it is desirable to measure these concentrations directly at the mucous membrane of the small intestine.

Considering all disadvantages of current techniques, a sensor is wanted that can detect relevant concentrations "on the spot" in the bowel system, does not require reagents, works as a direct assay, is applicable in "point-of-care" context and gives a fast "real time" result.

Therefore in this project a biosensor is under development for intestinal detection of such compounds.

1.3 An immunosensor: biological recognition by means of immunoglobulins

The first step in the development of a biosensor for histamine detection is creating a sensor with a biological recognition layer based on antibodies or immunoglobulins, a polymer transducer layer and an impedimetric method of detection. It is schematically depicted in Figure 1-7. All components are explained in following subsections.

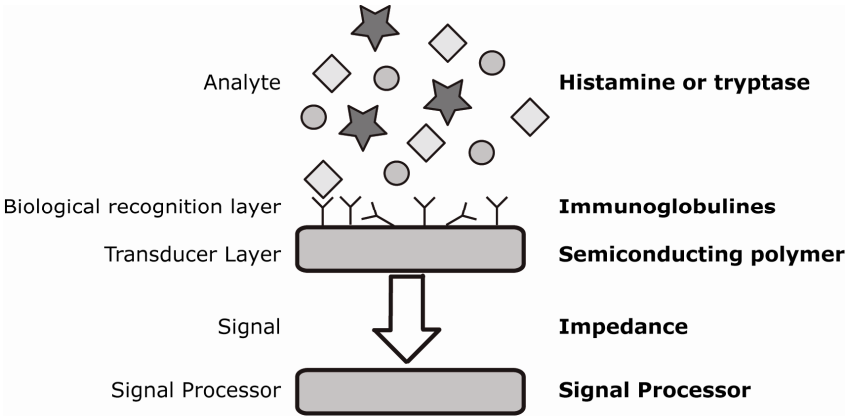

Figure 1-7: Schematic layout of an immunosensor.

1.3.1 Analyte

For IBS research applications the focus lies on the development of a sensor for 2 possible target molecules. Histamine and tryptase are both released by the mast cells. Histamine is synthesized from the decarboxylation of the amino acid histidine, a reaction which is catalyzed by the enzyme L-histidine decarboxylase. Histamine is a small molecule with a low molecular weight (111 Da) and a chemical formula $C_5H_9N_3$ [42]. The resembling molecules histidine (155 Da) and histamine are both depicted in Figure 1-8.

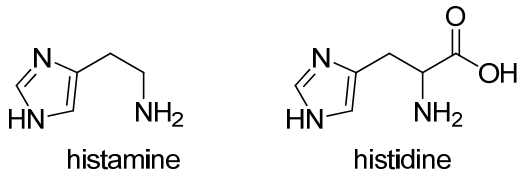

Figure 1-8: Chemical structure of histamine and histidine.

Human tryptase is a neutral protease with a tetrameric structure [43] and a molecular weight of 135 kDa [44,45]. Its structure is shown in Figure 1-9.

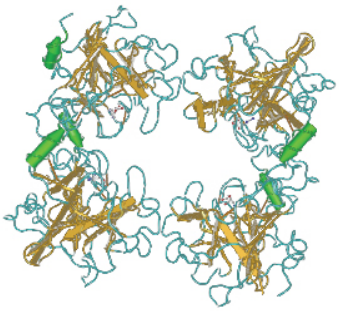

Figure 1-9: Representation of tryptase [46].

1.3.2 Biological recognition layer

The biological recognition layer consists of biological antibodies. The detection system is based on the biological recognition of molecules by using the appropriate antibody for the antigen one wants to detect.

An antibody is a protein which occurs in blood and other body fluids When a hostile antigen enters the human body, this body responds by creating an antibody which specifically can bind this antigen. Antibodies are thus proteins that are used by the immune system and can identify antigens and neutralize viruses or bacteria.

Figure 1-10 shows the simplest structure of an antibody. It has a symmetrical shape resembling the letter Y with on each side an identical recognition spot where it can bind an antigen. Each half consists of a large heavy chain and a small light chain. Each chain has a variable part on top, making the antibody specific to its antigen. In this way the antibody can recognize specific foreign objects. The heavy chain contains a constant part at the bottom, determining the biological activity. Antibodies that have an identical constant part of the heavy chain are antibodies of the same isotype. Based on the type of heavy chain, antibodies are grouped into five isotypes, known as IgA, IgD, IgE, IgG, and IgM. Isotypes E have heavy chains ε, and occur on mast cells and basophiles. Isotype G has heavy chains ψ and a molar mass of 150 kDa. IgG is

present mostly in serum and provides the majority of antibody based immunity against invaders. Depending on the unique function of each region of an a antibody, they can be labeled in a different way. The tips of the Y-shape are the fragment of the antibody that serves for antigen binding, the Fab region. The base of the Y-shape is a crystallizable fragment, called the Fc region. It plays a role in immune cell activity.

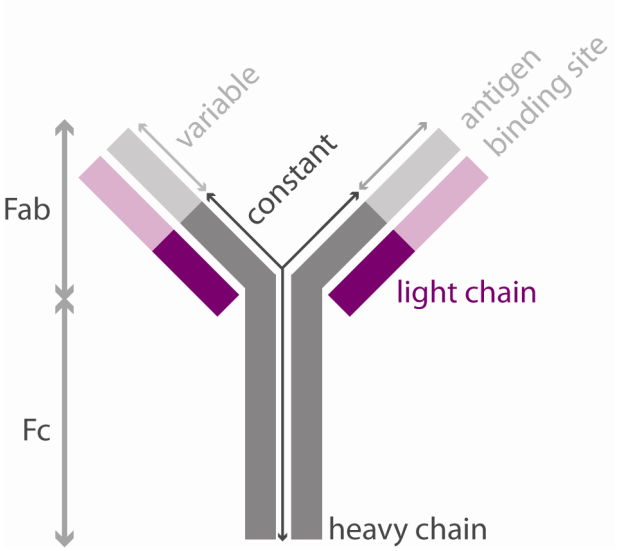

Figure 1-10: Structure of an antibody.

The binding between an antigen and the amino acids of the binding site of the antibody is a non-covalent binding. A series of weak intermolecular forces, namely hydrogen bonds, electrostatic forces between charged side chains, van der Waals forces and hydrophobic forces all work together to make it a strong and specific binding.

The biological recognition layer is created by physical adsorption of antibodies on this film, as has been reported in literature [47]. The Vroman effect describes the adsorption of body proteins to medical implants and how the proteins can bind with the polymer matrix by weak non covalent bonds [48]. This effect is also applicable in our sensor when antibodies physically adsorb to the polymer transducer layer. Forces controlling the process of physical adsorption are also intermolecular forces, of which there are the van der Waals force, hydrogen bonds, electrostatic forces and hydrophobic forces.

It is proven that antibodies remain biologically active after physical adsorption [49]. This is a cheap, easy and reproducible method of immobilization. However, they are severely affected by external conditions such as temperature, ionic strength and pH. Instead of the weak non covalent bonds created by physical adsorption, it is also possible to covalently bind the antibodies to the polymer. This will result in more stable recognition layers.

1.3.3 Transducer layer

When target molecules bind to the receptors on the electrode surface, a change in dielectric properties will occur at the biological interface. To be able to measure these capacitive and other electrical changes, a conducting or semiconducting transducer is needed. For other types of detection other transducer materials are also possible. For example microgravimetric detection occurs based on the mass change of a quartz crystal when target molecules bind to the recognition layer applied onto a quartz crystal.

Polymer is being used as semiconducting transducer layer. Although polymers initially have been considered to be insulators, it has been found that they can also conduct electricity. When polymers have alternating single and double bonds, i.e. conjugated polymers, they are organic semiconductors. The discovery of conduction in polymers in the 80's has lead to the birth of various new research areas [50,51]. LEDs and solar cells are just a few examples of the wide range of applications of the material formerly considered as an insulator. A hot topic in contemporary applied research is biotechnology where polymers play an important role, like here in biosensors. Opposed to polypyrrole and polyaniline, which are often referred to in literature [52, 53], IMO biosensor group strives for implementation of poly(phenylene-vinylene) (PPV) in their biosensors. Throughout the years a lot of expertise has been acquired, specifically on the PPV-polymers by the research group Organic Electrical Materials at IMO [54,55]. Combined with the easy handling and the possibility to vary the side chains these materials looked promising and indeed the Biosensor group has succeeded at activating thin polymer films for biosensing [1].

A polymer serves both transducer purposes, as a transducer and as an immobilization platform. Firstly, it is a semiconductor and can thus convert the signal of the biological receptors into an electrical signal. Secondly, receptors can be immobilized on polymers. By means of physical adsorption or covalent bonding antibodies can be immobilized. Synthetic receptors can be immobilized through stamping.

The polymer used in this work is MDMO-PPV, the monomer of which is shown in Figure 1-11. Poly[2-methoxy-5-(3,7-dimethyloctyloxy)-1-4-phenylene vinylene] is known as MDMO-PPV and synthesized via the so called Gilch or sulphinyl route. It is a p-type semi-conductor with a band gap of 2.1 eV [56].

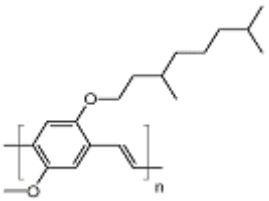

Figure 1-11: Monomer of MDMO-PPV [57].

These polymer-based sensors offer several advantages. They have a beneficial low production cost, making them cheap disposable sensors. They can also be used for bedside diagnostics.

1.3.4 From building blocks to creating a biosensor

There is a need for a rapid and sensitive detection method. Therefore a sensor with electronic readout has been constructed using all the different building blocks described above.

The sensor lay-out is schematically shown in Figure 1-12. A sensor starts with 8 electrodes on glass, each measuring channel contains a pair of electrodes. All channels are covered with the transducer layer. Each measuring channel can be individually functionalized according to the experiment.

Antibodies against the specific target-molecule are immobilized on the transducer layer, for which the conjugated polymer MDMO-PPV is used. The

biological recognition layer is created by physical adsorption of antibodies on this film. In the schematic drawing three channels are functionalized with immunoglobulines and one channel is bare polymer.

When the appropriate antigen is present in the analyte, it will bind to its antibody and a biological recognition will occur. The translation of the biological recognition to an electrical signal is based upon impedance measurements of the polymer film. The actual binding of the detected antigen to its immobilized antibody induces changes in the resistive, capacitive and dielectric properties of the biological interface. This binding event will thus cause a change in impedance over the recognition layer and an impedimetric read-out of the biosensor is established. Impedance is measured by an impedance analyzer, which applies an AC voltage to the sensor and measures the resulting AC current. Each channel is measured separately for preventing leaking currents form one electrode to the other. Data are sent to a computer where they are visualized, stored, processed and analyzed.

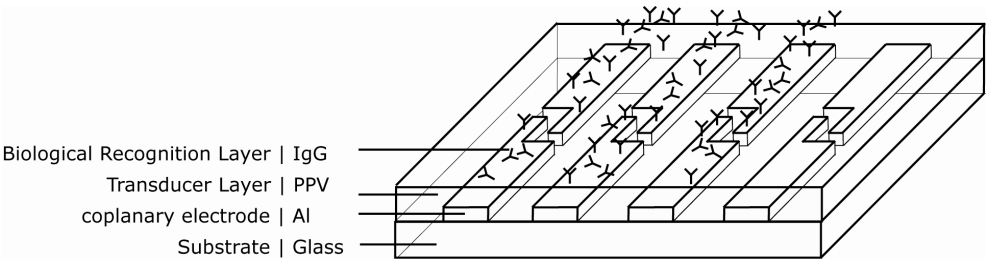

Figure 1-12 : Schematic representation of the coplanar polymer-based immunosensor.

1.4 A MIP-based sensor: chemical recognition by means of synthetic antibodies.

In section 1.3.2 the use of antibodies as biological receptors has been discussed. It has also been pointed out that physical adsorption of these antibodies is not a stable immobilization technique. This may be resolved by establishing a covalent binding between the antibody and the polymer layer, however some disadvantages remain. Existing sensing systems based on biological recognition

elements have restrictions limiting their use [58, 59]. Firstly, a biological recognition element is not always available for the desired target. It wasn't until 1984 when researchers were first capable of creating an antibody for histamine e.g. Secondly, not every molecule has a suitable antibody. Thirdly, antibodies are hard to produce in mass quantities. Furthermore they are instable in organic solvents, high temperature or changing pH. For the envisaged intestinal application of our biosensor in IBS research, a receptor that can withstand such conditions is desirable, with the same specific binding capacity and selectivity as an antibody. A chemical recognition element can be more inert and stable in a wide range of conditions such as temperature or pH [60]. Molecularly imprinted polymers (MIPs) have this similar specific binding characteristics and selectivity towards their target as antibodies [60, 61, 62, 63] and they are excellent candidates for use as synthetic receptors for the creation of a chemical recognition layer.

A biosensor for histamine detection has been developed using a biomimetic recognition layer based upon synthetic receptors, a polymer transducer layer and the same impedimetric method of detection. It is schematically depicted in Figure 1-13 and these synthetic receptors are treated in detail in this section.

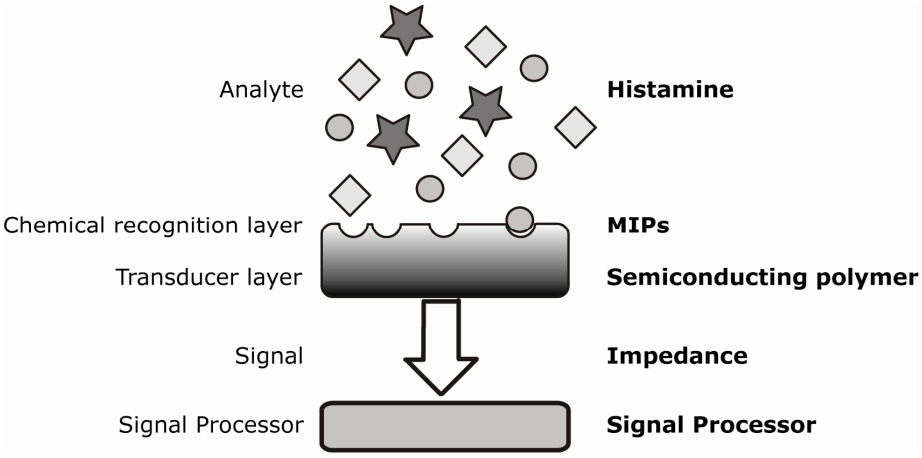

Figure 1-13: Schematic layout of a biomimetic sensor using MIPs as chemical recognition element.

1.4.1 Analyte

MIPs are suitable for target molecules for which no natural antibody is available. Previously they have also been successfully developed for low molecular weight molecules [64, 65]. This type of sensors is therefore focused on the detection of the small molecule histamine, which has been treated in section 1.3.1.

1.4.2 MIPs

As mentioned the biological receptors are replaced by synthetic receptors, or artificially created antibodies, as MIPs are often referred to [66, 62]. MIPs are polymers in which the target molecule is imprinted. This imprinting is according the shape and functional groups of the target molecule. Subsequent removal of the target molecules results in cavities being created within the polymer in the exact size of the target molecule with on the interior functional groups complementary to the target molecule.

The ingredients for synthesis of a MIP are a target molecule, a functional monomer, a crosslinker solvent and an initiator in case of radicalary polymerization. The target molecule is the molecule one wishes to detect or bind. For an optimal selectivity and sensitivity the target molecule needs different functional groups.

The recipe for synthesis of a MIP is described below and schematically depicted in Figure 1-14. A functional monomer has groups that interact with the complementary groups of the target molecule. This interaction results in the formation of a complex, called a pre-polymerization complex (step 1). The interaction between the monomer and the target molecules can be covalent or non-covalent. In non-covalent imprinting, used in this work, the interaction is usually based on hydrogen bridges but electrostatic and hydrophobic interactions are also possible. The choice of functional monomer depends therefore not only on the target molecule but also on the desired method of imprinting.

This pre-polymerization complex is then mixed with a cross-linker, which fixates the complex for maintaining the molecular structure after extraction of the MIP.

The cross-linker makes sure that the nanocavities remain. The stronger the cross-linker, the less other reagents will bind to the MIP. A weak cross-linker does not fixate the nanocavity well, allowing deformations which cause other reagents to bind. The stabilization of these complexes by means of the cross-linker is the polymerization process. Polymerization may be initiated by an initiator in the case of radical polymerization.

During these 2 steps of pre-polymerization and polymerization a solvent is used. Before polymerization the solvent keeps everything in solution, and during the polymerization it creates pores. These pores allow easier extraction of the target molecule and easier access to the nanocavity later on.

Now that the mixture has polymerized the target molecule is extracted by washing with specific solvents. In this way a cavity remains in the polymer which is tailor-made to the desired target molecule.

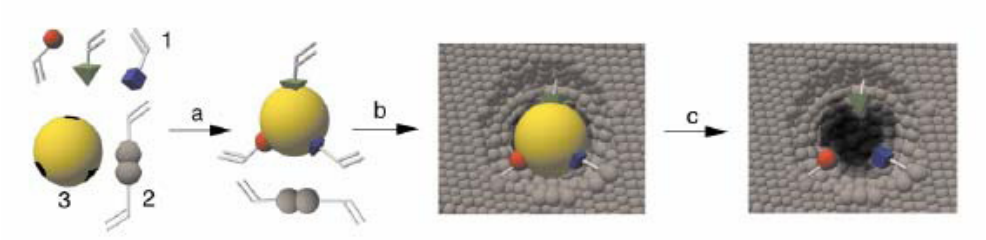

Figure 1-14: Schematic representation of MIP synthesis [67] with functional monomers (1), cross linker (2) and target molecule (3). Components undergo following steps. a) Step 1: complex formation of functional monomers with the target molecule, b) step 2: copolymerization with cross linker to c) step 3: a solid polymer with nanocavity after extraction.

Here it is aimed to integrate these MIPs into an impedimetric sensing device, which has recently been successful in the nicotine sensor [68]. MIPs are also applied in electrochemical [69], piezo-electric [70] and optical sensors [71]. The applications of MIPs are numerous, and the interest in these synthetic receptors his increased tremendously. The number of publications increased exponentially over the last couple of years (Figure 1-15). The same remark as with Figure 1-2 is made, as 2009 only accounts for 7 months.

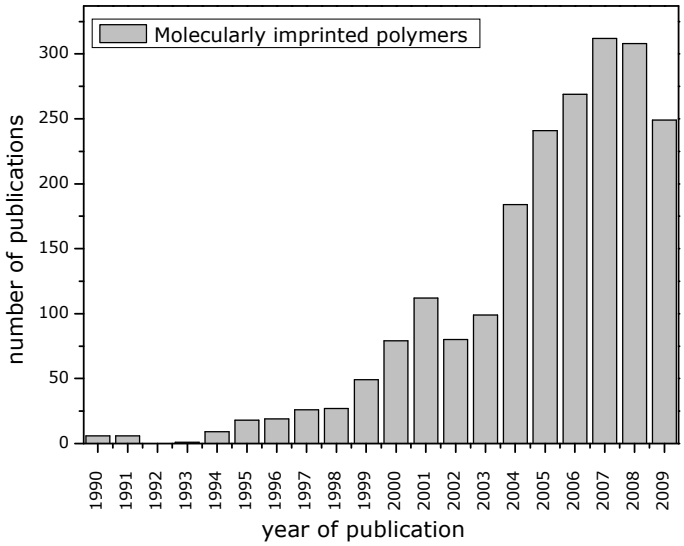

Figure 1-15: Growing number of publications on the topic 'molecularly imprinted polymers' on Science Direct (www.ScienceDirect.com).

1.4.3 Transducer layer

For impedimetric measurements a semiconducting transducer material is required. As explained before, organic semiconductors make suitable transducer platforms due to their low production cost. To immobilize the non-conducting MIP particles onto the electrode surface, a conjugated polymer is used that can amplify the signal. The polymer used for immobilization of biological antibodies, i.e. MDMO-PPV, is also suitable for immobilization of MIPS, the plastic antibodies. For microgravimetric purposes polyvinyl chloride (PVC) is a suitable immobilization platform. This polymer has been used by Tan et al. when they first successfully implemented MIPS for nicotine in a quartz microbalance device (QCM) by immobilization in a PVC matrix [72]. A detection limit of 25nM was obtained, while relevant medical concentrations for nicotine in urine are 0.3 μM for non-smokers and 6.3 μM for smokers.

The MIP microparticles can easily be immobilized onto the polymer layer. Microparticles are placed on the polymer, which is then heated to the glass transition temperature. At this temperature the polymer undergoes a transition from the glass state to the rubbery state, causing the polymer to become less rigid, softer and flexible. This allows for the microparticles to softly sink into the polymer layer. The sinking of the MIP particles into the polymer layer has been investigated by Thoelen et al. [68], who describe the sinking as an "ice-berg" effect. From the cross-section of the device they found that the sunken particles have a typical diameter of 300 nm.

With the different layers described in this paragraph MIP-based sensor substrates are made with exact dimensions of the immunosensor substrates. Samples are mounted into the addition setup in the same way as described in detail in 1.3.4.

2 Materials and Methods

In this chapter it is discussed how bio- and chemosensors are made and the techniques used for either characterization of the sensors or as detection method.

2.1 Sensor preparation

The different steps involved in the making of immuno- or MIP-based sensors are discussed in the same order as they are carried out.

2.1.1 Glass substrates

Glass substrates are used for all samples due to their cheap price and optical transparency. They can easily be cut to the desired dimensions using a diamond pen. The sensor samples are 12 x 20 mm² and samples prepared for characterization measurements usually have dimensions of 10 x 10 mm². For good attachment of electrodes and transducer materials the glass surfaces need to be cleaned: substrates are rinsed in an ultrasonic bath for 30 min in a Buehler Ultramet 2 Sonic cleaning solution, which has been diluted 1:20 and subsequently twice for 10 min in demineralized water with a resistivity of 18 MΩcm. 10 minutes in an ultrasonic bath in acetone will remove organic components. Finally samples are placed in hot iso-propanol for 10 minutes. The substrates are dried under N_2-flow.

2.1.2 Electrodes

Four electrodes are placed onto these glass substrates. Electrodes can be made of various materials such as gold (Au), aluminum (Al), titanium (Ti), titanium nitride (TiN) or platinum (Pt). Coplanar electrodes with an interspace of 1 mm (Figure 2-1) are made from 50 nm thick, sputtered TiN for the immunosensors and later 70 nm evaporated Al for the MIP-based sensors.

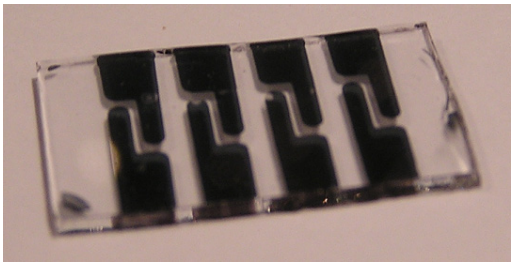

Figure 2-1: Coplanar electrodes with a 1 mm interspace.

As will be explained in the following of this section, interdigitated electrodes (IDE) can be useful alternative to coplanar electrodes. IDE's are prepared using optical lithography. On a 20 nm evaporated Al layer photo resist is spincoated at 4000 rpm during 30 s and then baked at 120°C for one minute. The samples are then covered with a photolithographic mask and UV-illuminated with a light-source MJB3 Karl Süss MA during 16 sec at 220 W. Microdeposit Developer 351 (1:4 MD351:H_20) and Al etcher OPD 5262 are then used to develop and simultaneously etch the substrates under slight motion during a couple of minutes. This creates interdigital structures with 15 fingers of 50 μm on each side with an interspace of 25 μm [Figure 2-2]. Afterwards, the samples are cleaned in demineralized water.

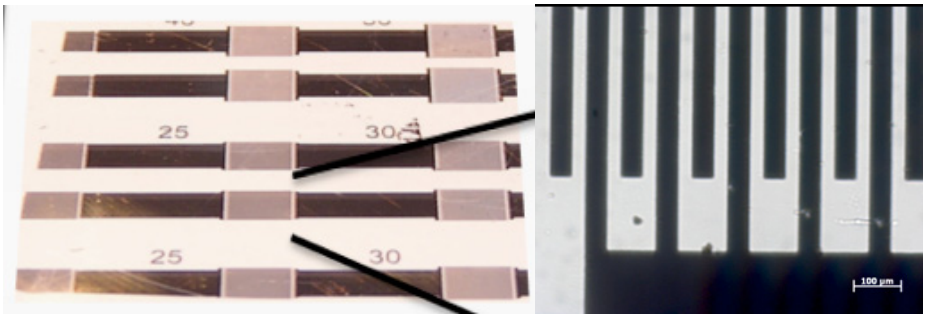

Figure 2-2: Interdigitated electrodes containing 15 fingers of 50 μm on each side with an interspace of 25 μm.

Obviously, the coplanar and interdigitated electrodes differ in electrode interspace. This is beneficial for the sensitivity of our sensor, due to the following. When electrodes are at a distance L apart from each other, it is assumed that 95 % of the electrical field lines are located at a height L above the surface, as is schematically drawn in Figure 2-3 [73]. For coplanar

electrodes with a distance of 1 mm, the electrical field lines are located mainly in the electrolyte solution while only a small part is focused on the interface layer which is where the biological recognition takes place. Interdigitated electrodes have an interspace of 25 μm. Field lines are now closer to the surface. The signal contains more information about the interface and less information from the electrolyte. This way, the sensor is more sensitive to small molecules such as histamine. Also the field lines itself are smaller and easier to disturb, again increasing the sensitivity of the sensor. Interdigitated electrodes are supposed to have increased their sensitivity by a factor of 20, compared to coplanar electrodes [74].

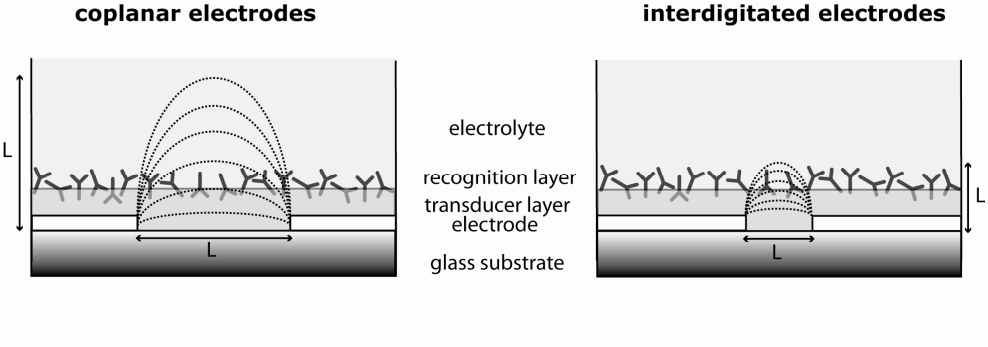

Figure 2-3: Field line distribution of coplanar (left) and interdigitated (right) contacts.

2.1.3 Transducer layer

Four electrodes are placed on one substrate, coplanar or interdigitated depending on the experiment. These electrodes are covered with a thin film of MDMO-PPV, a p-type semiconductor with a bandgap of 2.1 eV [Figure 2-4], which was synthesized via the sulphynil precursor route [56] by the Organic & Polymeric chemistry group of IMO. All chemical and physical properties of this conjugated polymer were in agreement with previously reported data.

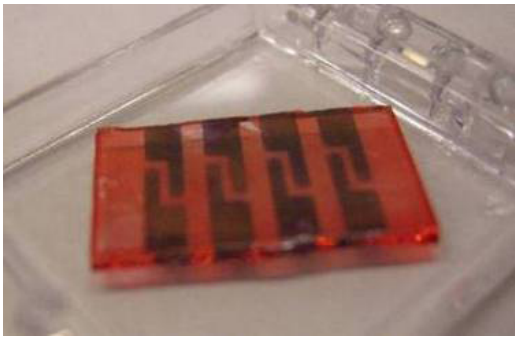

Figure 2-4: Four coplanar Al electrodes covered with PPV.

For obtaining thin layers of this polymer on the glass substrates, the spincoating technique [Figure 2-5] is used with a 0.7 wt% chlorobenzene solution. This technique occurs in a glovebox under inert N_2 atmosphere. This prevents any reactions between MDMO-PPV and O_2 to occur before drying, as this could damage the sample. The spincoating process technique consists of 4 steps in total, 1 dispensing step and 3 rotation steps. An excessive amount of dissolved MDMO-PPV is applied to the sample in a static phase (step 1). A first rotation step of 10 seconds at a speed of 300 rpm at an acceleration of 300 rpm/s spreads the dissolved polymer equally and uniformly over the substrate (step 2). The second rotation step determines the thickness of the polymer film. The speed is rapidly increased to 3000 rpm at an acceleration of 500 rpm/s for 10 seconds (step 3). Increasing the time or the speed decreases the layer thickness. Finally the substrate is spun at a low speed of 500 rpm again with a low acceleration of 500 rpm/s for 50 s. This slow and long rotation step allows for evaporation of the solvent. In this way a thin film of polymer remains on the substrate. With these settings and a concentration of 0.7 wt% chlorobenzene thicknesses of 100 nm are obtained. Higher concentrations lead to thicker layers. An increased speed in the second rotation step results in thinner layers.

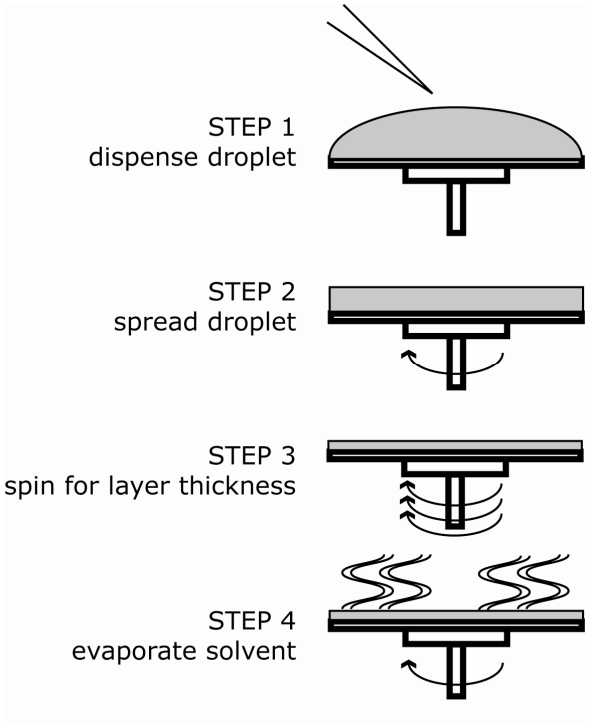

Figure 2-5: Steps of the spincoating process.

2.1.4 Recognition layers

Both biological (IgG's) and chemical (MIPs) types of recognition elements have been used. The materials for each type of receptor layer are explained in their respective following sections.

2.1.4.1 Biological receptors: antibodies

Monoclonal mouse antibodies IgG1 against free histamine (Argene D-22.12, 500 μg/ml) and against human mast cell tryptase (Genetex GTX75011) are dissolved in phosphate buffered saline (PBS). These antibodies are physically adsorbed onto the polymer layer by incubation during 1 hour at 37°C. The process is schematically depicted in Figure 2-6. The adsorption occurs in a closed environment in the presence of PBS to ensure a saturated atmosphere. After incubation, the samples are carefully rinsed in both PBS (1x) and demineralized water (2x) to wash off non-adsorbed immunoglobulines. The

immobilized antibodies can specifically bind their desired antigen, respectively histamine or tryptase from human lung, both obtained from Sigma-Aldrich. Antibodies immobilized via physical absorption have a random orientation. Therefore, some antibodies will have both recognition spots available, while others have only one or no recognition fragment.

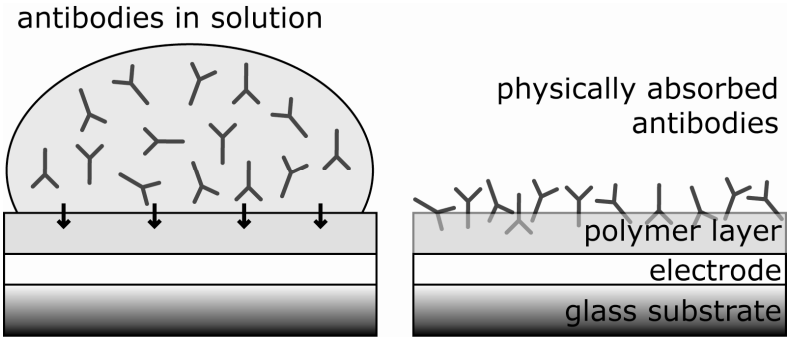

Figure 2-6: Physical adsorption of antibodies on polymer: during incubation (left) and after incubation (right).

2.1.4.2 Synthetic receptors: MIPs

MIP synthesis is performed by the Organic & Polymer Chemistry group of IMO [75] based upon previous successful preparation of MIPS for nicotine for integration in impedimetric sensing devises [68]. The MIP synthesis was optimized to obtain MIPs with a high affinity and selectivity for histamine detection in biomimetic sensors. The most suitable MIP, which was utilized in all biosensor experiments described hereafter, was made according to the following procedure:

A mixture of methacrylic acid (MAA) (17.8 mmol), Ethylene glycol dimethacrylate (EGDM) (36 mmol) and Azobisisobutyronitrile (AIBN) (0.66 mmol) was dissolved in 7 ml dimethylsulfoxide (DMSO) together with the template molecule histamine (8.99 mmol). MAA, which functions as monomer, the crosslinker EDGM, and the solvent DMSO were purchased from Acros. The stabilizers in the MAA and EGDM were removed by filtration over alumina. AIBN, the initiator for the polymerization, was purchased from Fluka. The target molecule histamine was obtained from Aldrich. This mixture was degassed for 5 min with N_2 to remove oxygen. For polymerisation the solution was sealed and

kept in a thermostatic oil bath at 65°C for 12 h. The process is schematically depicted in Figure 2-7. After polymerisation the bulk polymer was grounded with a mechanical mortar for 24 h and sieved through a 25-µm sieve. Only particles with a size smaller than 25 µm were used. Next, the histamine was removed from the MIP powders by Soxhlet extraction with methanol (48 h), followed by a mixture of acetic acid/acetonitrile (1/1) (48 h) and finally again methanol (12 h). The extracted MIP powders were dried in vacuum for 12 h. A non-imprinted polymer (NIP) was synthesized in the same manner, but without the presence of the target molecule.

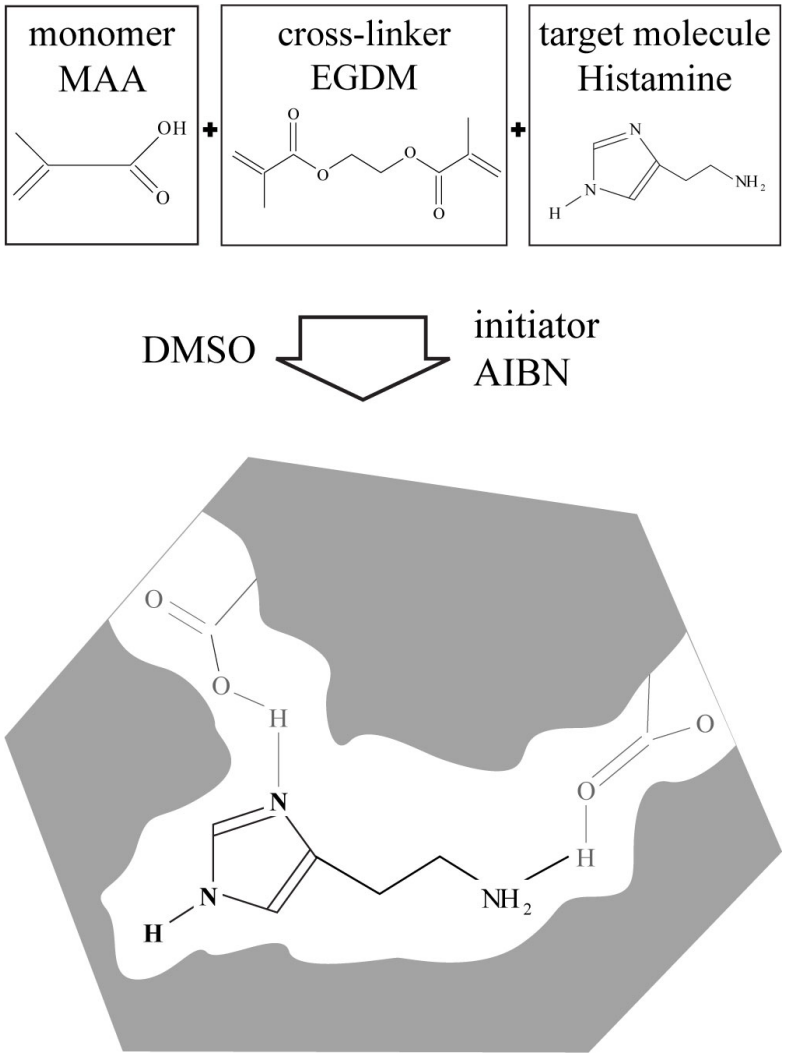

Figure 2-7: Schematic representation of MIP synthesis using histamine as target molecule.

Immobilization of these MIPs onto the transducer layer occurs via stamping of MIP microparticles in powder form. With this stamping method a PMMA stamp in the shape of the electrode is placed in the MIP microparticles, causing an excessive amount to stick to the stamp. Next the stamp is placed on the substrate and pressed for a few seconds and the MIP microparticles are in place. The electrodes can be accordingly functionalized with NIP microparticles as the experiment desires. The functionalized samples are then placed on a hotplate for 10 minutes at 120°C, which is above the glass transition temperature of the

MDMO-PPV (45°C). At this temperature microparticles become fixated in the surface of the polymer layer. Afterwards samples are rinsed with iso-propanol for removal of excessive and non-adsorbed microparticles and dried under N_2-flow.

2.1.5 Sensor lay-out

An addition setup is used for impedimetric sensing experiments. Figure 2-8 illustrates how samples are mounted into a PCB sample holder. Electrical contact between the sample and the PCB sample holder is established by means of wire bonding with 20 μm Al wires (Marpet Enterprises Inc) with a 1204W Hybrid Wedge Bonder.

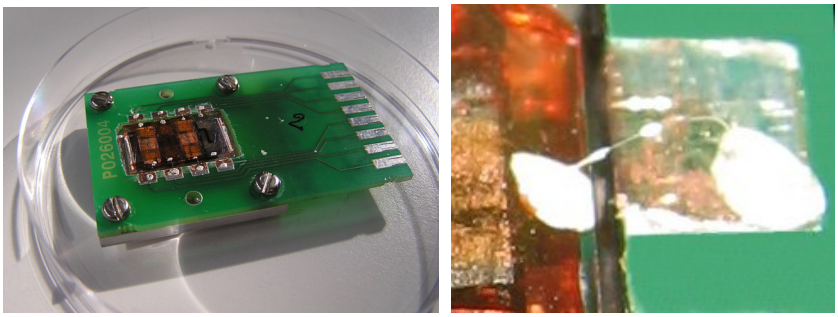

Figure 2-8: Samples are wire bonded onto a PCB sample holder.

A Teflon hood is placed on top of the PCB. The Teflon hood contains an opening at the top for addition of analyte concentrations. An addition setup is obtained [Figure 2-9]. With this static measuring device the interface behavior is not affected by turbulences in the liquid within the cell. To prevent leakage a small poly-dimethylsiloxane (PDMS) sealing rind is placed between the sample and the Teflon hood. Measurements occur at room temperature (20°C) and later in a temperature controlled environment of 37°C. During measurement the opening on top is covered from light.

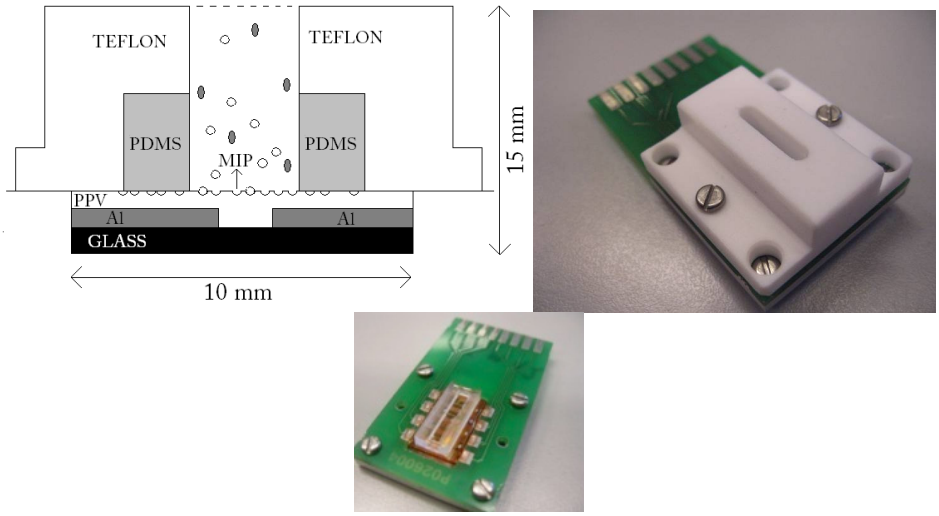

Figure 2-9: Schematic representation of the addition setup (left), containing a Teflon hood (right) and a PDMS ring (bottom).

2.1.6 Analyte

As target molecule the immunosensor uses histamine or tryptase from human lung, both obtained from Sigma-Aldrich.

For the MIP-based sensor histamine is also obtained from Aldrich. The analogue molecule, histidine, was obtained from Fluka and was used to test the specificity of the MIPs. For measuring a dose response curve, the concentration of histamine was increased in a 0 to 12 nM range. This is achieved by preparing a histamine concentration range of 9 to 31 nM in 12 equal steps. By sequentially adding constant volumes of 25 μl of these concentrations to the 200 μl PBS inside the reservoir, 1 nM increments of concentrations are obtained from 0 to 12 nM. The histidine concentrations were increased by repeatedly adding 50 μl of a 29 nM histidine solution to the starting volume of 200 μl PBS inside the reservoir. This results in unequal steps of 5.8 nM, 9.7 nM and 12.4 nM of concentration present within the sensor device. The dose response measurements occur at a pH neutral environment of pH 7.

2.2 Characterization techniques

For characterization of the sensor building blocks, several surface analytical techniques have been used, which are discussed in the following sections.

2.2.1 DEKTAK

DEKTAK is a height profiling equipment. A small needle scans the surface giving information about the height of the surface. Layer thicknesses can be measured by introducing an incision into the material. A DEKTAK measurement can then give information in the incision height which corresponds to the layer thickness.

This technique is an interesting tool for measuring layer thickness. Thickness of the electrode needs to be monitored as a thin electrode will have a high resistance. An electrode which is too thick will make it difficult to obtain a smooth surface when covering the electrodes with the polymer transducer layer. The thickness of the polymer layer is also investigated. A thin layer may contain pinholes in the film. This will cause the electrodes to be directly exposed to the electrolyte and all current will skip the recognition elements on the polymer layer and go straight to the electrode. When the polymer layer is too thick it will have a high resistance making it difficult to measure impedimetrically. A layer thickness of 100 nm is an experimentally determined compromise.

2.2.2 Contact angle measurements

Contact angle measurements allow for surface characterization. The contact angle between a solvent and the investigated surface gives information on the hydrophobic/hydrophilic properties of the surface.

A solvent droplet is placed on a surface. The contact angle between the surface and the droplet can be monitored in time with a video camera and software can model this contact angle measurement [Figure 2-10]. [76].

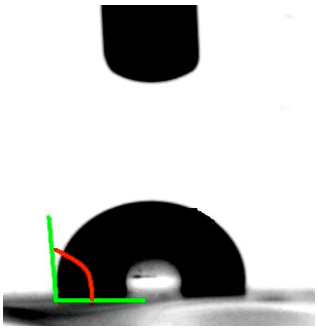

Figure 2-10: Solvent droplet on a surface and measuring of the contact angle.

When a droplet of water is placed on the surface, the change in hydrophilic/hydrophobic properties gives us information about the effect of certain surface treatments. As illustrated in Figure 2-11 a hydrophobic surface could repel an electrolyte solution, which has a negative impact on biosensing measurements.

Figure 2-11: Contact angle of a hydrophobic (left) and a hydrophilic (right) surface.

2.2.3 Atomic Force Microscopy

Atomic Force Microscopy (AFM) is a scanning probe technique for studying surface properties of materials from the atomic to the micron level. It has first been described in 1986 [77]. The operating principle is schematically drawn in Figure 2-12. A sharp tip, located at the end of a cantilever, probes the surface of a sample on a piezo-electric platform, allowing measurements in 3 dimensions. Atomic forces between the sample and this tip will cause the cantilever to bend. The movement of the cantilever and the tip is detected by an optical system consisting of a laser and photodiodes. The laser signal is focused to the

cantilever so that the photodiodes can measure the laser deflection, which is a measure for the forces acting between the sample and the tip [78].

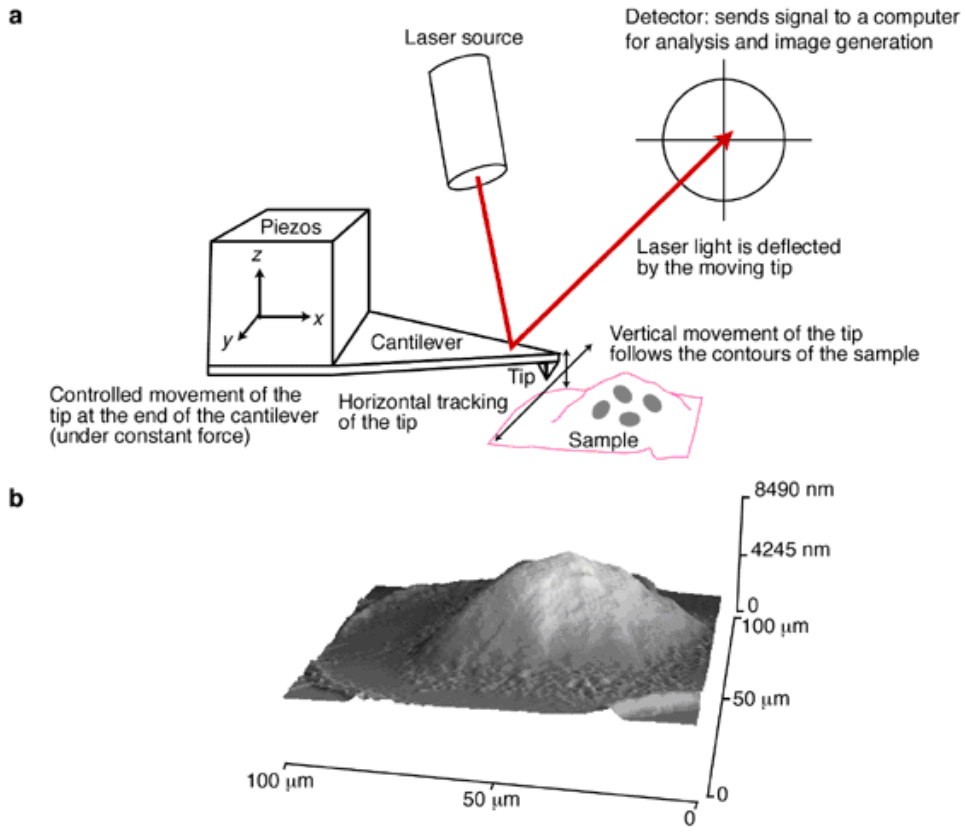

Figure 2-12: (a) Working principle of an atomic force microscope, (b) An example of the resulting three-dimensional image of the surface topography of the sample in (a). This AFM image was obtained in contact mode [79].

Regarding the interaction between sample and tip 3 different measuring modes can be distinguished. In "contact mode" the tip will slightly touch the surface to scan an (x,y) pattern. A constant deflection of the cantilever is maintained by continuously adjusting the Z position. A topographic image of the sample surface is obtained by plotting this Z position. Contact mode can be used in air and liquids but is less suitable for biological samples as the tip may damage the sample.

In "non-contact mode" (NC-AFM) a distance of several tens to hundreds of angstroms is maintained between tip and sample, where attractive van der Waals forces will act. Within this short distance, a tunneling current will flow between the tip and the sample surface. When this distance is decreased a higher tunneling current will be recorded. A feedback loop can then adjust the tip height in such a manner that the tunneling current will stabilize at its original value. In this way topographic images can be obtained with little or no contact between tip and sample.

A third method is "intermittent contact mode" (IC-AFM) or tapping mode. Just like non-contact mode it is also a "vibrating cantilever" mode but for IC-AFM the vibrating tip is brought close enough to the surface so that the tip can gently "tap" the substrate. Just like with NC-AFM the space between tip and sample changes the oscillation amplitude of the tip. Imaging these changes represents a topography image of the sample surface. Both non-contact and tapping mode are less likely to damage surfaces, making them both suitable for measuring biological samples. Tapping mode however is supposed to be more efficient for scanning larger areas of samples with more variation in topography.

AFM images have been acquired by a Veeco Dimension Microscope connected to a Nanoscope III Controller using Nanosensors probes (PPP-NCHR) with a diameter ranging from 5 to 10 nm.

2.3 Readout technique: Impedance Spectroscopy

With impedance spectroscopy (IS) the impedance is usually measured as a function of the frequency, by applying a known ac-voltage at a certain frequency and bias voltage and measuring the amplitude and phase shift of the resulting current. Doing so for an entire frequency range, a frequency spectrum can be obtained, which can provide a lot of information on the properties of the measured device.

Impedance spectroscopy can be used to determine an equivalent circuit that serves as a model of the electrical behavior of the sample. For this purpose the

impedance measured as function of the frequency can be represented by a Nyquist plot, as shown in Figure 2-13. The complex impedance Z consists of two parts, i.e. the real and imaginary part. In this figure Re{Z} is plotted against the negative of Im{Z}. The data can be represented as a vector with |Z| the length and ϕ the angle between the vector and the x-axis. Each point of the Nyquist plot -also called Cole Cole plot- corresponds to a fixed frequency f, but presenting data in a Nyquist plot looses information on the frequency. Note that $\omega=2\pi f$.

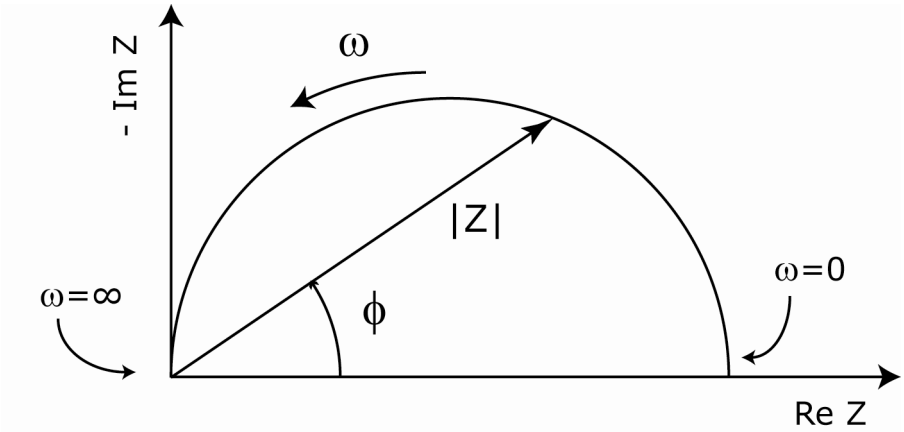

Figure 2-13: Nyquist plot.

$Z(\omega)$ can also be represented in a Bode plot as shown in Figure 2-14. In this figure the log(|Z|) and phase ϕ are plotted as function of log(f) [80].

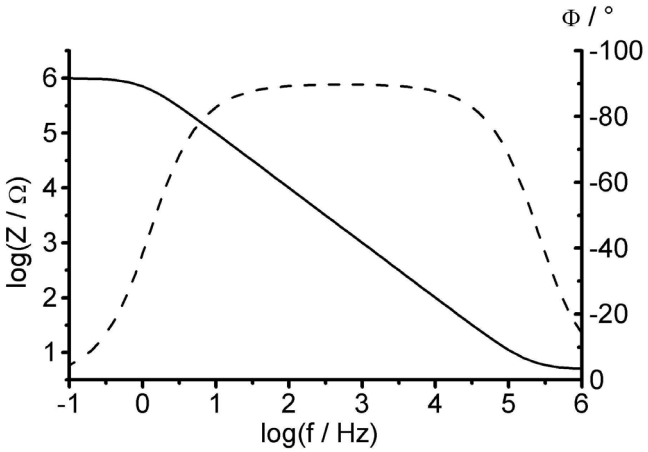

Figure 2-14: Bode plot.

For data interpretation these graphs are fitted with an equivalent circuit to model the impedance behavior. Elements in this circuit can be resistors, inductors, capacitors, constant phase elements… and one measurement can often be fitted with multiple circuits. The objective is to fit the data with the most useful circuit with the best correspondence to the system under study. This is a simple and realistic circuit in which the components have a physical meaning to the system.

Two parallel measuring contacts, like the coplanar electrodes, provide the capacitive behavior. The capacitance is partially determined by the dielectricum separating the two plates, being the polymer, hence the name C_p. Between these contacts is the polymer layer, which will have a resistance R_p when a current runs through it. Both components are parallel to each other. A simple model like this would look like Figure 2-15 (left) and the Nyquist plot would look exactly as in Figure 2-13.

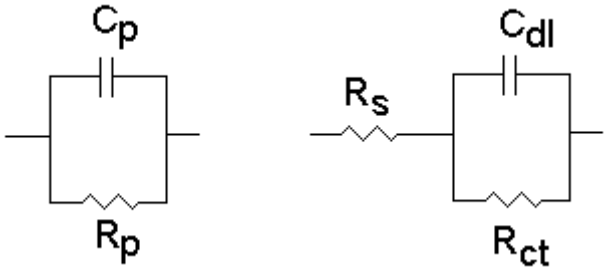

Figure 2-15: Simplified equivalent circuit (left) and the Randles cell (right).

Another model for fitting impedance measurements data (often used for electrolytes) is the Randles cell [81], as shown in Figure 2-15 (right). The main component of this model is the double layer capacity, C_{dl}. According to the Helmholtz model [81], this double layer is formed as ions from the solution "stick on" the electrode surface. Charges in the electrode are separated from the charges of these ions by an insulator and thus form a capacitor $C_{dl,}$ as shown in Figure 2-16, where Au is used as example. Au is a hole injector, thus positively charged, so negative ions in the electrolyte (or electrons in the polymer) will be attracted to the electrode surface. The separation is very small, in the order of Angstrøms.

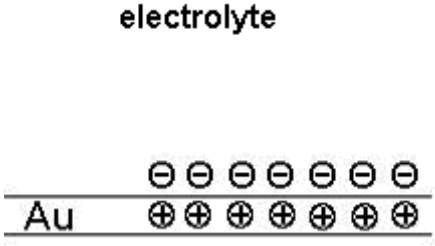

Figure 2-16: Schematic representation of the formation of a double layer capacity at the electrode, according to the Helmholtz model.

The charge transfer resistance R_{ct} of the electrolyte is formed by a single electrochemical reaction at equilibrium. When a metal substrate is placed in contact with an electrolyte the metal molecules can dissolve into the electrolyte. Electrons enter the metal, metal ions diffuse into the electrolyte and thus charge is being transferred. Another resistance is present in series with the other two

components. It represents the actual resistance of the electrolyte solution, R_s,. The total impedance of the Randlles cell can then be calculated using Eq. 2-1. When the frequency increases, Rs becomes of increasing importance in the total impedance. Therefore at high frequencies the resistive component of the electrolyte can be found. For information on the capacitive and resistive components of the interface data at low frequencies is relevant.

$$Z_{tot} = R_s + \frac{R_{ct}}{1+(\omega R_{ct} C_{dl})^2} - i\frac{\omega R_{ct}{}^2 C_{dl}}{1+(\omega R_{ct} C_{dl})^2} \qquad \textit{Eq. 2-1}$$

When impedance measurement data can be accurately fitted with the components of the Randles circuit (Figure 2-15 right), $-Z_{im}$ and Z_{real} can be calculated by Eq. 2.2 and Eq. 2.3. The Nyquist plot of this model is a semi-circle like in Figure 2-17.

$$Z_{real} = R_s + \frac{R_{ct}}{\omega^2 C_{dl}^2 R_{ct}^2 + 1}. \qquad \textit{Eq. 2-2}$$

$$Z_{im} = \frac{\omega\ C_{dl} R_{cp}^2}{\omega^2 C_{dl}^2 R_{ct}^2 + 1}. \qquad \textit{Eq. 2-3}$$

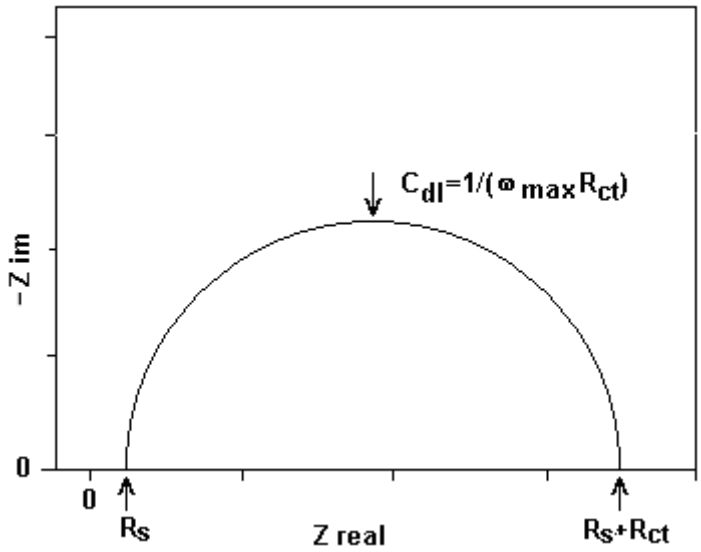

Figure 2-17: Nyquist plot of a Randles cell.

The minimum value of the two values where $Z_{im}=0$ corresponds to R_s. The maximum of both corresponds to R_s+R_{ct}. The maximum of Z_{Im} is reached at an angular frequency ω_{max}, which is determined from experimental data. With this value an average value of C_{dl} can be calculated using the relation (Eq. 2-3) below.

$$C_{dl} = \frac{1}{\omega_{\max} R_{ct}} . \qquad \textit{Eq. 2-4}$$

Although the Randles cell is a useful model in its own, it is often the starting point for more complex models, in which other elements might appear besides the elements discussed above. Table 2-1 gives different elements that can be used in modeling the sensor devices in this research.

Component	Symbol	Complex Impedance
Resistor	R	$Z = R$
Inductor	L	$Z = i\omega L$
Capacitor	C	$Z = \frac{1}{i\omega C}$
Constant Phase Element	CPE	$Z = \frac{1}{Q_0}(i\omega)^{-n}$
Warburg component	W	$Z = \frac{1}{Y_0}\omega^{-1/2}$

Table 2-1: Components for equivalent circuit fitting.

Capacitors in IS experiments often do not behave ideally. Instead, they act like a constant phase element (CPE) as defined in Table 2-1. The CPE takes into account semi-infinite diffusion, a kind of imperfect, leaking capacitor. The double layer has non-ideal behavior and the "double layer capacitor" in real cells therefore often behaves like such a CPE instead of like a capacitor. Diffusion can also create an impedance element known as the Warburg impedance. A Warburg element is a special type of CPE. As opposed to the CPE which accounts for semi-infinite diffusion, W accounts for a diffusion layer with an infinite thickness. At high frequencies the Warburg impedance is small since diffusing reactants do not have to move very far. At low frequencies the reactants have to diffuse further, thereby increasing the Warburg impedance. On a Nyquist plot the infinite Warburg impedance appears as a diagonal line with a slope of 0.5. On a Bode plot, the Warburg impedance exhibits a phase shift of 45°.

Possible models used for biosensors are illustrated in Figure 2-18. An R(QR)(QR) model is depicted used for impedimetric polymer-based immunosensor where measurements occur in a top-bottom electrode configuration [1]. The polymer is modeled with a constant phase element and a resistor in parallel. Next the

interface is modeled in the same way with a resistance and such a leaking capacitor in parallel. Thirdly a resistance is connected in series to account for the electrolyte resistance. For coplanar and interdigitated measurements the model could be expanded to the schematic drawing in Figure 2-19. However, in reality the interface and polymer elements are modeled in one semi-circle each, resulting again in the same model from Figure 2-18. Other models can also be used. For example, for coplanar measurements with IDE's the same elements can be used in a different circuit, containing two paths in parallel: one with the dielectric capacitance C_{di} of the solvent, and the path containing the resistance of the solution R_{sol} in series with the double layer capacitances C_{dl} at the electrodes [74]. One of the criteria for a good model is an accurate fit with the measured data. Secondly, the model needs to reproducible for other measurements. Finally, all components must have a physical meaning.

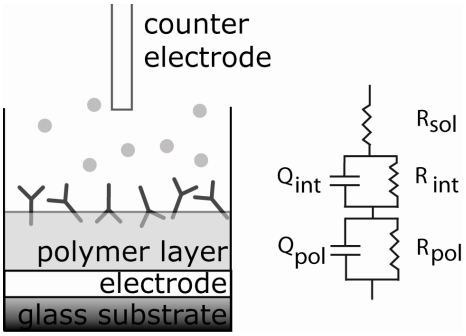

Figure 2-18: An R(QR)(QR)-model for a top-bottom electrode configuration.

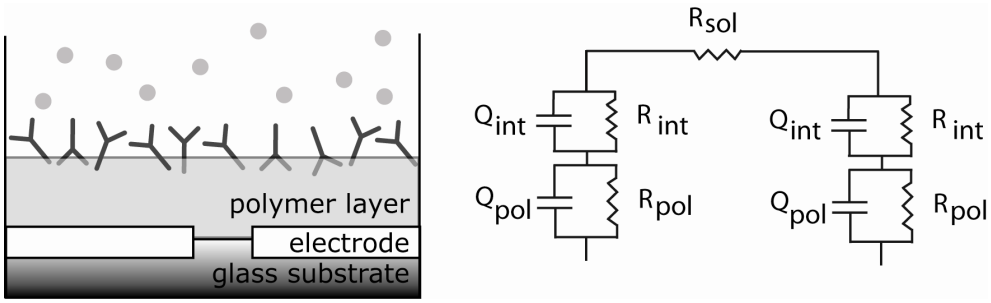

Figure 2-19: An adapted model for a coplanar electrode configuration.

Time-resolved analysis of the impedance spectra is performed in the low frequency range. At low frequencies the sensor is more sensitive for surface

interactions between the MIP binding sites or the IgG's on the one hand, the target molecules and the electrolyte on the other hand. It is found that upon binding, electrical changes occur at the interface [11]. The double layer at the electrode surface, which is reflected in the capacitive changes at the lower frequency range, affects the charge transfer from the electrolyte to the electrode. For each experiment an optimal frequency is chosen in this most useful frequency range, to obtain a maximal signal to noise ratio and stability.

Impedance Spectroscopy on immunosensors is performed using a HP 4194A Impedance/gain phase analyzer (Figure 2-20, left). Impedance is measured in a frequency range of 100 Hz-1 MHz with an oscillating voltage of 50 mV and zero bias voltage over 4 channels subsequently. The hardware is Labview steered and before each experiment an open circuit and a short circuit correction are performed. Impedance spectroscopy on MIP-based devices was performed using an Iviumstat electrochemical analyzer from Ivium Technologies B.V. (Figure 2-20 right). The frequency range for the Iviumstat is 10μHz to 2MHz and it offers a very stable signal at lower frequencies. For each sensing spot, spectra were measured sequentially in a low-frequency range from 1 Hz to 1 kHz, also with zero bias voltage and an oscillating voltage of 50 mV. Electrochemical Impedance Spectroscopy Analysis Software called ZSimpWin (Princeton Applied Research) is used for easy data processing and modeling data with equivalent circuits.

Figure 2-20: HP 4194A Impedance/gain phase analyzer (right) and an Iviumstat electrochemical analyzer (left).

3 An impedimetric immunosensor for the detection of histamine and tryptase

An immunosensor for the rapid and accurate detection of histamine and tryptase has been developed. For tryptase coplanar electrodes are coated with conjugated polymer and antibodies are immobilized on the polymer surface using physical adsorption. AFM and contact angle measurements confirm the electrode functionalization. The sensor detects the antigen impedimetrically. For the detection of the low-molecular weight antigen histamine (111 Da) Al interdigitated electrodes (IDE) are used for a direct impedimetric assay. In this chapter a proof-of-principle is established for direct detection of the low molecular weight molecule histamine. The most important findings of this chapter have also been described in Physicalia Magazine [82].

3.1 Sensor characterization

In this chapter the characterization of the biosensor focuses mainly on the immobilization of the antibodies onto the polymer surface. This is studied using contact angle measurements and AFM.

3.1.1 DEKTAK measurements

The thickness of the transducer layer is determined with a Dektak³ST. A scratch is induced into the polymer layer and the height difference between glass and polymer layer has been measured at 3 different places. This method has been repeated for a second sample. The results are shown in Table 3-1. With a 0.7 wt% PPV solution in chlorobenzene and spincoater settings as described in chapter 2, layer thicknesses of approximately 100 nm are obtained.

	Sample 1 (nm)	Sample 2 (nm)
Measurement 1	101.5	117.8
Measurement 2	105.4	114.5
Measurement 3	110.0	119.0
Sample average	105.6 ±4.4	117.1 ± 2.3
General average	**111.4 ± 8.1**	

Table 3-1: DEKTAK measurements of the thickness of the PPV film.

3.1.2 Contact angle measurements

3.1.2.1 Experimental set-up

Contact angle measurements are performed with a Dataphysics Instruments GmbH (Germany, Filderstadt) OCA 15 plus. A droplet of 1 μl distilled water is placed on a surface. This droplet is detected by the camera and the contact angle between the droplet image and the surface is fitted. Data are averaged over 5 measurements and taken after 10 seconds to ensure stabilization. The error bars obtained in this way indicate the stability of the contact angle between water and polymer surface in time.

3.1.2.2 Results & discussion

Firstly, the antibody adsorption is investigated. Different concentrations of antibodies have been incubated on the polymer samples. Each concentration is incubated at 37 °C during 1 h. For reference MDMO-PPV is measured incubated with the PBS buffer solution without IgG's. This sample represents a concentration of 0 nM. After one hour samples are rinsed in PBS (1x) and in demineralized water (2x). The contact angle is measured every second during 20 seconds. As placement of the droplet is performed manually data from the first few seconds might be affected by the speed and force applied by the user. Data are averaged from 15 to 20 seconds resulting in one value for the contact angle. 3 measurements are performed on each sample and averaged. The result of the contact angle measurements are shown in

Figure *3-1:* Graph (a) and fitting results (b) of the logistic relation between the physically adsorbed concentration of antibodies and the resulting surface contact angle.

. Upon increasing the concentration of antibodies the contact angle decreases systematically. After incubation with the zero concentration of antibodies, a polymer layer without biological activation is obtained with a contact angle of 102°. Due to this large contact angle, pure MDMO-PPV is a hydrophobic material. A polymer layer incubated with 100 pmol/ml antibodies against histamine has a contact angle of 72°. The hydrophobic surface has turned hydrophilic due to antibody incubation. The antibodies have physically adsorbed to the transducer layer successfully.

In Figure 3-1(a) at low and at high concentrations two saturated regimes can be seen. This is best described by a logistic fit (Figure 3-1 (b)). The logistic function is a sigmoid function, a mathematical function with an S-shape. The functional form of the sigmoid fit depends on the x-scale. For a linear scale the resembling Boltzmann function is used, while a logistic fit serves a logarithmic x-scale. In this equation A_1 is the highest saturation level, A_2 the lowest saturation level, x_0 represents the middle of the regression and ρ indicates how fast the evolution occurs between the two saturated regions. This logistic fit is often used for biological processes and growth models, but finds also applications in a range of fields. In medicine it can be used for the growth of a tumor. In ecology the logistic model is typically used for the population growth of a certain species. Applying this fit to the data in Figure 3-1(a) means x equals the concentration in pmol/ml and y represents the contact angle. The results of this fit are shown in the table in Figure 3-1(b). Saturated polymer surfaces for anti-histamine and anti-tryptase result in comparably low contact angles, as they are functionalized with comparable biomolecules. The logistic fit shows that saturation of incubated surfaces occurs at high concentrations of 100 pmol/ml.

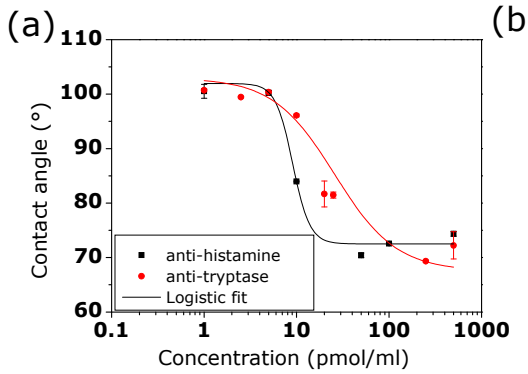

(b)

$$y = A_1 + \frac{A_1 - A_2}{1 + (\frac{x}{x_0})^{\rho}}$$

	anti-tryptase	anti-histamine
A1 (°)	103.0 ± 0.1	102.0 ± 0.7
A2 (°)	67.5 ± 0.4	72.5 ± 0.1
x_0 (pmol/ml)	26 ± 1	9.1 ± 0.2
ρ	1.31 ± 0.05	4.7 ± 0.7
R^2	0.98	0.99

Figure 3-1: Graph (a) and fitting results (b) of the logistic relation between the physically adsorbed concentration of antibodies and the resulting surface contact angle.

Secondly, the incubation time has also been optimized experimentally for times of approximately one hour. Samples have been incubated with 100 pmol/ml antihistamine for different times. Data are averaged from 15 to 20 seconds resulting in one value for the contact angle. 3 measurements are performed on each sample and averaged, for obtaining error bars. The results of the contact angle measurements are shown in Figure 3-2. After one hour the contact angle has sharply dropped and the surface has turned hydrophilic, indicating a successful adsorption of the antibodies. Longer incubation times do not decrease the contact angle any further. Even more, a slight increase is noticeable when antibodies are incubated longer than one hour. The adsorption process reaches a maximum after one hour, when the surface is saturated with antibodies.

The iso-electric point (pI) depends on the type of immunoglobulin. Monoclonal IgA's have an iso-electric point between 4.5 and 6.5, monoclonal IgG's have an iso-electric point between 7-9.5. Now the pH of the environment determines the actual charge of a protein. Because the pH of the buffer solution, at a pH of 7, is lower than the pI of the antibody, the antibody will absorb more protons from the solution and become positively charged. Once the surface is saturated, no new antibodies will absorb onto this layer because all IgG's are identically positively charged, causing them to retract each other. Therefore the functionalization process stabilizes after approximately one hour.

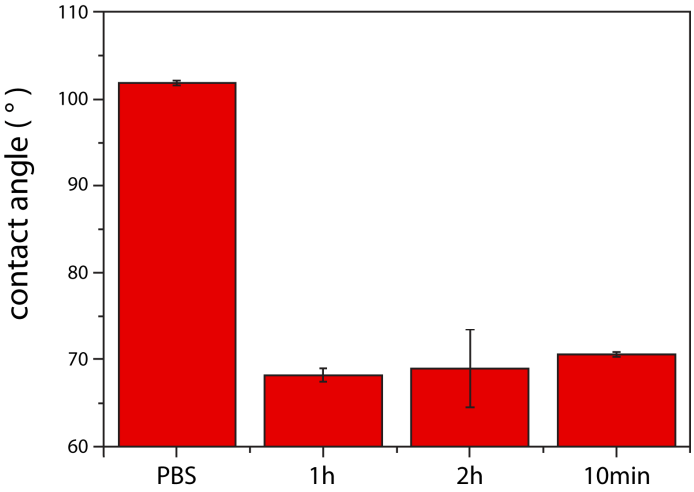

Figure 3-2: Effect of incubation time of antihistamine antibodies on the surface saturation.

Thirdly, the stability of these saturated antibody layers in a sensor setup is under investigation. When these functionalized surfaces are used as sensors they are placed in a small volume of buffer solution for varying times, depending on the stabilization period of the sensor and the number of measurements. The effect of this buffer solution on the functionalization of the surface is investigated. In the following, polymer samples have always been incubated with 100 pmol/ml antibodies against histamine (labeled aHis) for one hour, as these parameters have been previously optimized. Afterwards, samples have then been exposed to PBS for increasing amounts of time. Contact angle measurements have subsequently been performed and the results are shown in Figure 3-3.

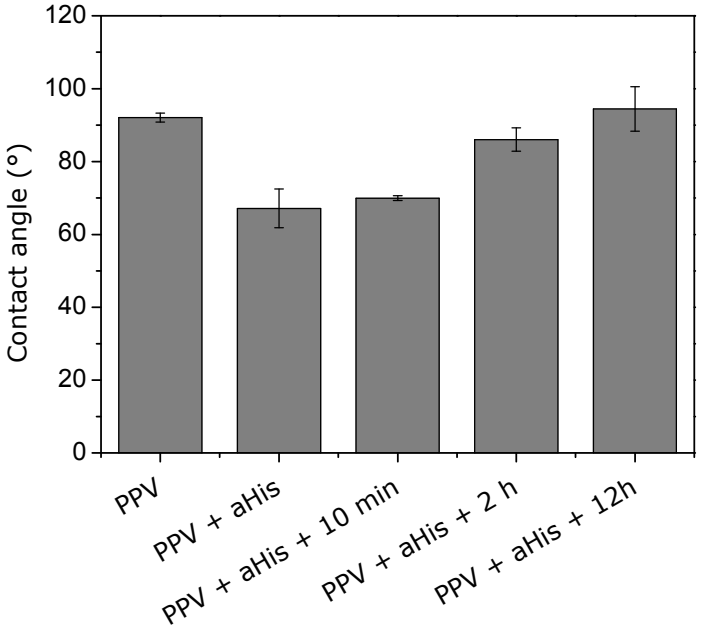

Figure 3-3: Influence of PBS on physically adsorbed antibodies.

Normally incubated samples confirm that hydrophobic polymer turns hydrophilic due to antibody adsorption. After 2 hours, however, the contact angle increases to (86±3)° indicating that the polymer surface is turning hydrophilic again. PBS has the possibility of breaking the weak bonds of the immunoglobulines to the polymer. Antibodies are washed away in presence of PBS and are no longer absorbed to the polymer. The surface tends to be hydrophobic again. On the other hand the increasing contact angle may also be due to an additional effect, caused by degradation of the polymer film. These measurements confirm the slightly increasing contact angle noticeable in Figure 3-2. At this moment, from these measurements, it is not possible to draw any conclusion. However, it can be assumed that the antibodies are no longer immobilized onto the polymer layer. Another option is the destabilization of the polymer layer itself.

During preparation of the samples for sensing purposes, they are blown dry with a N_2 nozzle. The effect of this strong airflow on the weak physical adsorption of the immunoglobulines has also been tested. Polymer samples have been

incubated with 100 pmol/ml antibodies for tryptase (labeled 'aTryp'). These samples have been air dried while one sample has been blown dry. The results of contact angle measurements are shown Figure 3-4.

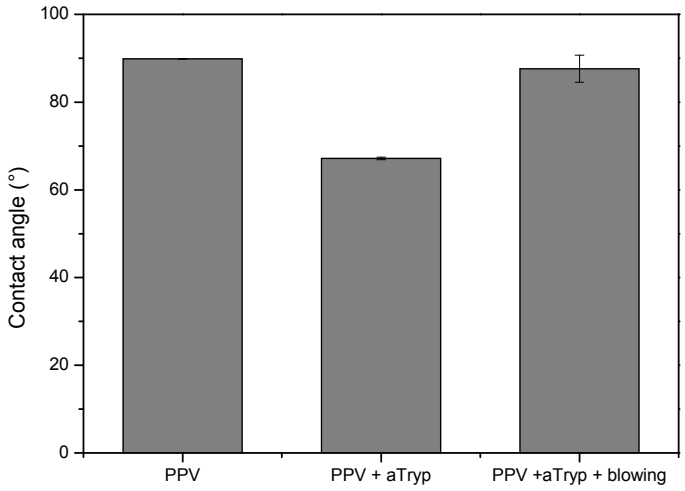

Figure 3-4: Influence of air flow on physically absorbed antibodies.

Again it is seen that a hydrophilic polymer surface turns hydrophobic upon successful immobilization of 100 pmol/ml antibodies for tryptase. The contact angle is decreased below 70°. Blow-drying the samples however results in increased contact angles, comparable to the hydrophilic surfaces before antibody incubation. After blow-drying, the antibodies are no longer present at the surface. This result shows that the sensor preparation influences the performance of the sample, which is a major disadvantage of immobilization by means of physical absorption.

Due to the weak binding mechanism of physical adsorption, these types of sensor samples thus have a short lifetime in biosensing applications. Possible alternatives could be the covalent binding of the immunoglobulines to the polymer surface. Covalent attachment of DNA to diamond has already been established [2, 83, 84, 85]. Current research focuses on covalent attachment of antibodies to diamond and polymers. Nowadays, a new generation of click-

chemistry polymers opened an alternative route and publications on the first results of this method are under preparation. They will also be the topic of following chapters.

3.1.3 AFM

Atomic Force Microscopy is a surface analytical technique used to observe an characterize surfaces of the sensor substrates.

3.1.3.1 Experimental setup

For biological samples little or no contact between tip and sample is desired, as this may damage the soft sample. Therefore, the measurements discussed here are performed in non-contact mode.

3.1.3.2 Results and discussion

Firstly, it is investigated how the surface is functionalized with antibodies The samples have been studied by AFM. The resulting images of 1 x 1 μm are shown in Figure 3-5. A polymer layer incubated during 1 hour with PBS, the "zero concentration", is shown on the left for reference. The sample in the middle is incubated with 100 pmol/ml antibodies for tryptase and the one on the right is incubated with the same concentration of antibodies for histamine. By comparing these samples with the reference sample on the left, one can clearly notice the presence of these antibodies. In the height profile of the incubated samples, peaks can be seen with a height difference of 5 nm, in correspondence with the 10 nm diameter of an antibody. These height peaks are most noticeable in the height profile of the sample with antibodies against tryptase in the middle. The height profile of the reference sample, on the left, has a maximum height peak of only 2 nm.

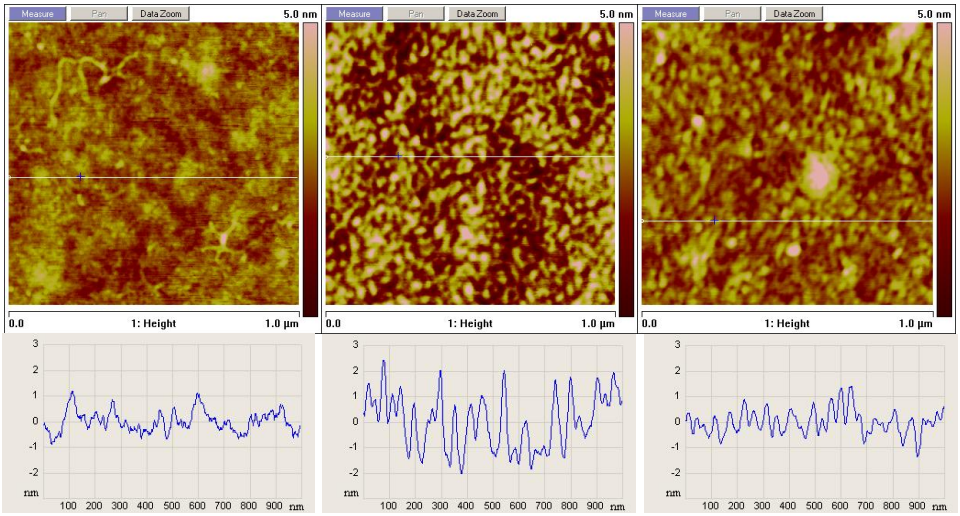

Figure 3-5: AFM images of antibody immobilization on PPV layers. Left: PBS without antibodies, middle: 100 pmol/ml antibodies for tryptase, right: 100 pmol/ml antibodies for histamine.

Secondly, the stability of these functionalized surfaces in a sensor setup is investigated with AFM. Contact angle measurements indicated problems with the physically absorbed antibodies when samples are placed in a PBS buffer solution for certain periods of time. The samples have been investigated using AFM. Results are shown in Figure 3-6. Samples were incubated with antihistamine antibodies according to the experimentally established protocol. Next they have been placed in a PBS solution for respectively 2 and 12 hours. A polymer surface with 100 pmol/ml antihistamine antibodies is measured as a reference to these samples.

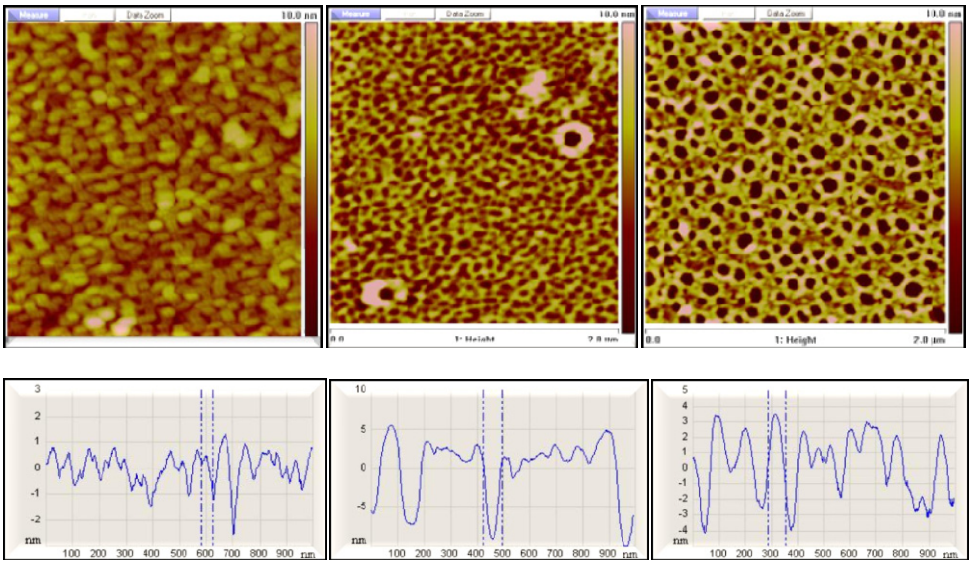

Figure 3-6: AFM images and corresponding height profile of PPV incubated with 100 pmol/ml and treated with PBS for 0 minutes (left), 2 hours (middle) and 12 hours (right).

After 2 hours small deviations in surface topography appear compared to the reference sample. After 12 hours large topographical differences can be seen. Ring shaped structures appear at the surface of the polymer. It is now clearly seen that not only the physically absorbed antibodies are removed but also the polymer is negatively affected by the presence of PBS during biosensing experiments.

3.2 Impedimetric readout of the tryptase sensor

To translate the biological recognition occurring between tryptase and anti-tryptase at the polymer surface directly into an electrical signal, impedance spectroscopy is performed.

3.2.1 Experimental setup

Electrochemical Impedance Spectroscopy (EIS) is used for the electronic readout of the sensors. An addition setup is used as has been extensively described in

section 2.1.5. Four channels are measured simultaneously. Impedance is measured at room temperature with a HP 4194A impedance/gain phase analyzer in a frequency range of 100 Hz - 1 MHz with an oscillating voltage of 50 mV over 4 channels subsequently. The hardware is Labview steered and before each experiment an open circuit and a short circuit correction are performed. Relative signals shown in time-resolved impedance spectra are normalized by dividing them with a value prior to addition.

3.2.2 Results & discussion

For the impedimetric detection of tryptase, coplanar electrodes made of TiN were used, and covered with a polymer layer. One polymer-based electrode is biologically activated with antibodies for the specific antigen tryptase, as described above. This is measured simultaneously with a reference polymer electrode without IgG coating and one bare TiN electrode. For this measurement the addition setup is filled with PBS to simulate a biological environment. After a stabilization period of 2 hours 100 pmol/ml tryptase is added to the sensor. Impedance data, shown in the time resolved impedance graph, at 312 Hz, are normalized relative to their initial impedance value, several minutes prior to the addition of the target molecule. The resulting value is referred to as the relative impedance signal and it is shown in Figure 3-7. After addition of 100 pmol/ml tryptase the impedance of all channels drops. Tryptase is dissolved in a solution with a high NaCl concentration (1 mol/l). The addition of these extra ions creates more charge carriers, resulting in an impedance drop for all channels. However, the impedance drop varies for each channel. The anti-Tryp channel 1 has the highest drop of approximately 38%, while PPV and anti-Tryp 2 decrease only 20% and TiN only 13%. The specific binding of antitryptase to the newly introduced tryptase molecules causes the Anti-Tryp 1 channel to decrease more than the PPV channel. The decrease of channel Anti-Tryp 2 is similar to PPV, making it seem like all the antibodies are washed off from this channel, hence no specific binding is possible.

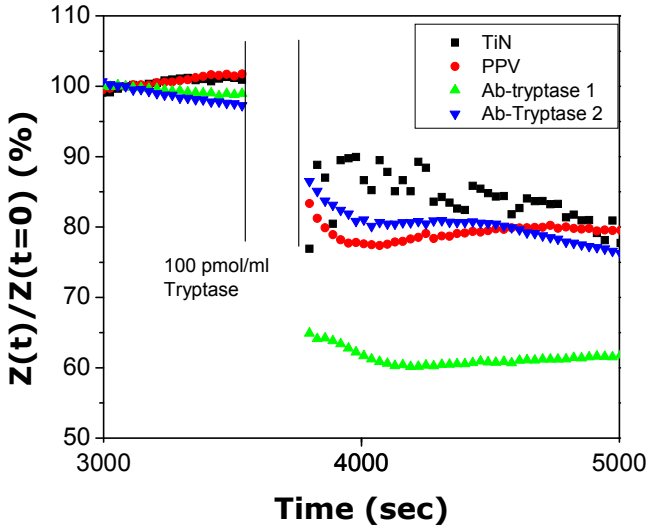

Figure 3-7: Relative impedance signal as function of time during the addition of 100 pmol/ml tryptase.

To get more insight in the processes that occur in the sensor, the Bode plots are shown in the following figures. In a Bode plot both the amplitude and the phase of the channels are logarithmically shown as a function of frequency. Now the entire frequency spectrum can be seen. For each channel the Bode plots before and after the addition of target molecule are compared to investigate which changes happen within the sensor.

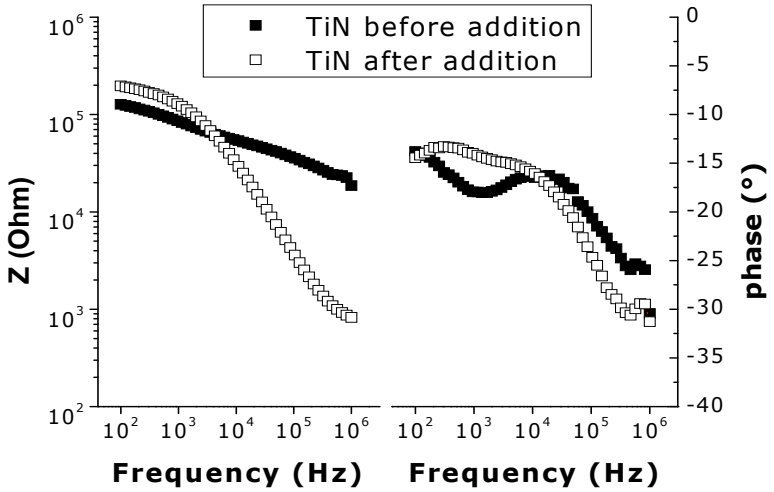

Figure 3-8: Bode plot of a TiN electrode before and after the addition of tryptase.

The TiN channel in Figure 3-8 shows a resistive impedance spectrum as the impedance does not vary much with the frequency. After addition of the tryptase its impedance decreases with increasing frequency. The impedance of the TiN channel is frequency dependent and shows capacitive behavior. Unspecific binding of the tryptase molecules at the electrode surface may occur. This bound tryptase enhances the double layer at the electrode, which provides the capacitive characteristics.

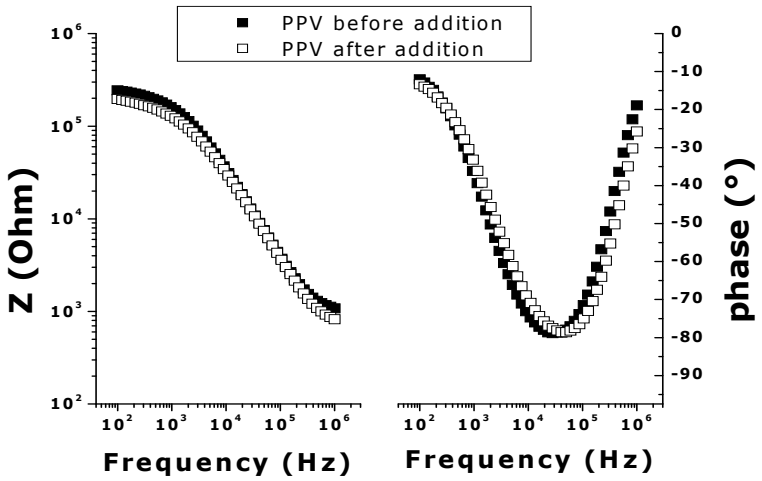

Figure 3-9: Bode plot of a PPV covered electrode before and after the addition of tryptase.

Firstly, non-specific adsorption is discussed. Therefore the TiN electrode covered with a PPV film is shown in Figure 3-9. Due to the polymer film on the electrode the Bode plot shows a capacitive behavior, meaning that the phase is near to the characteristic -90° for capacitors. After addition the phase does not change. However, a slight decrease in impedance can be noticed at low frequencies due to unspecific adsorption of tryptase, which will absorb onto the polymer layer. Also at high frequencies a decreased impedance is measured. The addition of the buffer solution, which contains the tryptase molecules, induces more extra ions and thus more free charge carriers. This decreases the resistance of the electrolyte, which is what is measured in the high frequency range.

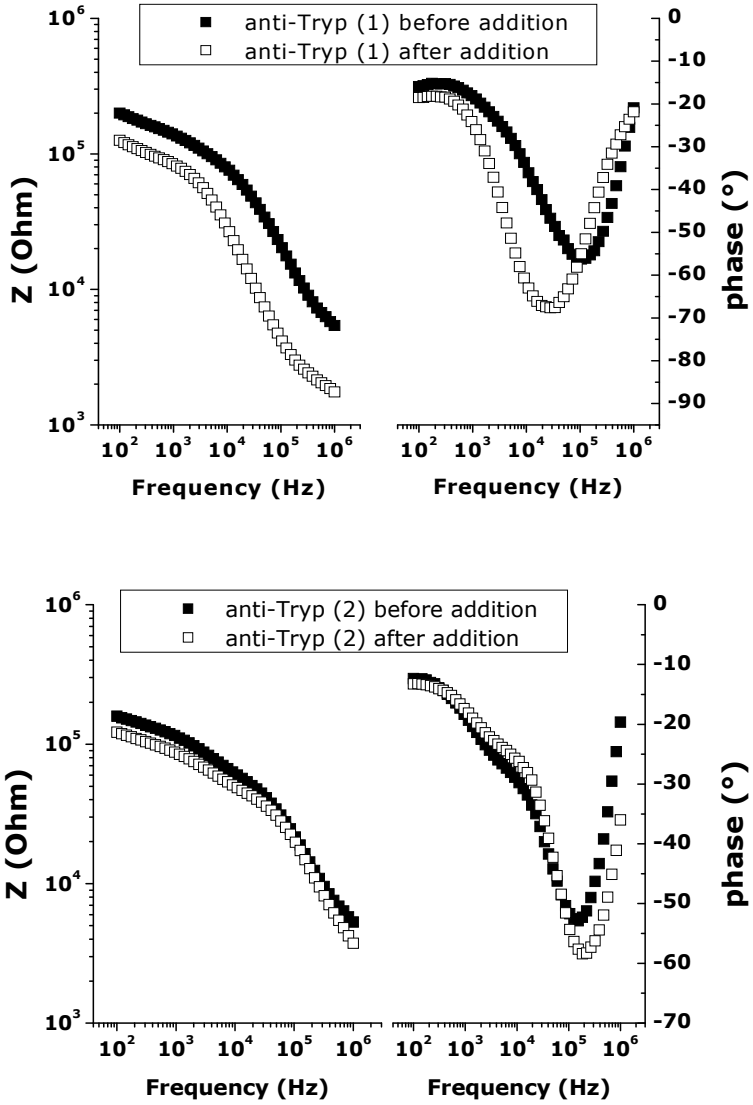

Figure 3-10: Bode plots of two polymer electrodes functionalized with antibodies for tryptase, labeled (1) and (2).

The two polymer channels functionalized with antibodies against tryptase are presented with a Bode plot as well in Figure 3-10. Two channels are functionalized in the same manner for testing reproducibility. The first antibody functionalized channel 'anti-Tryp (1)' shows a similar Bode plot to the PPV Bode

plot. The capacitive behavior only shows a smaller phase angle of 55°, which is 25° less than the phase angle of the polymer channel, see Figure 3-9. After addition of tryptase its capacitive behavior remains, however the impedance has dropped significantly over the entire frequency spectrum. Addition of tryptase also decreases the phase angle by 25°, meaning it is now more capacitive than before the addition of tryptase.

Although initially it appeared as if the second functionalized channel 'anti-Tryp(2)' resembles the polymer channel more than the first functionalized channel, the Bode plots show that its behavior is indeed similar to the other functionalized channel, only less prominent. The phase angle is also 35° smaller than the phase of the PPV channel. After addition of tryptase the impedance decreases in the same order of magnitude as the PPV channel. However, the Bode plot shows that the phase angle has qualitatively decreased in the same way as the 'anti-Tryp (1)' channel, but with a minor decrease of 8° as opposed to the 25° of the other functionalized channel. It needs to be pointed out that the phase angle of the non-functionalized polymer layer does not change due to the addition of tryptase. Sensitivity is sample-dependent, which makes it difficult to obtain a dose-response curve.

For the functionalized channel 'anti-Tryp (1)' and the reference channel the Nyquist plots are shown in Figure 3-11, before and after addition of tryptase. These show the negative imaginary part of the impedance (-Im(Z)) versus the real part of the impedance (Re(Z)). This type of plots allows for the easy modeling of the measured data with an equivalent electrical circuit. ZSimpWin, as described in section 2.3, can perform the calculations on this type of data. A number of equivalent circuits may fit, however it is objective to find the most appropriate one in which al components have a physical meaning. This way the different behavior of a polymer electrode and a polymer electrode functionalized with antibodies can be explained.

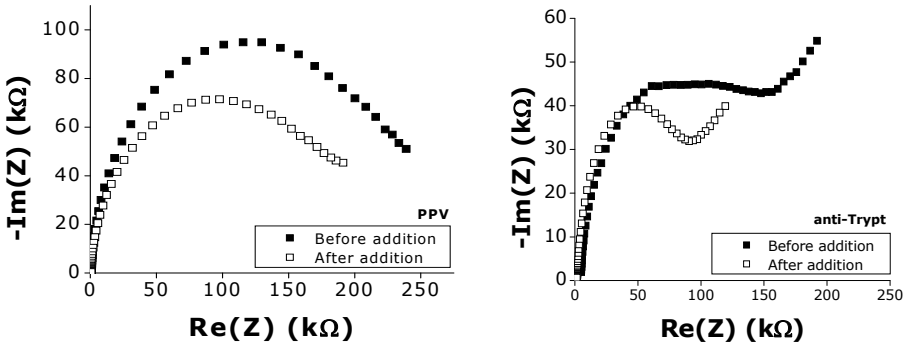

Figure 3-11: Nyquist plot for PPV (left) and the channel functionalized with tryptase antibodies (right), before and after the addition of tryptase.

The polymer coated electrode without antibodies is best fit with the electrical circuit shown in Figure 3-12. This RQ(RQ) circuit consists of a resistor in series with a constant phase element Q and a parallel block of again a resistor and a Q. In this model R_{sol} is the resistance of the solution, Q_{int} is the double layer capacitance of the interface between the polymer and the electrolyte. The third block represents the polymer, which is best represented by a resistor and a capacitor in parallel for the respective resistance and capacitance of the polymer layer.

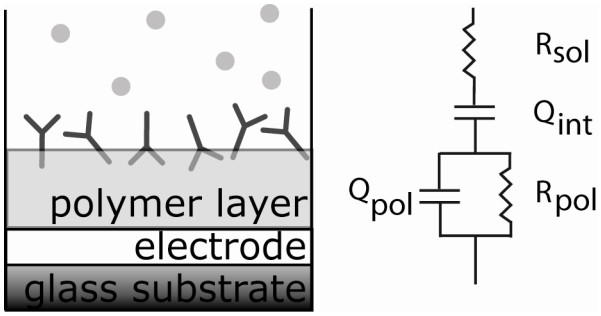

Figure 3-12: Equivalent circuit RQ(RQ).

The fitting results are shown in Table 3-2. χ^2-values of 3.58×10^{-3} and 5.62×10^{-3} are obtained for the fits of the PPV Nyquist plots before and after the addition of tryptase. The parameter α is dependent on how much the CPE

resembles a normal capacitance. The fact that α hardly varies before and after antigen binding allows comparing the different values of Q_{int} directly.

RQ(RQ)	Before	After	Difference (%)
R_{sol} (Ω)	967	669.2	**-30.8**
Q_{int} (nS.s$^{\alpha}$)	96.4	111	**15.3**
α	0.8281	0.8029	**-3.0**
R_{pol}(Ω)	2.08 E+05	1.59 E+04	**-92.3**
Q_{pol}((S/cm).s^{n})	8.28 E-10	1.03 E-09	**24.2**
n	0.9543	0.9399	**-1.5**
χ^2	3.58 E-03	5.62 E-03	

Table 3-2: Fitted results for the PPV electrode.

Firstly, the resistance of the solution R_{sol} decreases significantly, due to the extra charge carriers that are introduced in the electrolyte when a high concentration of antigen solution is added. Secondly the double layer at the interface increases. This is caused by the non-specific binding of target molecules at the polymer surface. Hereby the dielectrical constant decreases from ε=81 for water to ε=2 for proteins. The dielectric constant is directly proportional to the capacitance, which then also decreases. However, an increase is observed. This can be explained by a change in active surface. By non-specific adsorption of molecules to the polymer film, the coating will have a increased roughness. This will increase the dielectric constant of the double layer capacitor that is formed at the electrode. Thirdly the effect of the polymer layer is discussed. The capacitance of the polymer increases while the resistance decreases. Adsorption of PBS molecules into the polymer layer may be a possible explanation.

The Nyquist plot of the functionalized electrode from Figure 3-11 (right) is also fitted with the RQ(RQ) circuit from Figure 3-12. The fitting results are displayed in Table 3-3. The functionalized electrode also measures a decrease in resistance of the solution, R_{sol}, like the PPV electrode. The interface capacitor increases by 35.5%, which is 20% more than the interface of the non-functionalized PPV electrode. This may be attributed to the specific binding of the tryptase molecules to their antibodies. The n-value of a constant phase element has a value between 0 and 1 and is a measure for the roughness of the surface. The PPV electrode has a n~0.8 while the functionalized electrode has an n~0.5. This value is 0.3 lower, indicating the functionalized electrode has a more rough

surface. This can be explained by the presence of antibodies on this electrode. Also the PPV channel showed a decrease in n-value after addition of tryptase. Non-specific binding of tryptase to the polymer will make the interface less smooth. The functionalized electrode, however, shows an increase in n-value of the constant phase element that represents the interface layer. Finally the polymer layer's Q remains rather constant, while the resistance of the polymer decreases. As antibodies are present at the surface, they inhibit the non-specific adsorption of tryptase molecules and the entering of Na and Cl ions from the PBS solution into the polymer matrix. Another explanation could be that the polymer suffers swelling. All the holes in the matrix are now filled with conducting ions, decreasing the polymers resistance. This would also explain the increased n-value as the polymer has swollen and now has a smooth surface.

RQ(RQ)	Before	After	Difference (%)
R_{sol} (□)	3667	1448	-60.5
Q_{int} (nS.s□)	364	493	35.5
□	0.519	0.5544	6.8
R_{pol}(□)	1.15 E+05	7.56 E+04	-34.1
Q_{pol}((S/cm).s^n)	1.05 E-09	1.03 E-09	-2.3
n	0.8216	0.9567	16.4
□²	6.07 E-03	1.35 E-03	

Table 3-3: Fitted results for the functionalized electrode.

For sensor purposes the main interest goes out to information about binding events happening at the interface. As treated earlier for the Randles cell using Eq. 2-1, by looking at the impedance formula of the circuit, the frequency behavior can be further analyzed. At high frequencies the signal contains all information of the electrolyte. However data from the low frequency range contains the most information about the interface layer, which is where the binding events take place. Capacitive changes, due to the binding of the analyte to the antibody, are the most noticeable at these low frequencies. Hence a low frequency can now be chosen for displaying time resolved impedance analysis.

Unfortunately it is not always possible to apply the model from Figure 3-12 to all channels. Sometimes extra components are required in the model to obtain reasonable fits. A resistance (R_{int}) may be placed in parallel with the Q_{int} for better modeling of the double layer at the interface. A Warburg element (W_{ID}) may be added at the polymer layer which accounts for ion diffusion.

As most changes related to the specific binding events occur at low frequencies, another tryptase measurement occurs at a low frequency. This way, molecular recognition is most obviously. In this most useful frequency range a frequency of 211 Hz was chosen for its optimal signal to noise ratio and stability. The time-resolved measurement is shown in Figure 3-13, in which the low frequency change is now plotted as a function of time. The data is represented relative to the initial values (Z_0) of each channel: Relative Z (%)=Z/Z_0. The polymer electrode with tryptase antibodies shows a 10% response, while the bare polymer reference electrode remains constant. It can now quickly be concluded from a measurement that the sensor is capable of detecting the tryptase molecule and relating this to a measureable signal, simply by looking at one low frequency.

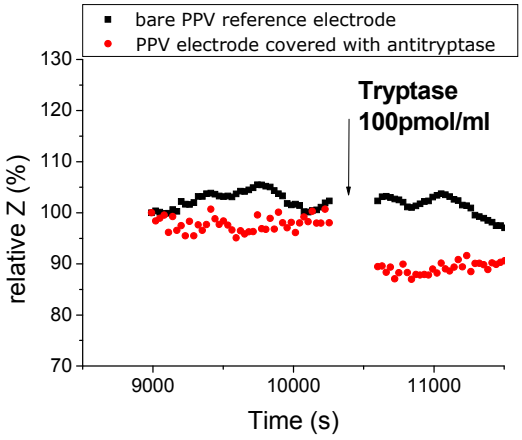

Figure 3-13: Impedimetric detection of tryptase at 211 Hz.

The detected concentration of 100 pmol/ml tryptase corresponds to physiologically relevant concentrations.

3.3 Impedimetric read-out of the histamine sensor

As opposed to tryptase, histamine is very difficult to be impedimetrically detected via a direct assay due to its small size. Several attempts with the

tryptase sensor set-up, using coplanar electrodes, remained unsuccessful for the detection of histamine in an impedimetric way. Possible solutions for the detection of low-molecular weight antigens, such as histamine, involve a competition assay, detected with e.g. enzyme immunoassay [86,87]. In this work, however, the first steps are made towards the direct impedimetric detection: the small molecules are outsmarted by downsizing the electrodes.

3.3.1 Experimental setup

Using interdigital electrodes with a reduced interspace of 25 μm an electrical field is created closer to the surface, as schematically represented in Figure 2-3. This way, electrical changes in the immediate neighborhood of the electrodes can be measured. The measurement data contain more information on the electrical changes at the interface, which is where the actual molecular recognition takes place and the buffer solution contributes less to the sensor signal. A thorough analysis and characterization of a palladium (Pd) IDE has already been developed, demonstrating its bulk-insensitive behavior in KCl solutions [73]. Gold (Au) IDE's have also been used in an impedimetric immunosensor [88], as well as titanium (Ti) IDE's [74]. In this experiment IDE's made of aluminum (Al) are used for the first time for the direct detection of a low-molecular weight antigen.

IDE's are used in the same setup as the tryptase measurement for the impedimetric detection of the low-molecular weight antigen histamine.

3.3.2 Results & Discussion

Al IDE's are used for the impedimetric detection of histamine with an immunosensor. One electrode is bare Al (name: Al), one is covered with PPV but non-functionalized (name: Al-PPV). The 2 remaining electrodes are both functionalized by immobilizing antibodies for histamine on the PPV layer (name: Al – PPV - anti-Hist). With these 2 identical channels can be monitored if both channels behave in the same way. The sensor stabilizes for half an hour, after which 50 nmol/ml is added to the sensor. The Bode plots of this experiment are

shown in Figure 3-14. For each channel the Bode plot before and after addition are matched on the graph for clearly noticing the differences.

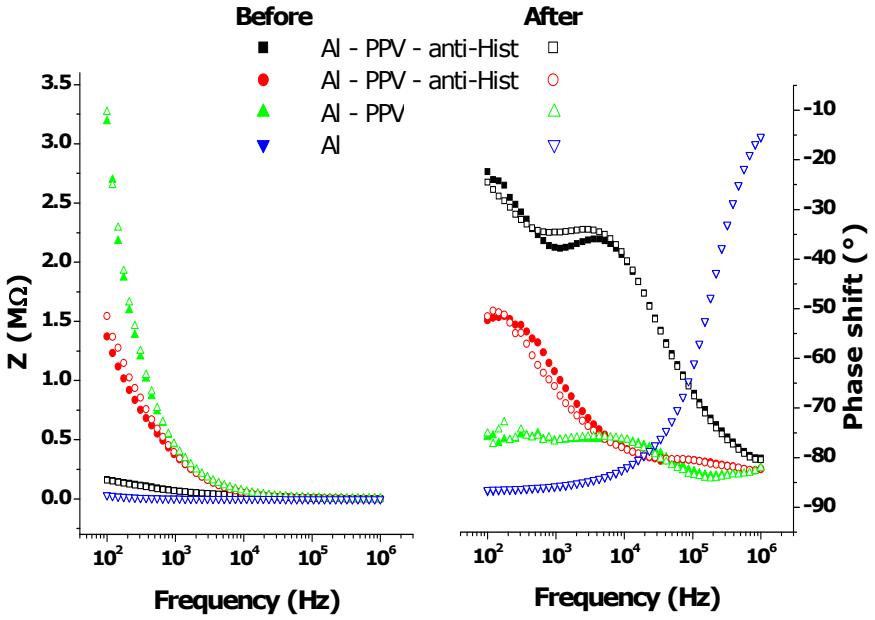

Figure 3-14: Bode plots for histamine addition.

For the Al channel the amplitude of the impedance does not change after addition of histamine, compared to the signal before addition. Also the phase remains similar. The same can be said about the PPV channel. It can be said that histamine does not absorb to Al, nor to Al coated with PPV. For the channels functionalized with anti-histamines the first channel (squares) shows a rather strange behavior. One assumption can be that the PPV film is unstable on this electrode. This channel is therefore no longer under investigation. The focus goes to the second functionalized channel (Al – PPV - anti-Hist, circles), that shows a difference in impedance signal before and after addition. Both the phase shift and the amplitude differ at low frequencies. The amplitude of the impedance increases, meaning that the capacitance of the interface decreases. The binding of histamine to the antibodies may increase the double layer at the interface. When the distance of the double layer is increased the capacitance decreases, according to Eq. 3-1, in which C is the capacitance of a capacitor, A is

the surface of the two parallel plates, d is the distance between the parallel plates and ε permittivity of the dielectricum between the parallel plates. This decreased capacitance causes an increase in the impedance, as described with Eq. *3-2*, where i is the imaginary unit and ω is the angular velocity of the sinusoidal signal.

$$C = \varepsilon \frac{A}{d} \qquad \textit{Eq. 3-1}$$

$$Z = \frac{1}{i\omega C} \qquad \textit{Eq. 3-2}$$

Nyquist plots could teach us which equivalent electrical circuit would best fit this sensor and modeling of the data with this circuit could show us many things. Unfortunately it is very difficult to obtain reliable and meaningful Nyquist plots, due to bad signal-to-noise ratio. Repeated attempts could not improve the signal. Nevertheless it is clear that the changes in response to histamine all occur at low frequencies. One of these frequencies is chosen for monitoring the amplitude of the sensor channels in time.

Time-resolved impedance analysis is done at a frequency of 211 Hz. Due to noise, data need to be filtered with a moving average filter of 20 data points. When histamine is added to the sensor, a concentration of 50 pmol/ml is obtained. After stabilizing for half an hour, the activated IDE changes 10% (Figure 3-15). Apart from the signal drift, the bare polymer reference IDE remains constant after addition of the antigen.

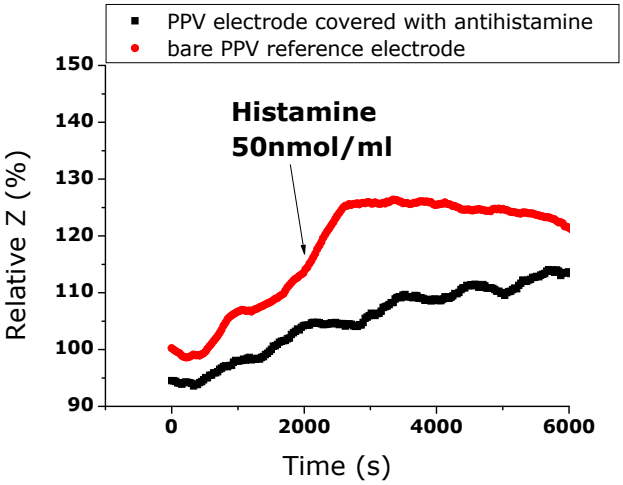

Figure 3-15: Impedimetric detection of histamine at 211 Hz.

Histamine concentrations in patients are about 200 pmol/ml. The high histamine concentration of 50 nmol/ml provides a good proof-of-principle for direct impedimetric detection of low-molecular weight antigens. Measuring conditions are not further optimized for estimating and decreasing the limit of detection, as meanwhile promising new materials have become available, which will be discussed in the following chapters.

3.4 Conclusion

In this chapter prototype immunosensors are developed for two target molecules, tryptase and histamine. Antibodies for tryptase and histamine were successfully immobilized on polymer-based electrodes. Physical adsorption of 100 pmol/ml antibody solution creates a saturated monomolecular surface. Higher concentrations do not lead to a better covered surface. This is a fast and easy way to build a recognition layer. The immunosensor shows a 10% response to 100 pmol/ml tryptase. The low-molecular weight molecule histamine was, for the first time, impedimetrically detected with a direct assay by using IDE's. The detection of 50 nmol/ml target molecules by their antibodies caused a 10% increase in impedance. IDE's are proven to be beneficial for use in future

electronic sensing of tryptase and histamine. However, there were reproducibility problems with the immunosensors due to bad adhesion of the antibodies to the polymer transducer layer. In future work, as described in chapter 4 and 5, a chemical recognition, based on molecularly imprinted polymers (MIP's), will replace the instable biological recognition layer. This chemical recognition element is developed for the low-molecular weight molecule histamine, which is equally useful as tryptase in IBS diagnostics.

4 A MIP based biomimetic sensor for the detection of histamine

The most important findings have been submitted to Biosensors & Bioelectronics [75].

As explained in the introductory chapter, existing sensing systems based on biological recognition elements have restrictions limiting their use. A biological recognition element is not always available for the desired target. Furthermore they are instable in organic solvents, at high temperature or changing pH. A chemical recognition element can be more inert and stable in a wide range of conditions such as temperature, pH or ionic strength [5].

Molecularly Imprinted Polymers (MIPs) are synthetic receptors which exhibit similar specificity and selectivity to the desired target molecules as their natural antibodies or enzymes [5-8]. Substituting the biological recognition element by a chemical one opens perspectives for applications in harsh environments. For application of the sensor in body fluids a chemical recognition element is necessary to withstand the acidic environments of fluids in which histamine occurs, such as stomach fluids, bowel fluids and saliva. Hence, a histamine sensor also requires such a chemical recognition element. MIPS are supposed to withstand a wide range of pH conditions.

In this chapter, a MIP is developed by the Organic & Polymeric chemistry group of Hasselt University. The MIP is synthesized as described in the materials & methods chapter in section 2.1.4. First the MIP has been characterized by UV-VIS (section 4.1). The MIP with the best result is then used for implementation in 2 sensor platforms. The first setup is based on the principle of quartz crystal microbalance (QCM) and it gravimetrically detects the target in the micromolar range (section 4.2). Secondly, impedance spectroscopy makes it possible to detect the target in the nanomolar range (section 4.3). This way the binding events of the MIPs can be monitored over a large concentration range.

4.1 Sensor characterization by UV-VIS spectroscopy

The content of this section is the result of collaborative work by the chemistry department. However, because they are of high importance for this thesis, their results are also reported here.

Optical adsorption measurements for batch rebinding experiments are performed with a Varian Cary 500 UV-Vis-NIR spectrophotometer.

The MIP synthesis is optimized by varying the amount of MAA and EGDM. A variety of MIPs and the corresponding NIPs have been synthesized with different ratios of MAA and EGDM. For all prepared MIPs and NIPs batch rebinding experiments have been performed to identify the binding characteristics. For batch rebinding experiments, the MIP or NIP powder (20 mg) was added to 5 mL of various concentrations of histamine (Scheme 1) in aqueous solutions. The resulting suspensions were shaken at room temperature during 4 hours on a rocking table. After filtration, the free concentration (C_f) of histamine in fluid was measured using UV-Vis spectroscopy. Subsequently, the amount of histamine bound per gram MIP was calculated (S_b). Binding isotherms and corresponding affinity distributions for the imprinted and non-imprinted polymers towards histamine are created. These affinity distributions are based on the Freundlich model. The Freundlich model is based on the Langmuir model, used for adsorption of molecules to a solid surface, thereby forming a monomolecularic layer. However, this is a limiting model, neglecting intermolecular interaction between adsorbed solute particles The Freundlich model is a more sophisticated model which is known to give a good description of the binding characteristics in MIPs. Each binding site has a different affinity and such heterogeneous distribution of the binding sites results in a binding isotherm. This is best analyzed with the Freundlich model, displayed in Eq. 4-1 [68 and references therein, 89, 90, 91]. In this formula q is the amount of absorbed material per gram, K_f the Freundlich constant and ν the Freundlich heterogeneity parameter.

$$q = K_f C_f^{\gamma}. \qquad \text{Eq. 4-1}$$

Using the Freundlich model, the total number of binding sites, N_{tot}, within the range of affinity constants K_i = 1 to 100 mM^{-1} can be calculated (Table 4-1) [90].

MIP	Histamine	MAA	EGDM	N_{tot}(mol/g)
MIP1	1	0.5	1	219
MIP2	1	1	2	270
MIP3	1	2	4	524
MIP4	1	3	6	84
MIP5	1	1	4	84
MIP6	1	2	8	98

[a] The total number of binding sites within the range from 1 to 100 mM^{-1}, as obtained after fitting with Freundlich isotherms.

Table 4-1: Relative composition of selected MIPs with the corresponding amount of binding sites.

From these batch rebinding experiments, it is clear that MIP3 has the best performance for integration into biosensors. Therefore, MIP3 and its corresponding NIP counterpart were selected for the biosensor experiments. The binding isotherms and affinity distributions of MIP3 are shown in Figure 4-1. In the remainder of this thesis, they will be referred to as MIP and NIP. The results confirm the higher binding affinity of histamine for MIP compared to the corresponding NIP. For the region between 1 and 100 mM^{-1} the amount of binding sites for histamine is 524 µmol/g for MIP and 137 µmol/g for the corresponding NIP. This indicates that the MIPs have, within this integration range, almost four times more binding sites for histamine as the corresponding NIP.

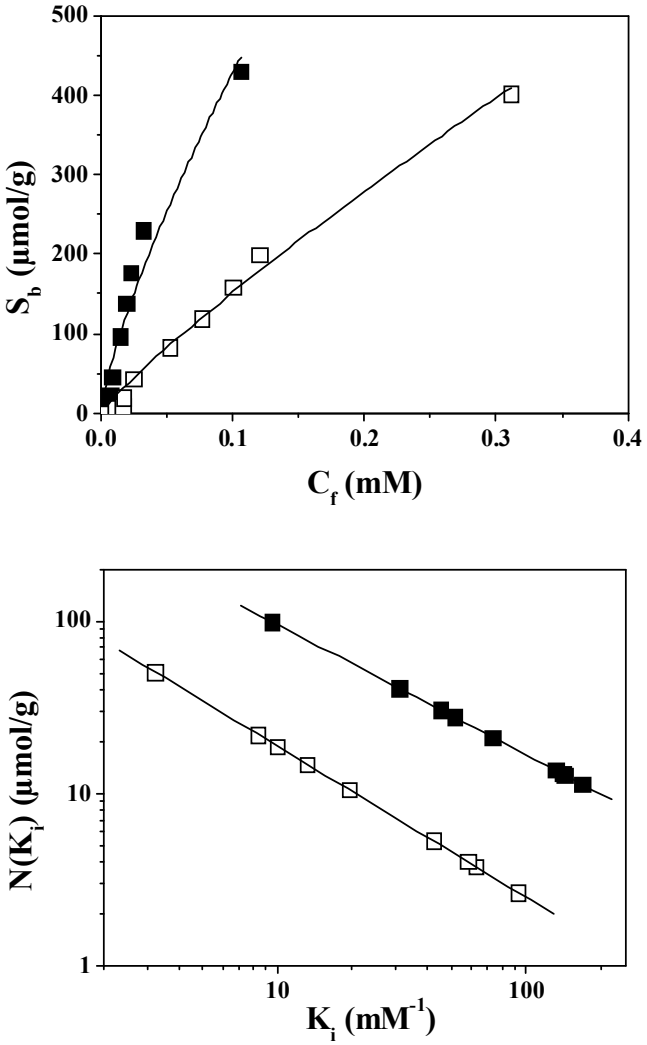

Figure 4-1: Binding isotherms for MIP (solid squares) and corresponding NIP (open squares) exposed to histamine (top) and resultant affinity distributions after fitting with Freundlich isotherms (bottom).

One can also estimate an overall binding constant for the MIP and NIP by assuming that every binding site present has the same affinity for histamine by using a Langmuir isotherm. This assumption is obviously incorrect, but can still provide a rough comparison of the MIP and NIP systems. In this way, binding constants for the MIP and NIP are found of 6.4 mM^{-1} and 1.2 mM^{-1}, respectively.

This indicates that, as expected, the MIP binds histamine significantly better than the NIP. This specific chemical recognition of histamine is to a large degree the result of the presence of directional hydrogen bonds in the cavities of the MIPs, as illustrated in Figure 2-7. For comparison, typical affinity constants for IgG-protein recognition are of an order of magnitude of 10^6 and more.

The same MIP and NIP were also exposed to various concentrations of histidine. From an analysis of the binding isotherms and affinity distributions, it can be seen that the amounts of histidine bound to the MIP and NIP are more or less equal and significantly lower as compared to the histamine binding characteristics. For the region between 1 and 100 mM^{-1} the amount of binding sites for histidine is 20 µmol/g for MIP and 13 µmol/g for the corresponding NIP, as compared to 524 µmol/g for the amount of histamine binding sites on the same MIP.

4.2 Microgravimetric detection of histamine

The content of this section is the result of coworker J Alenus from our BIOS-group, as it was published in literature [75]. His results are also reported in this thesis as this gravimetric detection method is an excellent reference technique. The chemical recognition occurring at the MIP and NIP covered surfaces can be detected gravimetrically.

4.2.1 Materials and methods

Quartz Crystal Microbalance (QCM) is a technique which makes use of the piezoelectric properties of quartz crystal. When weight is deposited onto the crystal surface, its oscillation frequency will change in accordance to the weight and it will stabilize at a new resonance frequency. The relationship between this frequency shift and the deposited weight is described in the Sauerbrey equation Eq.4-2 (92, 93). From this equation the deposited mass Δm can be directly calculated from the resonance shift Δf. The resonance frequency of the crystal is f_0, A is the active surface of the crystal that is sandwiched between the electrodes, ρ_q the density of quartz and μ_q is the shear modulus of quartz.

$$\Delta f = -\frac{2 f_0^2}{A\sqrt{\rho_q \mu_q}} \Delta m \qquad \textit{Eq. 4-2}$$

The QCM measurements are performed using a PLO-10 phase lock oscillator from Maxtek Inc. The crystals are standard AT-cut, 5 MHz, Ti/Au polished with an active oscillation region of 34.19 mm². The pump used during the QCM experiments is a NE-500 syringe pump from Prosense B.V

The quartz crystals are prepared for sensor measurements by coating them first with an adhesive polymer layer. Since no conductive properties are needed for QCM measurements, a common non-conjugated polymer, *i.e.* PVC, is utilized for this layer, which was ordered from Sigma Aldrich. The QCM crystals are spincoated with a 0.7 weight-% PVC solution in tetrahydrofuran (THF). This layer serves as an immobilization layer for either the MIP or the NIP particles. These particles were applied to the polymer layer using the stamping method described in chapter 2. As the glass transition temperature of PVC is 80°C, this stamping method, where baking occurs at 120°C, is also applicable for stamping on PVC. The resultant surface coverage is assessed using optical microscopy on these stamped sensor surfaces with a Zeiss Axiovert 40 MAT. Microscope images were processed with the image analysis program ImageJ 1.37v from the National Institute of Health, USA. The obtained surface coverage was 27.1% and 28.7% for the MIP and NIP crystals respectively. This is similar to the previously reported surface coverage of nicotine-MIPs on OC_1C_{10}-PPV [68]. It is important that the surface coverage of the MIP and NIP on each crystal is very similar, since MIP and NIP surfaces can not be measured simultaneously and the QCM results would be difficult to compare.

The crystals are placed in the sample holder, which is on one side connected to the syringe pump and on the other side to an addition reservoir. Each measurement starts with a base volume of 10 mL of water in the addition reservoir. This water is then pumped through the crystal holder with a flow rate of 1 mL/min. When the signal stabilizes, the flow is stopped and the desired amount of histamine or histidine is added to the addition reservoir. This mixture is stirred for 20 seconds with a magnetic stirrer. After 20 seconds the stirrer is

stopped and the pumping resumes at the same flow rate. If binding occurs to the MIP or NIP the frequency will drop in accordance with the bound mass. After each measurement, the reservoir and the crystals are adequately rinsed to remove any remaining target molecules. Increasing concentrations of histamine and histidine are measured using both the MIP- and the NIP-covered crystals in the concentration range 1 µM to 100 µM with 10 µM increments. This results in typical dose-response curves. The dilution range of histamine and histidine is made with water which was demineralized with a Sartorius arium 611 (18.2 MΩ∗cm) and degassed using a MD4 diaphragm vacuum pump from Vacuubrand.

4.2.2 Results and discussion

In Figure 4-2 dose-response curves are shown for MIP and NIP, both exposed to increasing concentrations of histamine and histidine. Frequency shifts are obtained after stabilization of the frequency shift before addition of the next concentration.

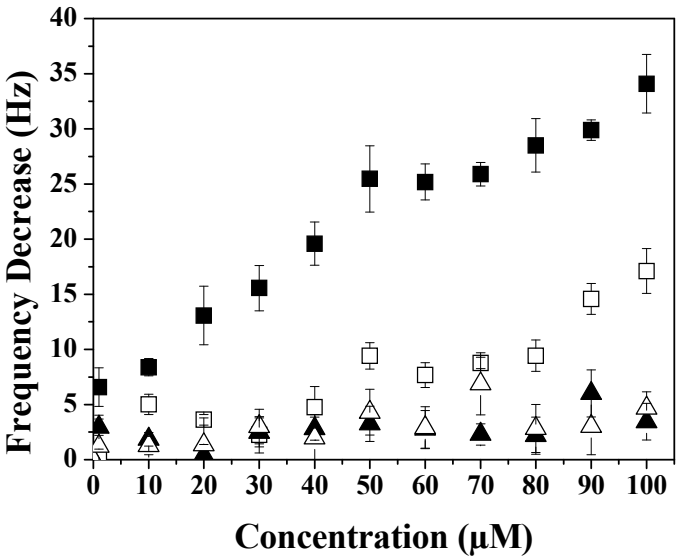

Figure 4-2: QCM dose response curves for MIP and NIP exposed to increasing concentrations of histamine and histidine (MIP exposed to histamine: solid squares; MIP exposed to histidine: solid triangles; NIP exposed to histamine: open squares; NIP exposed to histidine: open triangles).

From Figure 4-2 can be seen that the observed frequency shifts for the MIP exposed to histamine are significantly higher than for the NIP exposed to histamine as well as the MIP and NIP exposed histidine. For the MIP a concentration of 1 µM histamine causes a frequency shift of 6.57 Hz, which rises almost linearly until the highest measured concentration of 100 µM. This causes a frequency shift of 34.09 Hz. In contrast, for both the MIP and the NIP exposed to histidine, the frequency remains reasonably constant (minimum 0.38 Hz and maximum 6.87 Hz) over the entire concentration range, with only a minor rise towards the higher concentrations.

As expected, there are no specific binding sites for histidine and only aspecific binding is observed. Due to aspecific binding, the NIP exposed to histamine exhibits a similar behaviour, with a slightly higher frequency shift for the larger concentrations. This frequency shift is a little more pronounced than the one observed for histidine as a result of the fact that the MIP synthesis was optimized for the specific binding of histamine. Hence, the NIP synthesized from the same optimized mixture of monomers, cross-linkers and porogen (but without the template being present), can be expected to have also a somewhat higher amount of aspecific binding sites for histamine.

For a true comparison, the corresponding mass change was calculated for every frequency shift. It was found that the binding of 6.11 ng of target molecules corresponds to a frequency decrease of 1 Hz. The mass change of the sensor, obtained in this way, was compared to the total mass that passed the sensor for that given concentration. This gives an estimate of the percentage of molecules that bind to either the MIP or NIP. From these calculations it is found that histamine binds about 14 times better to the MIP based sensor surface than histidine does. Histamine binds also almost 5 times better to the MIP based sensor surface, compared to the NIP. This confirms the results of the batch rebinding experiments, which also demonstrated that the MIP has almost 4 times as many binding sites for histamine in comparison to the NIP.

4.3 Impedimetric detection of histamine

To translate the chemical recognition occurring at the MIP and NIP covered surfaces directly into an electrical signal, impedance spectroscopy is performed.

4.3.1 Sensor properties

A polymer sample is measured with 2 MIP imprinted electrodes and 2 NIP imprinted electrodes. The best and most stable channels, 1 MIP and 1 NIP, are displayed. The histamine concentration in the sensor is increased in 3 steps, resulting in concentrations of 3, 6 and 9 nmol/l. Measurements have been performed in a temperature-controlled environment of 37°C. Impedance is monitored as function of time. In the low-frequency region, a frequency of 213 Hz is chosen for its optimal signal-to-noise ratio. The signals are relative to their initial value 5 data points prior to the first addition of histamine. The MIP electrode is shown by solid squares and the NIP electrode by open squares. The full line indicates the concentration, with a secondary axis on the right.

Upon sequentially increasing the concentration of histamine, the MIP shows an increase in impedance amplitude. The NIP shows no significant change, as it does not have specific binding sites for the histamine molecules. Possible explanations for the increase in impedance can be found in Eq. 3-1 and 3-2. It may be caused by a decreasing capacitance or an increasing resistance after binding of histamine to the MIP nanocavities. Eq. 3-1 shows that the capacity is proportional to the permittivity and the surface, and inversely proportional to the thickness d of the capacitor. Upon binding of histamine the nanocavities are filled with histamine instead of water, meaning the permittivity decreases.

Another possible explanation is a decrease in active surface due to the filling of the nanocavities. For exact understanding of the recognition event occurring in the sensor the measured data should be modeled with an equivalent electrical circuit. This is discussed in the following of this chapter. With this first experiment the selectivity is established.

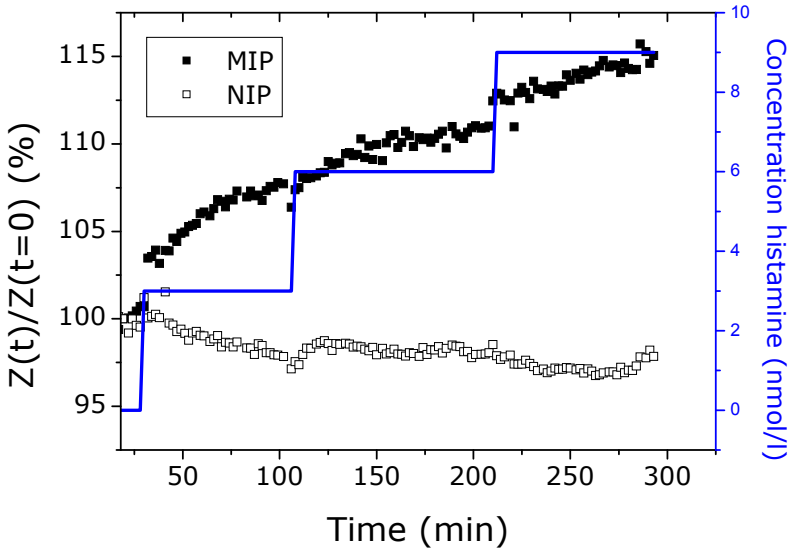

Figure 4-3: Impedance as function of time for a MIP and a NIP electrode. The step curve indicates the concentration of histamine as function of time.

A dilution range of histamine and histidine is made in a phosphate buffered saline (PBS) solution. For the dose response curve the concentration of histamine was increased in a 0 to 12 nM range. This is achieved by preparing a histamine concentration range of 9 to 31 nM in 12 equal steps. By sequentially adding constant volumes of 25 μl of these concentrations to the 200 μl PBS inside the reservoir, 1 nM increments of concentrations are obtained from 0 to 12 nM. The histidine concentrations were increased by repeated addition of 50 μl of a 29 nM solution, resulting in unequal steps of 5.8 nM, 9.7 nM and 12.4 nM. The dose response measurements occur at a pH of 7 (neutral environment).

After a stabilization period of 15 minutes, increasing concentrations of histamine are added stepwise. Impedance spectra are measured subsequently in a temperature-controlled environment of 37°C. At a chosen frequency of 213 Hz a clear dose-response curve is obtained in the 0-12 nM concentration range (Figure 4-4). It should be noted that all impedance data are normalized relative to their initial impedance value, prior to addition of the target molecule. The resulting value is referred to as the relative impedance signal. A response value

is obtained 20 minutes after addition of the target molecule by averaging 5 data points. The error bars obtained in this manner are an indication for the stability of the measured impedance signal. The actual error bars in Figure 4-4 are smaller than the symbols utilized, indicating a low noise level. At 213 Hz the MIP-based sensor shows a 45 % response to a concentration of 10 nM histamine. At higher concentrations the sensor will reach its saturation level. The NIP channel, which measures non-specific binding of histamine molecules to the sensor surface, shows no significant sensitivity towards histamine.

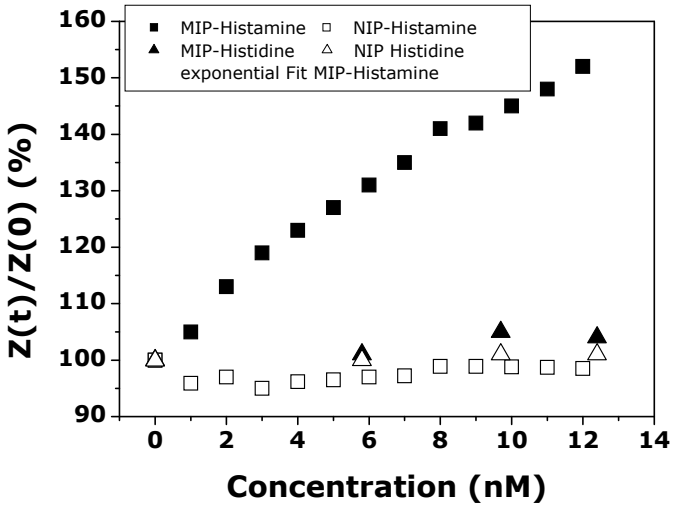

Figure 4-4: Dose response curves of MIP and NIP channels in response to addition of histamine and histidine obtained with impedance measurements.

The specificity is tested with the analogue molecule histidine. At 213 Hz both the MIP and NIP channel show no response to histidine concentrations in the same nanomolar range. For a better graphical representation of the specific binding events occurring at the sensor surface, the relative impedance signal of the MIP channel is subtracted from the relative impedance signal NIP channel, which is associated with non-specific binding (Figure 4-5).

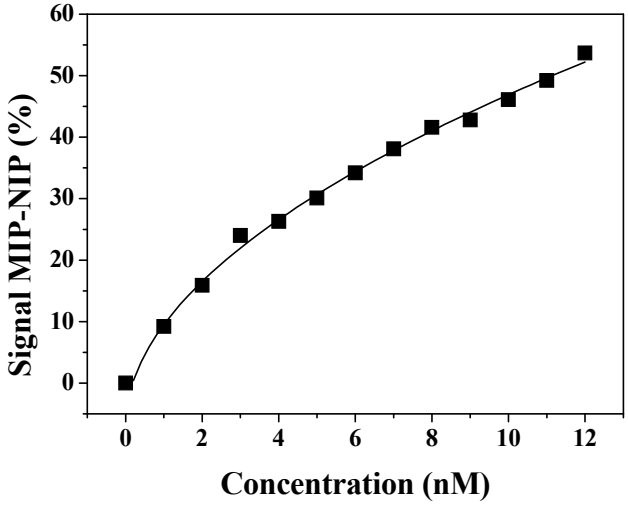

Figure 4-5: Difference between the relative impedance signals of the MIP channel and the NIP channel. The resulting fit is a good measure for the specific binding occurring at the sensor surface.

It can be seen that the histamine MIP-sensor exhibits a 40% response to 10 nM histamine. In addition, the sensor response can be represented by a simple allometric fit, as described by Eq. 4-3, where *x* is the concentration of target molecule and *y* the impedance signal representing the amount of target molecule that has specifically bonded to the MIP. An allometric fit reflects a typical binding isotherm.

$$y = ax^b \qquad \textit{Eq. 4-3}$$

The fitted values are displayed in Table 4-2.

parameter	Fitted value
a	10.8 ± 0.5
b	0.63 ± 0.02
R^2	0.99

Table 4-2: Parameters of the allometric fit of the differential dose response curve.

When, in real life, events are supposed to happen at a constant rate often an exponential function model is used. The exponential growth model is described by Eq. 4-4 and the dose response curve of the MIP-based biosensor matches this exponential growth model very well. In this exponential growth model, *t* represents the time-constant of the saturation process. In analogy with electronics of capacitor loading, the time-constant is the time to reach 64% of the saturated value. The results of the fit are displayed in Table 4-3. The saturation value is approximately 170% and at 9.3 nmol/l 64% of this value will be obtained.

Sensor sensitivity is not easy to be established with this type of sensor set-up. In comparable studies with different samples the sensitivity currently varies between 10 to 40% response to 10 nmol. This is sample dependent due to the stamping method and mainly due to the use of a semi-conducting polymer, which is susceptible to swelling in aqueous media. Another transducer material, like non-swelling conjugated polymers, would improve the quantitative reliability of the sensor output and the development of water-resistant polymers is currently under progress.

$$y = y_0 - A\exp\left(-\frac{x}{t}\right) \qquad \text{Eq. 4-4}$$

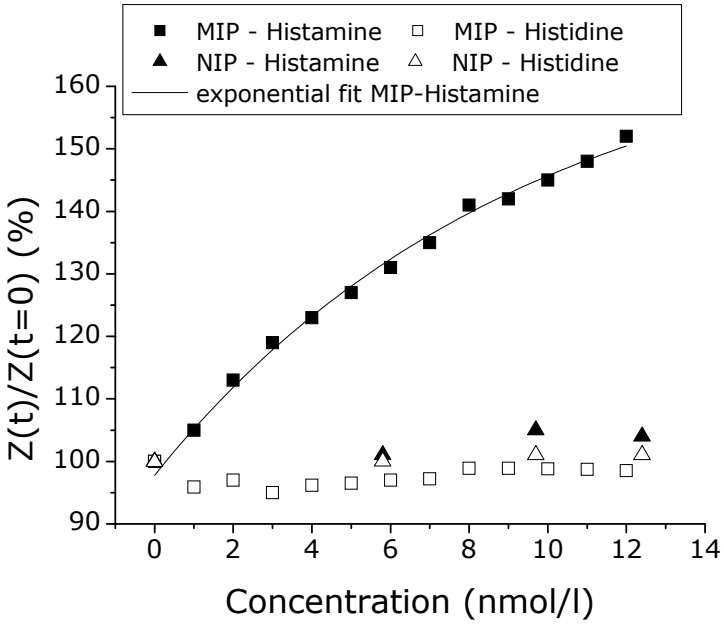

Figure 4-6: Dose response curves of MIP and NIP channels in response to addition of histamine and histidine, modeled with the exponential growth model.

Parameter	Fitted value
Y_0	1.70 ± 0.02
A	0.73 ± 0.02
t	9.3 ± 0.5
R^2	0.997

Table 4-3: Parameters of the exponential fit of the dose response curve.

4.3.2 Modeling of the impedimetric sensor

When modeling the recognition event within the sensor, the focus is on one single addition of analyte, in order to find an explanation for the increasing impedance of the MIP electrode. The addition setup is filled with PBS. The

Nyquist plots of the MIP and NIP channel show different behavior, indicating both channels have different properties. The MIP is supposed to be more porous than the NIP, which might explain the different behaviour. Next a histamine solution is added so that a concentration of 6 nmol/l is obtained. A Nyquist plot before the addition and one 45 minutes after the addition are compared in Figure 4-7.

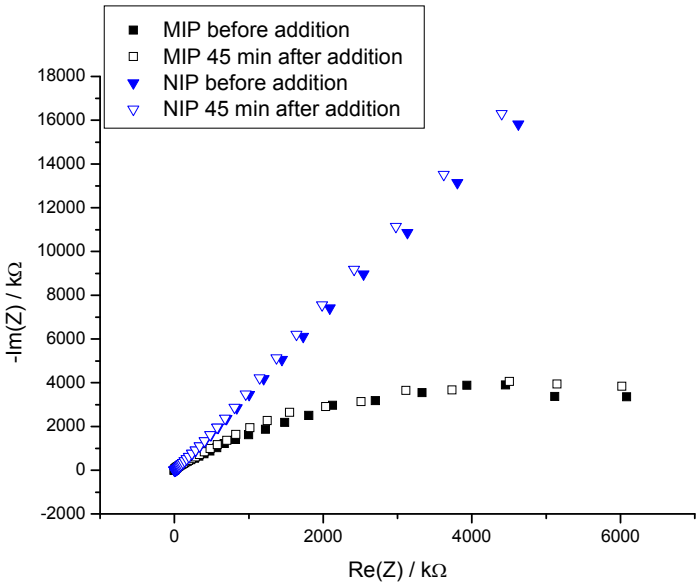

Figure 4-7: Nyquist plots before and 45 minutes after the addition of 6 nmol/l histamine.

A variety of models are tested and the most appropriate one is displayed below in Figure 4-8. The values resulting from the fit by ZSimpwin are displayed in Table 4-4. As expected, the double layer capacitance decreases after binding of histamine and the resistance increases. Both effects lead to an increase of the impedance. However, it should be noticed that these effects also occur at the NIP electrode, which ultimately does not show any increased impedance. Also, this kind of modeling of data suffers from bad reproducibility. Somehow, the modeled circuits do not always match the measured data and it is necessary to understand what is causing this difference.

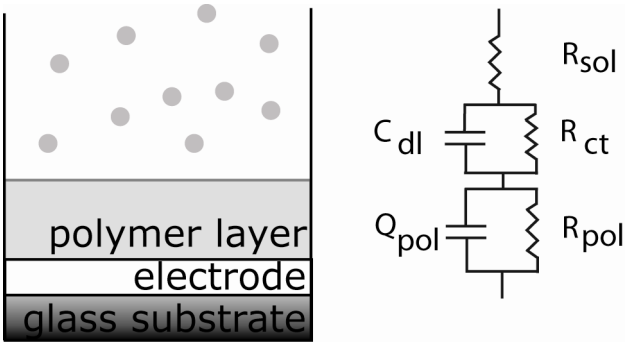

Figure 4-8: R(CR)(QR) model for a MIP-based sensor.

	MIP before	**MIP after**	**NIP before**	**NIP after**
X^2	6.649 e-3	4.123 E -3	1.653 E-2	9.653 E -3
R_{sol} (Ω)	7.152 ±1	(260±2)10^1	23 ± 6	(12 ± 3)10^2
C_{dl}(F)	(5.4 ± 0.6) 10^{-7}	(1.4 ± 0.1) 10-8	(7 ± 1) 10-8	(10±4)10-9
R_{ct}(Ω)	(43 ± 7) 10^2	(1.5 ± 0.2) 10^5	(13±2)10^1	(9±6)10^7
Q_{pol}(nS.s^{α})	800±40	16.5 ± 0.6	720 ± 40	70±31
α	0.848 ± 0.006	0.843 ± 0.004	0.804 ± 0.009	0.64 ± 0.03
R_{pol}(Ω)	(1.9 ± 0.1) 10^5	(1.03 ± 0.05) 10^7	(3 ± 2 e 10) 10^{13} (8 E11%)	(6±25) 10^6

Table 4-4: Fitted values for an R(CR)(QR) circuit.

To further investigate these results, the focus in the remainder of this paragraph is on one dataset only, namely the measured data of the MIP channel before the addition of histamine. The Nyquist plot of this measurement is represented as a Bode plot in Figure 4-9. Data is measured from 1 Hz to 100 kHz. An R(CR)(QR) circuit with component values as in the first column of Table 4-4, indicated in bold, is simulated over a larger frequency spectrum from 1 mHz to 1 MHz. The simulated data is also represented in the Bode plot in Figure 4-9. This way the difference between the measured data and the model can be clearly seen. The phase of the simulated data resembles the phase of the measured data well.

Some noise can be noticed at higher frequencies. However, the impedance amplitude of the fitted circuit is similar in shape, but over the entire spectrum it is a few orders of magnitude smaller than the amplitude of the measured data.

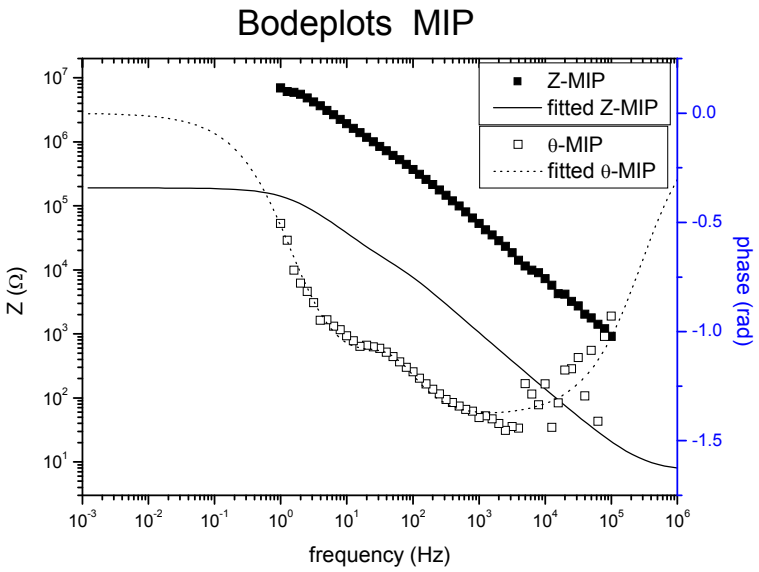

Figure 4-9: Bode plots of the measured MIP channel and the fitted MIP channel, both before histamine is added.

To find out which component is causing this difference, and hence most likely the cause of the bad reproducibility of modeling data, the parameters have been altered one by one. The most interesting ones were the polymer parameters R_{pol} and Q_{pol}. This resulted in 3 other models. All models are depicted in Figure 4-10. Model 1 is the model as it was fitted by computer software for the MIP channel before addition. This is indicated in bold in Table 4-4. In Model 2 the R_{pol} is increased by a factor 100. In Model 3 the Q_{pol} is decreased by a factor 100. In model 4 a combined effect is created by increasing the R_{pol} as well as decreasing Q_{pol}.

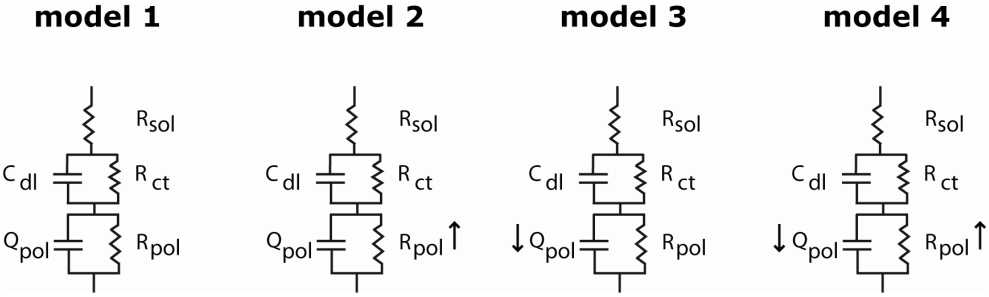

Figure 4-10: Four electronic models for the MIP-based sensor.

The effect of these parameters becomes clear from Figure 4-11, in which the impedance of all models is shown, together with the originally measured data. This way it is obvious how the parameters affect the outcome and which model hence fits the measured data best. For model 2 the amplitude at low frequencies is increased and now matches the value that the measured data would have in this region. In the middle and higher frequency range the impedance is not influenced by increasing R_{pol}. When looking at model 3 one can see the effect of decreasing Q_{pol}. This will increase the amplitude in the middle and high frequency range. Finally in model 4 the two former effects are combined and the amplitude of this circuit matches the measured data very well.

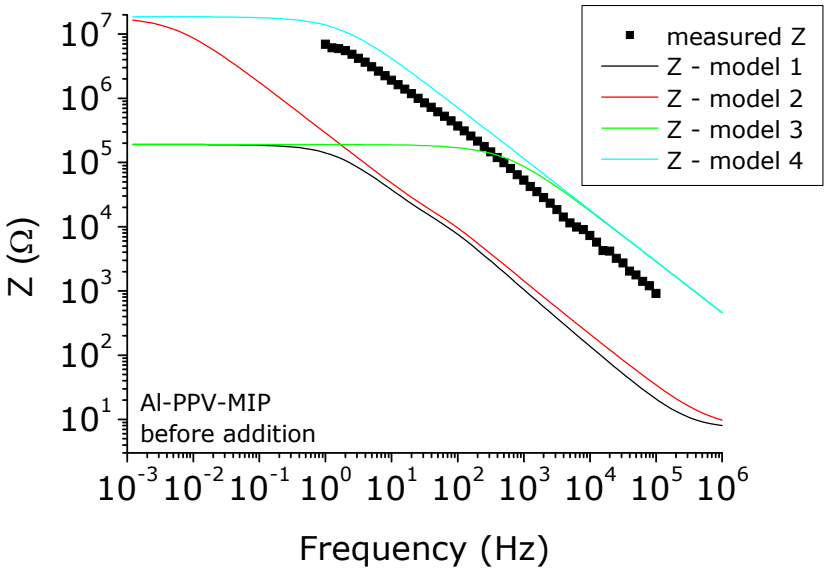

Figure 4-11: Amplitude as function of frequency for the measured impedance and 4 models.

Again the Nyquist plots are considered (Figure 4-12). Now the Nyquist plots of the modeled data are displayed as well, as is the data of model 4, which was now assumed to be the best fitting model. Model 1 for the MIP is displayed on the inset of Figure 4-12 on a different scale. It does not correspond to the measured MIP data. Model 1 for the NIP is also shown, with a straight line. However, this figure confirms that model 4 is a good fit for the MIP. The characteristic semi-circle is present in the Nyquist plot and corresponds well with the measured data.

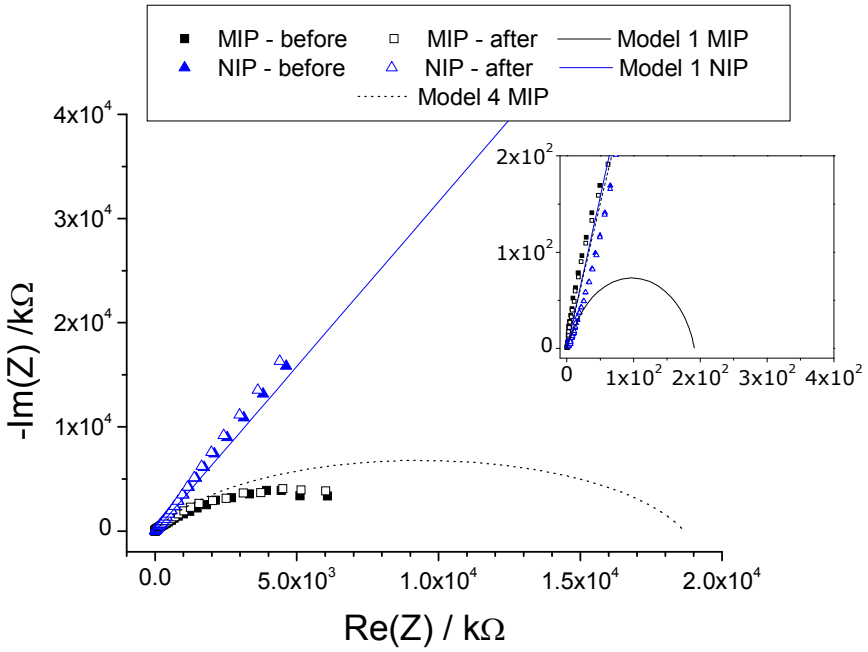

Figure 4-12: Nyquist plot of the measured data, computer models and a by hand adjusted model.

When fitting measured data with an equivalent circuit, a lot of problems occur while finding a good outcome that is reproducible for different data sets. Some parameters have unrealistic values. However, it is now found that the outcoming model fits the measured data and the absolute values are realistic, but are influenced by polymer-related parameters that can differ a factor 100 and more.

For accurate modeling of the recognition event occurring within the sensor, it would be desirable to develop a sensor that does not require the use of the polymer layer. When developing an immunosensor in the previous chapter, this component also caused instabilities and other artifacts that lead to irreproducibility of data. It would be desirable to immobilize the MIP particles directly onto the electrode. First steps towards this method have also been taken, however no successes have been booked in this field yet.

4.4 Conclusion

MIPs with high affinity and specificity towards histamine have been successfully developed by the Organic & Polymeric Chemistry group. Their batch rebinding experiments characterized the target binding phenomena to screen the MIPs and the corresponding NIPs to find the MIP most useful for integration into the biosensor systems. The optimized MIP binds significantly more histamine as compared to the corresponding NIP. Aspecific interactions between histamine and the polymer matrix cause limited binding of histamine on the NIP. In contrast, the binding isotherms for the MIP and corresponding NIP show even less aspecific binding towards the analogue histidine.

The optimized MIP and the corresponding NIP have both been successfully integrated as synthetic recognition elements for the detection of histamine into two sensing platforms, i.e. QCM and impedimetric detection. QCM can detect histamine in the micromolar range and serves as a reference technique for measuring the binding of histamine to the MIP. Impedimetric detection is a fast and specific technique for detecting low concentrations in the nanomolar range. Typical physiological concentrations in e.g. mast cells are around 200 nM.

The impedimetric MIP-based sensor shows a selective reaction to histamine. Impedance increases in response to histamine. By modeling this binding event with an equivalent circuit, it remains unspecified what precisely causes this response, but it can be assumed that it is a double effect. The resistance of the interface layer can increase, but mainly the capacitance of the double layer at the interface decreases, due to a decreased surface or a decreased permittivity. In this chapter again it can be concluded that the sensor would benefit from the use of a substitute material with respect to the semiconducting polymer MDMO-PPV.

The characteristics of the sensor have been determined, with a limit of detection as low as 2 nM. The sensitivity is up to 45% to 10 nM histamine. Although this result is sample dependent, all measured samples showed a similar trend. A dose response curve is measured in the 0 - 12 nM range. Sensor saturation

begins at 9.3 nmol/l. Specificity was confirmed by tests with histidine, showing no significant sensor response.

5 A MIP-based sensor in different pH environments

In this chapter the MIP-based impedimetric sensor is tested under various pH conditions to which it must withstand. It is investigated how the pH affects the functionality of the MIP. These findings have been submitted to Physica Status Solidi (a) [94]. A novel model is established to describe the pH dependent interaction between histamine and MIP.

5.1 Introduction

For application of the sensor in bodily fluids a chemical recognition element is necessary, which can withstand the acidic environments of fluids in which histamine occurs, such as stomach fluids, bowel fluids and saliva. As a result, the development of a histamine sensor containing such a chemical recognition element is of considerable interest. MIPs are supposed to withstand acidic and basic environments very well and are therefore very suitable for application in biosensors for measuring in vivo. For the envisaged intestinal application or applications in bodily fluids in general, the sensor is tested under various pH conditions. It is investigated in which way various pH environments affect the detection of histamine by the MIP-based sensor. The chapter ends with a straightforward model for treating the pH-dependent binding aspects.

5.2 Materials and methods

The sensor is impedimetrically tested under various pH conditions. Therefore the previously described four channel addition setup is used. PBS with pH 5, 7, 9 and 12 are prepared by adding small quantities of hydrogen chloride (HCl) or natrium hydroxide (NaOH) to the neutral buffer solution. A histamine concentration series is created with these PBS solutions in order to obtain 3 equal steps of 3, 6 and 9 nM. The fewer but larger steps result in shorter

measuring time while a similar concentration range is maintained, as in the dose-response curve in the previous chapter, see Figure 4-6.

5.3 Result & discussion

The results are shown in Figure 5-1 a to d. The three following addition steps of 3, 6 and 9 nmol/l are labeled from I to III. In an acid solution of pH 5 the sensor exhibits no response to the subsequent addition of histamine in both the MIP channel and the NIP channel (Figure 5-1-a). In neutral environments (pH 7), the MIP channel shows a response to the following addition steps while the NIP channel does not exhibit non-specific adsorption (Figure 5-1-b). When a concentration of 9 nM is present in the setup the signal has increased 12 % after 20 minutes. This is similar to the observations in the dose-response experiment. However in a more basic solution of pH 9 the sensor shows an increased response (Figure 5-1-c). When in the third addition step the concentration is increased to 9 nM the sensor signal increases 60 % after 20 minutes. Again, the NIP channel shows very little non-specific adsorption. The same measurement has been performed in a basic environment of pH 12 (Figure 5-1-d). Both signals remain constant after the first addition. After the second and third addition step both the MIP and the NIP channel show a slight signal drift. This may be caused by minor disturbances in the addition setup when analyte is added. Most importantly no specific response of the MIP channel is noticeable regarding the three subsequent addition steps in this experiment.

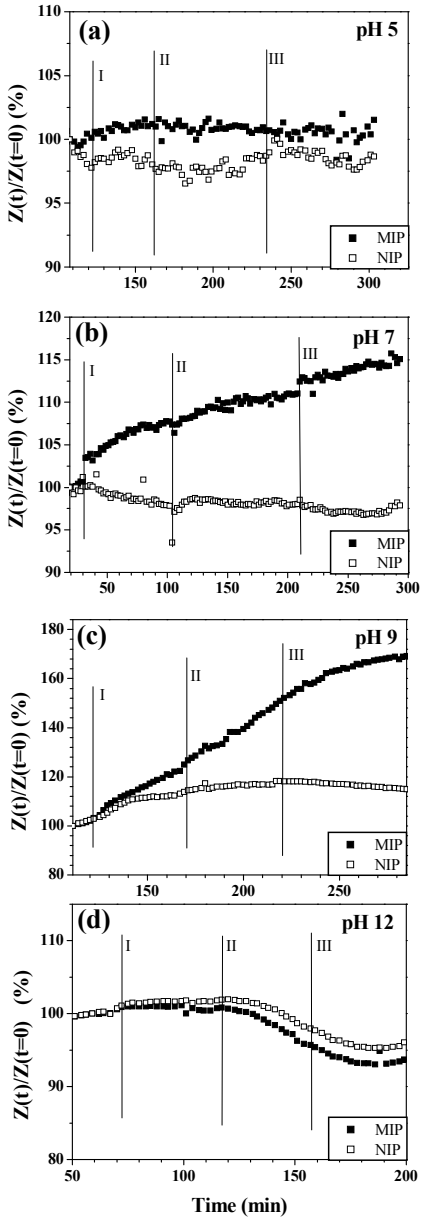

Figure 5-1: Relative impedance signal of MIP and NIP channels in response to addition of histamine under various pH conditions: pH 5 (a), pH 7 (b), pH 9 (c) and pH 12 (d). Additions of 3 nM, 6 nM and 9 nM are labeled I, II, and III respectively (MIP exposed to histamine: solid squares; NIP exposed to histamine: open squares)

This pH dependency of the sensor response can be explained by the behavior of the molecules in solution. The appearance of a molecule depends on the pH of the solution in which it is dissolved [95]. In an acidic environment protons from the solution might stick to molecules, resulting in protonated molecules. This ionization occurs at a specific pH value. Histamine has pKa values of 6.9 and 10.4 [96]]. A third pKa value of about 15-20 has been reported but does not fall within the pH range of aqueous solutions [96]. The resulting behavior of histamine in various pH solutions is modeled with Hyperquad simulation and speciation (HySS) [97]. This is a utility program for the investigation of equilibria involving soluble and partially soluble species. The result is depicted in Figure 5-2.

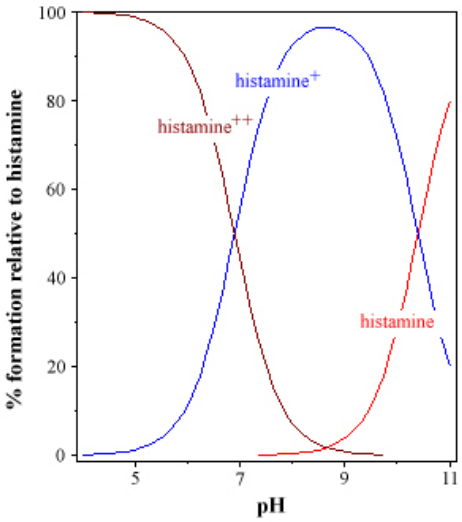

Figure 5-2: Equilibrium ratios of an aqueous solution of histamine at varying pH values, modeled with HySS [97].

In solutions, histamine becomes protonated at specific sites. They are depicted in Figure 5-3. In strongly basic environments above pH 10.4, histamine will be predominantly present in its neutral form. Upon lowering the pH, the aliphatic amino group will be able to increasingly bind a proton, creating single-protonated histamine or histamine^{+}. At pH 10.4, when the pH is exactly the pKa value, the neutral histamine and the single-protonated histamine are present in equal concentrations. In neutral environments (pH 7) histamine is still mostly present in its single protonated form. However, decreasing the pH of the buffer

solution will further increase the protonation of histamine. At lower pH, the imidazole ring can bind a proton and hence a double protonated form of histamine, histamine^{++} will be formed. At pH 6.9 the single protonated and double protonated histamine are present in equal concentrations. Below pH 6.9 double protonated histamine is predominant in the buffer solution.

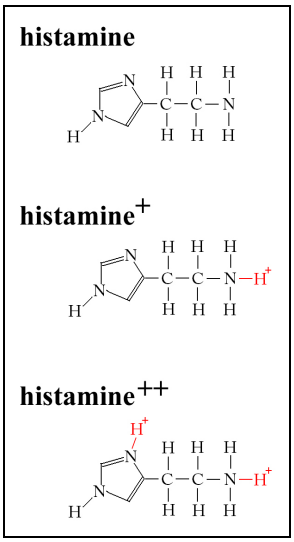

Figure 5-3: Protonation sites of histamine.

Not only the histamine will be affected by changing the pH, but also the MIP will exhibit protonation and deprotonation reactions. As a model for the MIP, PMAA, poly-methacrylic acid, can be used. This can be obtained from the same monomer, i.e. methacrylic acid (MAA), which is also used to make the MIP. PMMA has a pKa between 6 and 7 [98]. Its protonation behavior can also be modeled using HySS as depicted in Figure 5-4.

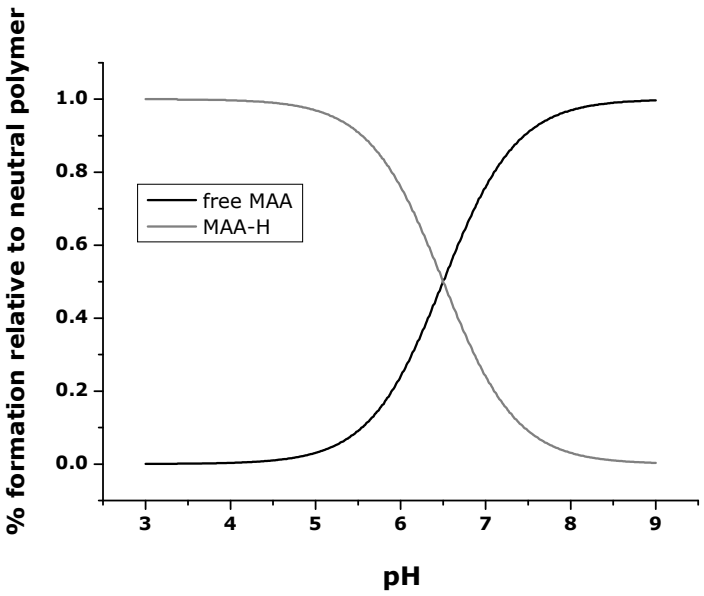

Figure 5-4: Equilibrium of poly-MMA in solutions, modeled with HySS [98].

For a successful selective binding event of histamine to the MIP, at least one, but preferably more, hydrogen bond has to be formed between histamine and the MIP. This binding will ultimately result in detection in the sensor. However, the formation of hydrogen bonds is strongly pH dependent, which explains the results from Figure 5-1 as follows. In buffer solutions of pH 5, histamine is mostly double protonated (histamine^{++}) and there are almost no histamine^{+} molecules left. Since in such acidic solutions also the MIP is almost fully protonated, only very weak hydrogen bonding is possible between the target molecule and the MIP. As a result, the molecule now is unlikely to bind to the nanocavity of the MIP and hence the sensor shows no response to addition of this molecule. At pH 7 the MIP is partially deprotonated. At the same time, about 44 % of the histamine remains double protonated, while the remainder has become single protonated. The histamine^{+} and the histamine^{++} molecules can form hydrogen bonds with the partially deprotonated MIP. As a result, the sensor shows a good response at pH 7.

At even higher pH (pH 9) histamine$^+$ is predominant, while the MIP is now almost fully deprotonated. This allows the formation of a hydrogen bond and thus the sensor shows a strong response. It is assumed that this condition is close to the optimal balance between protonation of histamine and deprotonation of the polymer.

At a pH of 12, histamine$^+$ has mostly been converted into neutral histamine, which is now the predominant molecule. Since, both histamine and the MIP have become deprotonated, no large amount of hydrogen bonds can be formed. The MIP channel shows no response to the analyte addition at a pH of 12 and no specific match with the nanocavity is established.

5.4 Modeling of the pH measurements

For a thorough understanding of the binding processes occurring within the biomimetic sensor, a simplified model is applied. Histamine can be represented as one of the shapes and corresponding names as in Figure 5-5. HisN represents the neutral form of histamine. His+ is singly protonated at its aliphatic tail. Theoretically, protonation could also be possible on the aromatic ring of histamine, the third situation sketched in the Figure 5-5. In reality, however, this is not possible regarding the pKa value of histamine. The third form of histamine does not exist in practice. His++ represents the state that is double protonated. Here both the tail and the aromatic ring have absorbs one proton. The same idea can be applied to the monomer MAA, and thus the MIP. Its corresponding states are indicated in the right of Figure 5-5. The four situations are labeled A to D. This leads to 12 possible situations where one of the three histamine types matches one of the 4 MIP-models. All these possible situations are now further investigated.

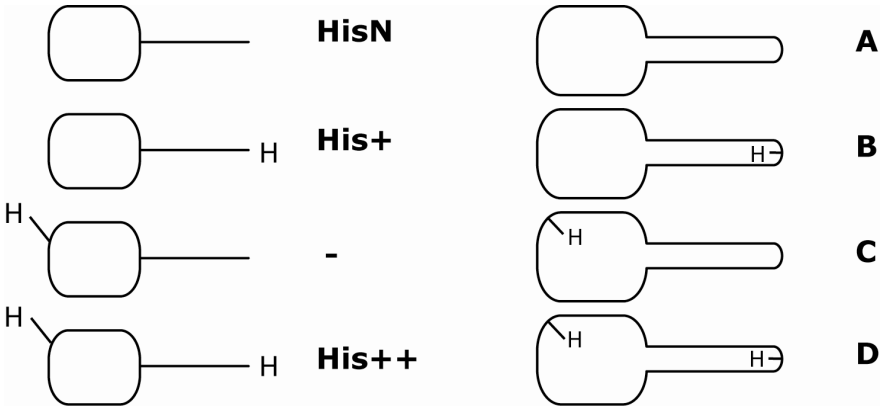

Figure 5-5: Schematic representation of the protonation of histamine (left) and MIP (right).

Binding of histamine to PMMA occurs when only 1 hydrogen is present. When both components have a hydrogen atom no hydrogen bond can be created. The same is true for when no hydrogen atoms are present. A variety of binding options are possible. Histamine can bind with PMMA by means of 2 hydrogen bridges, one left and on right, to create a strong binding. This happens when HisN meets MIP D, when His+ finds MIP C and when His++ binds with MIP A. The resulting matches are shown in Figure 5-6. In each of these cases two hydrogen bonds will be created. Histamine and MIP are now strongly bonded together.

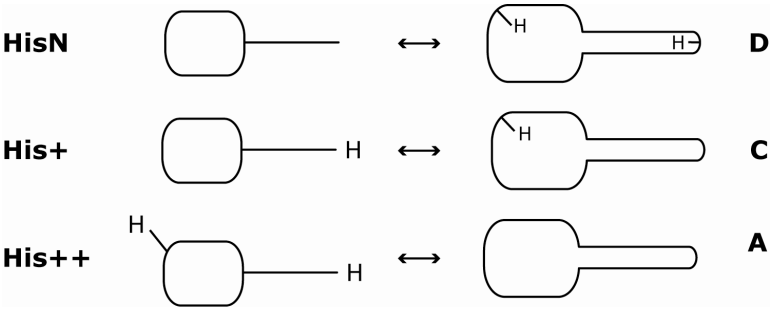

Figure 5-6: Histamine and MIP matching with 2 hydrogen bonds, causing good binding.

There is also some binding if only 1 hydrogen bond is formed. All possibilities are depicted in Figure 5-7.

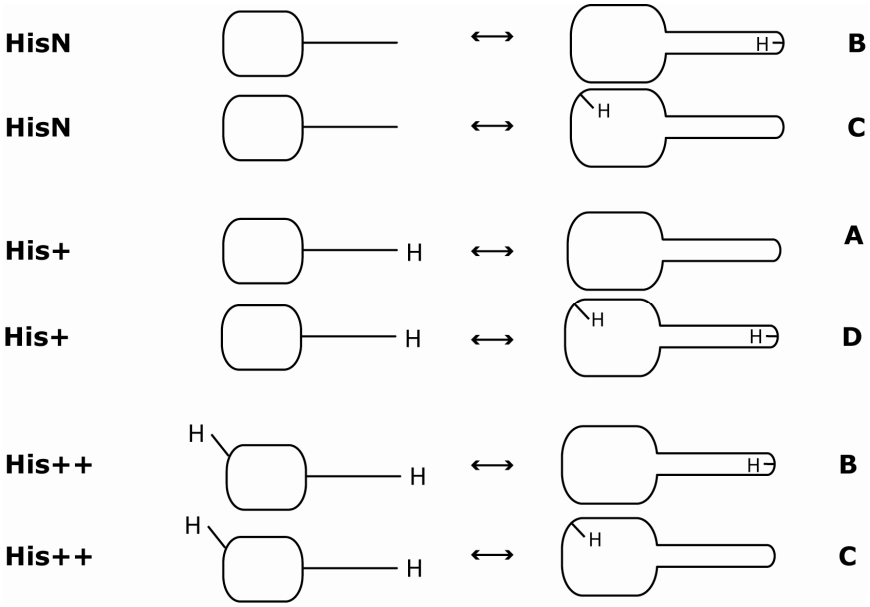

Figure 5-7: Histamine and MIP matching with 1 hydrogen bond, causing weak binding.

When no hydrogen atoms are present at either component, no hydrogen bonds can be created and there will be no binding of histamine to the MIP. When 2 hydrogen atoms are present no bond can be established either. The situations in which these no binding occurs are depicted in Figure 5-8.

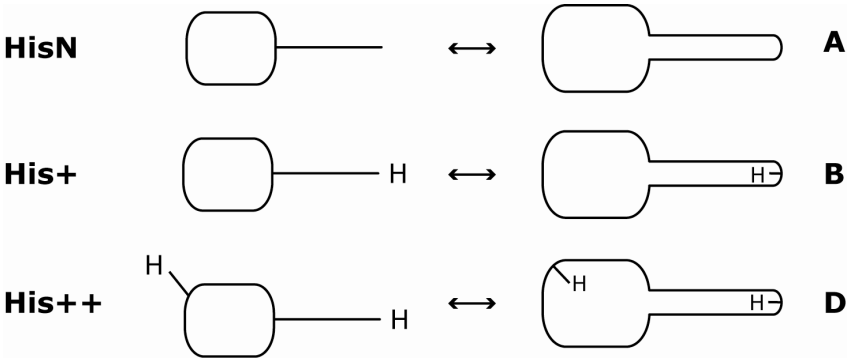

Figure 5-8: Situations in which no hydrogen bonds can be established.

Upon the impedimetric detection of histamine, hydrogen bonds have been formed. Either one of the combinations in Figure 5-6 or Figure 5-7, or a number of these combinations have been formed. By means of statistical analysis it can

be determined which matches are causing the binding. When no histamine is detected, no hydrogen bonds between histamine and MIP have been established, thus the processes occurring within the sensor are mainly those as in Figure 5-8.

The prevalence of a molecule at a certain pH can be calculated when the pKa value is known as follows. From the known chemical formule Eq. 5-1 a ratio of [HA]/[A-] can be calculated as in Eq. 5-2.

$$pKa = pH + \log\left(\frac{[HA]}{[A^-]}\right). \qquad \textit{Eq. 5-1}$$

$$\frac{[HA]}{[A^-]} = 10^{pKa-pH}. \qquad \textit{Eq. 5-2}$$

Using the definition of pH (Eq. 5-3) the $[H^+]$ can be calculated, which equals $[A^-]$ (Eq. 5-4).

$$pH = -\log([H^+]). \qquad \textit{Eq. 5-3}$$

$$[A^-] = [H^+] = 10^{-pH}. \qquad \textit{Eq. 5-4}$$

From $[A^-]$, now [HA] can be also found (Eq. 5-5).

$$[HA] = \frac{[HA]}{[A^-]} \cdot [A^-]. \qquad \textit{Eq. 5-5}$$

Ratios of [HA] and [A-] can be calculated as in Eq. 5-6 and Eq. 5-7.

$$\%[HA] = \frac{[HA]}{[A^-] + [HA]}. \qquad \textit{Eq. 5-6}$$

$$\%[A^-] = \frac{[A^-]}{[A^-] + [HA]}. \qquad \textit{Eq. 5-7}$$

Applying these formulas to histamine and MIP, results in the following prevalence numbers displayed in respectively Table 5-1 and Table 5-2. All numbers have been rounded to 2 decimals. The MIP at pH 9 is rounded to 3 decimals as the third decimal is of importance.

PH	His++	His+	HisN	Sum
5	0.99	0.01	0.00	1.00
7	0.44	0.56	0.00	1.00
9	0.01	0.95	0.04	1.00
12	0.00	0.02	0.98	1.00

Table 5-1: Prevalence of histamine.

PH	MIP A	MIP B	MIP C	MIP D	Sum
5	0.00	0.03	0.03	0.94	1.00
7	0.58	0.18	0.18	0.06	1.00
9	0.994	0.003	0.003	0.00	1.00
12	1.00	0.00	0.00	0.00	1.00

Table 5-2: Prevalence of MIP.

Two hydrogen bonds are established in the situations depicted in Figure 5-2. One can now estimate the chance of 2 hydrogen bonds occurring at pH5 by adding the probabilities of each matching pair. To estimate the chance of the first situation, HisN and MIP D occurring together, the chances of each independent event need to be multiplied.

$$P(HistN \ \& \ MIPD) = P(HistN) \cdot P(MIPD) \, . \qquad \textit{Eq. 5-8}$$

The individual chances are displayed in Table 5-1 and Table 5-2. The probability of all of the three matches can be calculated. The resulting chance is the likeliness of a double hydrogen bond between the MIP and the histamine at pH 5 and can be found in the left of Table 5-3. At pH 5 only 0.1% of the histamine and MIP molecules are protonated or deprotonated in such a way that 2 hydrogen bonds can be established. In the middle, the chances at pH 5 are calculated of all 6 possible configurations that can lead to a single hydrogen bond. Adding these chances, only 7.04 % of the molecules might contribute to

the recognition event via a single hydrogen bond. However, 92.8 % of the histamine and MIP is protonated or deprotonated in such a way that no hydrogen binding is possible (Figure 5-8), and hence no binding can be impedimetrically detected. This is in correspondence with the biosensor experiment, where at pH 5 no binding between histamine and MIP could be detected (Figure 5-1 (a)). It has been verified that the sum of all probabilities at pH 5 equals 1.

		2 H-bonds			1 H-bond			no H-bond
HisN	D	0.0000	HisN	B	0.0000	HisN	A	0.0000
His+	C	0.0004	HisN	C	0.0000	His+	B	0.0004
His++	A	0.0009	His+	A	0.0000	His++	D	0.9280
			His+	D	0.0117			
			His++	B	0.0293			
			His++	C	0.0293			
pH 5		**0.0013**			**0.0704**			**0.92832**

Table 5-3: Prevalence of hydrogen bonds at pH 5.

The same method can be applied to the situations of pH 7, 9 and 12. The results are given in Table 5-4, Table 5-5 and Table 5-6, respectively. It has been verified that the sum of all probabilities at a pH of 7, 9 and 12 also equals 1. At a pH of 7, 35.7 % of the molecules can establish double hydrogen bonds and 51.6 % can establish single bonds. Combining these results, 87.3 % of the molecules will contribute to the binding of histamine to the MIP, which is detected in the impedimetric measurement in Figure 5-1 (b).

		2 H-bonds			1 H-bond			No H-bond
HisN	D	0.0000	HisN	B	0.0001	HisN	A	0.0002
His+	C	0.1017	HisN	C	0.0001	His+	B	0.1017
His++	A	0.2555	His+	A	0.3216	His++	D	0.0256
			His+	D	0.0322			
			His++	B	0.0808			
			His++	C	0.0808			
pH 7		**0.3572**			**0.5155**			**0.1275**

Table 5-4: Prevalence of hydrogen bonds at pH 7.

At a pH of 9, only 1.1 % of the molecules can establish double hydrogen bonds. However, a majority of 94.8% of the molecules is protonated or deprotonated in a way that allows the establishment of single bonds. Therefore histamine can

also be specifically detected. At pH 7 approximately 13 % does not participate in the formation of hydrogen bonds, whereas at pH 9 only 4 % does not contribute to the detection. This explains the stronger detection that was measured at a pH of 9 (Figure 5-1 (c)).

		2 H-bonds			1 H-bond			no H-bond
HisN	D	0.0000	HisN	B	0.0001	HisN	A	0.0380
His+	C	0.0030	HisN	C	0.0001	His+	B	0.0030
His++	A	0.0078	His+	A	0.9481	His++	D	0.0000
			His+	D	0.0000			
			His++	B	0.0000			
			His++	C	0.0000			
pH 9		**0.0108**			**0.9484**			**0.0410**

Table 5-5: Prevalence of hydrogen bonds at pH 9.

In Figure 5-1 (d) can be seen that no binding of histamine is impedimetrically detected at a pH of 12. The results in Table 5-6 confirm this result. Only 2 % of the molecules can contribute in the binding process through single hydrogen bonds, while 98 % of the molecules is not capable of establishing any hydrogen bond. As almost no molecules can play a role, almost no binding can be detected. This can be seen clearly the impedimetric signal in Figure 5-1 (d), apart from the small drift that is noticeable.

		2 H-bonds			1 H-bond			no H-bond
HisN	D	0.0000	HisN	B	0.0000	HisN	A	0.9755
His+	C	0.0000	HisN	C	0.0000	His+	B	0.0000
His++	A	0.0000	His+	A	0.0245	His++	D	0.0000
			His+	D	0.0000			
			His++	B	0.0000			
			His++	C	0.0000			
pH 11		**0.0000**			**0.0245**			**0.9755**

Table 5-6: Prevalence of hydrogen bonds at pH 12.

All results are combined into one master table. In this table the probabilities of each type of bond are shown per pH. Also the total probability of any bound molecules can be found per pH value. In this table it can be clearly seen, that at a pH of 9, 96 % all molecules will have bound though 1 or 2 hydrogen bonds. This is the optimal pH for measuring with the MIP used in this thesis.

pH	2 H bonds	1 H bond	0 H bond	Total bound
5	0.0013	0.0704	0.9283	0.0717
7	0.3572	0.5155	0.1275	0.8727
9	0.0108	0.9484	0.0410	0.9593
12	0.0000	0.0245	0.9755	0.0245

Table 5-7: Master table, showing the probabilities of each bond, and the total probability of bound material.

Some important remarks must be made regarding this model. Firstly, this model only accounts for the binding of histamine to the MIP by means of hydrogen bonds, the most important method of binding. However, in reality, there are other processes involved. Secondly, from literature, the pKa value of the monomer, used to synthesize the MIP, can be between 6 and 7. For the calculations in this model a pKa value of 6.5 is assumed, which might deviate from its real value.

For application of the sensor in bodily fluids or in the intestines, it needs to withstand a wide range of pH values, but also operate under these extreme pH conditions. Histamine is a given fact in this situation. It is the target molecule to trace down in a solution and it can not be modified. Therefore the only option is to modify the MIP. Using the newly constructed model some "design-rules" can be established for the pH-dependent modification of the MIP. A MIP with a different pKa value might allow for binding of histamine at a pH of 5. Only one input parameter was used in the model that is constructed in this section, being the pKa value of the relevant molecules. This model can now be easily used to find a pKa value for which binding would still occur at a pH of 5, or by single or by double hydrogen bonds. In Table 5-8 the most right column contains the percentage of the molecules that can establish zero hydrogen bonds. These molecules can not contribute to the binding process. For the actual pKa value of the MIP of 6.5, it is calculated that at pH 5 92% of the histamine molecules can not bind to the MIP. With this model it has been found that with a higher pKa value of the MIP an even higher percentage can not bind to the MIP at pH 5. However, decreasing the pKa value of the MIP, also decreases the amount of molecules that cannot bind. By means of a MIP with a pKa value of 5.5, 5.9% of the molecules can establish double hydrogen bonds and already 36.8% binds

through single hydrogen bonds. The results are also represented in a graph in Figure 5-9.

pKa	2 H bonds	1 H bond	0 H bond
7	0.000	0.032	0.968
6.5	0.001	0.070	0.928
6	0.009	0.174	0.817
5.5	0.059	0.368	0.572
5	0.250	0.500	0.250
4.5	0.572	0.368	0.059
4	0.817	0.174	0.009

Table 5-8: Formation of hydrogen bonds at pH 5.

As impedance spectroscopy is a very sensitive method of detection, this amount of binding is enough to be distinguished impedimetrically. Nevertheless, lowering the pKa value of the MIP, increases the number of hydrogen bonds that might be established. A MIP with a pKa value of 5 could be used to detect histamine in a pH of 5. The lower the pKa value, the better the histamine binding is established and detected.

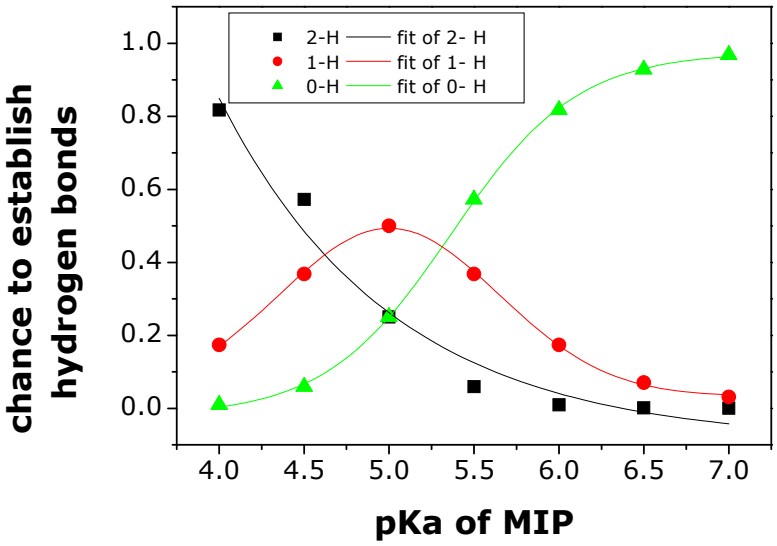

Figure 5-9: Prevalence of hydrogen bonds as function of the pKa value of the MIP.

In collaboration with the chemistry department, work can now be initiated for the development of a MIP with a pKa value of 5.5 or preferably even lower.

5.5 Conclusion

The detection of the MIP-based sensor is affected by the pH of the environment. Although the MIP can withstand a wide range of pH values, the pH of the electrolyte affects protonation or deprotonation of the target molecule and the MIP. This has a substantial impact on the formation of hydrogen bonds, which are needed for binding of the target molecule to the MIP. A novel model has been established to verify the impedimetric results. This model is useful for adapting this type of MIP-based sensor for the use in lower pH values. The protonation of histamine is a given, with a fixed pKa value. However, finetuning of the pKa value of the MIP creates a situation that allows for the formation of hydrogen bonds at lower pH values. This makes it possible for histamine to be impedimetrically detected at low pH conditions by means of synthetic receptors.

6 Conclusions & Outlook

In this thesis a sensor is developed for the detection of histamine or tryptase. These are two compounds which play an important role in IBS. Upon a physical or emotionally stressful event, the mast cells in the bowel will degranulate. Thereby the substances histamine and tryptase are released, which have a negative impact on the bowel system.

A first step towards this sensor was to develop biosensors with a biological recognition element. Immunoglobulins have been used for the development of immunosensors for the detection of 2 antigens, tryptase and for histamine. As proof-of-principle, the tryptase immunosensor detected 100 pmol/ml with a signal response of 10 % in buffer. The detected concentration of 100 pmol/ml tryptase corresponds to physiologically relevant concentrations. As opposed to tryptase, the direct impedimetric detection of histamine was complicated by the small size of the molecule. However, a successful sensor was created using interdigitated electrodes, allowing to measure closer to the surface. This way, the signal is optimized and the little information about histamine binding can be found within the signal. By means of IDE's, low-molecular weight molecules can now be impedimetrically detected with a direct assay. The detection of 50 nmol/ml histamine by their antihistamines caused a 10 % increase in impedance. IDE's are proven to be beneficial for use in future electronic sensing of tryptase and histamine. However, reproducibility was hampered due to several elements. Firstly, physical adsorption was not an adequate immobilization method of the immunoglobulines onto the polymer transducer layer. New methods for the covalent attachment of antibodies to polymer are under development. Secondly, it was shown by AFM and contact angle measurements that the polymer itself is attacked by the buffer solution after a period of time, causing instabilities during the measurements. This will be solved in the future by a new generation of conjugated polymers, specially designed to withstand aqueous solutions and with the possibility to bind immunoglobulin-type antibodies covalently to functional side chains.

The second step was to replace the biological recognition element by a chemical one, which can be described as a biomimetic receptor. As histamine is a low-molecular weight molecule, it is very suitable for the development of a Molecularly Imprinted Polymer (MIP) towards the detection of histamine. MIPs with high affinity and specificity towards histamine have been successfully developed by the Organic and Polymeric Chemistry group. These synthetic receptors have been implemented in a MIP-based sensor. Concentrations in the millimolar range can be detected using Quartz Crystal Microbalance (QCM). Even more, the impedimetric sensor can detect concentrations in the nanomolar range. The sensor has a limit of detection of 2 nM. The sensitivity is 45 % to 10 nM histamine, although this result is sample dependent. A dose response curve is measured in the 0 - 12 nM range. Sensor-response id widely linear for concentrations up to 9~10 nmol/l and becomes sub-linear for higher concentrations, indicating that the output tends towards saturation. Tests with the resembling molecule histidine, which is a precursor of histamine, show no significant sensor response. Thereby the specificity is confirmed.

When a sensor for the detection of histamine in bodily fluids or in the intestines is developed, the pH of the environment is an important factor to be considered as the third step in the development of an intestinal sensor for the detection of histamine. The sensor was tested under various pH environments between pH 5 and pH 11. Although MIPs can withstand a whole range of pH values, there functionality is affected by the pH of the electrolyte. Histamine and the MIP itself can be protonated or deprotonated at certain positions, influencing the number of hydrogen bonds that can be established. With a combinatory model this effect is envisaged. The model accounts for all possible protonated and deprotonated positions and corresponds qualitatively with the sensor output, measured in a range of pH 5 to 12.

For future application of the sensor in acid environments, which bodily fluids usually are, fine-tuning of a MIP is possible. Altering the pKa of the MIP can create possibilities for the establishment of hydrogen bonds at lower pH values. For future work on the sensor development other research goes to the use of the polymer film PPV. This material causes not only immobilization problems for antibodies, but also reproducibility problems when measuring impedimetrically,

and problems in the modeling of the measured data. Currently the option is tested for applying the MIP precursor directly onto electrode material without the use of the polymer transducer layer. Dipcoating of wire electrodes in MIP-precurser followed by polymerization of the MIP on the electrode-wires is one possibility. Another option is electropolymerization on wire electrodes. Wire-shaped electrodes are first choice for integration of active electrodes, together with reference electrodes, in existing catheders for intestinal studies. Typically, the inner diameter of these catheders is 3 mm only, putting stringent boundary conditions on the final sensor dimensions, keeping also in mind that the sensors are best to be integrated with a miniaturized pH electrode. Also, PMMA, the polymer imprinted to create the MIP in this thesis, is biocompatible. It is therefore suitable for *in vivo* applications, or, in a first step, intestinal applications.

In this work the first steps are made towards a sensor for the detection of histamine. However, a lot more steps are yet to follow before the medicinal world can get to the bottom of IBS and bring relief to the many IBS patients that are suffering every day

References

[1] P. Cooreman, R. Thoelen, J. Manca, M. vandeVen, V. Vermeeren, L. Michiels, M. Ameloot, and P. Wagner, *Biosensors and Bioelectronics* **20,** 2151-2156 (2005).

[2] V. Vermeeren, N. Bijnens, S. Wenmackers, M. Daenen, K. Haenen, O.A. Williams, M. Ameloot, M. vandeVen, P. Wagner, L. Michiels, *Langmuir* **23**, 13193- 13202 (2007).

[3] E. Eltzov, R. Marks, S. Voost, B. A. Wullings, and M. B. Heringa, *Sensors and Actuators B,* article in press (2009).

[4] M. Pohanka, P. Skladal, and M. Kroca, *Def. Sci. J.* **57,** 185-193 (2007).

[5] W.G. Thompson, G.F. Longstreth, D.A. Drossman, K.W. Heaton, E.J. Irvine, S.A. Muller-Lissner, *Gut* **45**, 1143-1147 (1999).

[6] C.J. DeLor, *Am. J. Gastroenterol.* **47**, 427-434 (1967).

[7] J. Santos, E. Saperas, C. Nogueiras, M. Nourelle, M. Antolin, A. Cadahia, J.R. Malagelada, *Gastroenterology* **114**, 640-648 (1998).

[8] G. Barbara, V. Stanghellini, R. De Giorgio, C. Cremon, G.S. Cottrell, D. Santini, G. Pasquinelli, A.M. Morselli-Labate, E.F. Grady, N.W. Bunnett, S.M. Collins, and R. Corinaldesi, *Gastroenterology* **126**, 693-702 (2004).

[9] R.Y. Lin, L.B. Schwartz, A. Curry, G.R. Pesola, R.J. Knight, H.S. Lee, L. Bakalchuk, C. Tenenbaum, and R.E. Westfal, *J. Allergy Clin. Immunol.* **106**, 65-71 (2000).

[10] J. Chhabra, Y-Z. Li, H. Alkhouri, A.E. Blake, Q. Ge, C.L. Armour, and J.M. Hughes, *Eur. Respir. J.* **29**, 861-870 (2007).

[11] M. Adlesic, M. Verdrengh, M. Bokarewa, L. Dahlberg, S.J. Foster, A. Tarkowski, *Scand. J. Immunol*. **65**, 530-537 (2007).

[12] D.A. Drossman, Z. Li, E. Andruzzi et al. *Dig. Dis. Sci.* **38**, 1569-1580 (1993).

[13] M. Camilleri, M.G. Choi, *Aliment. Pharmacol. Ther*. **11**, 3-15 (1997).

[14] R.S. Sander, *Gastroenterology* **99**, 409-415 (1990).

[15] D.A. Drossman, W.E. Whitehead, M. Camilleri, *Gastroenterology* **112**, 2120-2137 (1997).

[16] D.A. Drossman, W.G. Thompson, *Ann. Intern. Med*. **116**, 1009-1016 (1992).

[17] A. Manning A, W. Thompson W, K. Heaton K, and A. Morris, *Br. Med. J.* **2** 653–654 (1978).

[18] P.M. Boyce, N.J. Talley, C. Burke, N.A. Koloski, *Intern. Med. J.* **36**, 28-36 (2006).

[19] P.L. Lee, *Korean J. Gastroenterol.* **47**, 94-100 (2006).

[20] T.T. Ashburn, M.S. Gupta, The IBS Market. *Nat. Rev. Drug Discov*. **5**, 99-100 (2006).

[21] S. Maxion-Bergemann, F. Thielecke, F. Abel, R. Bergemann*, PharmacoEconomics* **24**, 21-37 (2006)

[22] Project application Impuls financing "Intestinal histamine sensor", transnational University Limburg.

[23] P.A. Shore, A. Burkhalter, V.H. Cohn Jr., *J. Pharmac. exp. Ther.* **127**, 182-186 (1959).

[24] W. Lorenz, H.J. reimann, H. Barth, J. Kusche, R. Meyer, A. Doenicke, M. Hutzel, *Hoppe-Seyler's Z. Physiol. Chem.* **353**, 911-920 (1972).

[25] P.A. Shore, A. Burkhalter, V.H. Cohn Jr., *J. Pharmacol. Exp. Ther*. **127**, 182-186 (1959).

[26] R.P. Siraganian, *J. Immunol. Methods* **7**, 283-290 (1975).

[27] Y. Tsuruta, K. Kohashi, and Y. Ohkura, *Journal of Chromatography* **146**, 490-493 (1978).

[28] M.A. Beaven, S. Jacobsen, Z. Horakova, *Clinica Chim. Act*a **37**, 91-103 (1972).

[29] J.J. Keyzer, B.G. Wolthers, F.A.J. Muskiet, H. Breukelman, H.F. Kauffman, and K. de Vries, *Analytical Biochemistry* **139**, 474-481 (1984).

[30] V. Van Vietinghoff, G. Gäbel, J. R. Aschenbach, *J. Chromatogr. B.* Analyt. Technol. Biomed. Life Sci. **844**, 335-339 (2006).

[31] F. Nishiwaki, K. Kuroda, Y. Inoue, G. Endo, Biomed. *Chromatogr.* **14**, 184-187 (2000).

[32] H. Mita, H. Yasueda, T. Shida, S. Baba, *Agents and Actions* **14**, 5/6 (1984).

[33] H.L. Waldum, A.K. Sandvik, E. Brenna, B. Schulze Sognen, *Scand. J. Gastroenterol. Suppl.* **180**, 32-39 (1991).

[34] M. Yamaguchi, K. Sayama, K. Yano, C.S. Lantz, N. Noben-Trauth, C. Ra, J.J. Costa, S.J. Galli, *J. Immunol.* **162**, 5455-5465 (1999).

[35] A.W. Van Toorenenbergen and A.M. Vermeulen, *Inflammation Research* **30**, 278-280 (1990).

[36] B. Rotz, A. Savaser, I. Werthmann, S. Lau, and U. Wahn, *Allergy* **46**, 529 (1991).

[37] A. Ujike, Y. Ishikawa, M. Ono, T. Yuasa, T. Yoshino, M. Fukumoto, J.V. Ravetch, T. Takai, *J. Exp. Med.* **189**, 1573-1578 (1999).

[38] S. Wenzel, A.M. Irani, J.M. Sanders, T.R. Bradford, L.B. Schwartz, *J. Immunol. Meth.* **86**, 139-142 (1986).

[39] I. Enander, P. Matsson, J. Nystrand, A.S. Andersson, E. Eklund, T.R. Bradford, L.B. Schwartz, *J. Immunol. Methods* **138**, 39-46 (1991).

[40] E. Edston, M. Van Hage-Hamsten, *Forensic Science International* **93**, 135-142 (1998).

[41] L.B. Schwartz, T.R. Bradford, C. Rouse, A.M. Irani, G. Rasp, J.K. van der Zwan, P.W. van der Linden, *J. Allergy Clin. Immunol.* **14**, 190-204 (1994).

[42] M.A. Beaven, *Monogr. Allergy* **13**, 1-113 (1978).

[43] P.J.B. Pereira, A. Bergner, S. Macebo-Ribeiro, R. Huber, G. Matschiner, H. Fritz, C.P. Sommerhoff, and W. Bode, *Nature* **293**, 306-311 (1998).

[44] J. Hallgren and G. Pejler, *FEBS Journal* **273**, 1871-1895 (2006).

[45] C.P. Sommerhoff, W. Bode, P.J.B. Pereira, M.T. Stubbs, J. Stürzebecher, G.P. Piechottka, G. Matschiner, and A. Bergner, *Proc. Natl. Acad. Sci. USA* **96**, 10984-10991 (1991).

[46] J. Chen, J.B. Anderson, C. DeWeese-Scott, N.D. Fedorova, L.Y. Geer, S. He, D.I. Hurwitz, J.D. Jackson, A.R. Jacobs, C.J. Lanczycki, C.A. Liebert, C. Liu, T. Madej, A. Marchler-Bauer, G.H. Marchler, R. Mazumder, A.N. Nikolskaya, B.S. Rao, A.R. Panchenko, B.A. Shoemaker, V. Simonyan, J.S. Song, P.A. Thiessen, S. Vasudevan, Y. Wang, R.A. Yamashita, J.J. Yin, and S.H. Bryant, *Nucleic Acids Res.* **31**, 474-477 (2003).

[47] W. Schramm, S.-H Paek, and G. Voss, ImmunoMethods **3,** 93-103 (1993).

[48] L. Vroman and A.L. Adams, J*ournal of colloid and interface science* **111**, 391-402 (1986).

[49] J.N. Lin, J.D. Andrade, and I.N. Chang, *Journal of Immunological Methods*, **125**, 67-77.(1989).

[50] H. Shirakawa, E.J. Louis, A.G. MacDiarmid, C.K. Chiang, and A.J. Heeger, *J. Chem. Soc. Chem. Commun.* **16**, 578-580 (1977).

[51] H.S. Nalwa, Handbook of Organic Conductive Molecules and Polymers, Wiley, New York (1997).

[52] J.L. Bredas, J.C. Scott, K. Yakushi, and G.B. Street, *Phys. Rev. B* **30**, 1023-1025 (1984).

[53] B. Wessling, *Synth. Met*. **85,** 1313-1318 (1997).

[54] T. Martens, J. D'Haen, T. Munters, Z. Beelen, L. Goris, J. Manca, M. D'Olieslaeger, D. Vanderzande, L. De Schepper and R. Andriessen, *Synth. Met.* **138**, 243–247 (2003).

[55] T. Munters, T. Martens, L. Goris, V. Vrindts, J. Manca, L. Lutsen, W. De Ceuninck, D. Vanderzande, L. De Schepper, J. Gelan, N.S. Sariciftci, and C.J. Brabec, *Thin Solid Films* **403**, 247–251 (2002).

[56] F. Louwet, D. Vanderzande, J. Gelan, and J. Mullens, *Macromolecules* **28**, 1330-1331 (1995).

[57] H. Neugebauer, M.A. Loi, C. Winder, N. Serdar Sariciftci, G. Cerullo, A. Gouloumis, P. Vazquez, and T. Torres, *Solar Energy Materials & Solar Cells* **83**, 201–209 (2004).

[58] V.B. Kandimalla and H. Ju, *Anal. Bioanal. Chem.* **380**, 587-605 (2004).

[59] K. Yano and I. Karube, *Trends Anal. Chem.* **18**, 199-204 (1999).

[60] P.K. Owens and L. Karlsson, *Trends Anal. Chem* **18**, 146-154 (1999).

[61] S.A. Piletsky, S. Alcock, and A.P.F. Turner, *Trends in Biotechnology* **19**, 9-12 (2001).

[62] K. Haupt and K. Mosbach, *Trends Biotechnol.* **16**, 468–475 (1998).

[63] K. Haupt and K. Mosbach, *Chem. Rev*. **100**, 2495–2504 (2000).

[64] S.A. Piletsky, N.W. Turner, and P. Laitenberger, *Medical Engineering & Physics* **28**, 971-977 (2006).

[65] F.L. Dickert, P. Lieberzeit, S.G. Miarecka, K.J. Mann, O. Hayden, and C. Palfinger, *Biosensors & Bioelectronics* **20**, 1040–1044 (2004).

[66] F.L. Dickert, P. Lieberzeit, and M. Tortschanoff, *Sensors and Actuators B* **65**, 186-189 (2000).

[67] K. Haupt, *Anal. Chem* **1**, 376-83 (2003).

[68] R. Thoelen, R. Vansweevelt, J. Duchateau, F. Horemans, J. D'Haen, L. Lutsen, D. Vanderzande, M. Ameloot, M. vandeVen, T.J. Cleij, P. Wagner, *Biosensors and Bioelectronics* **23** 913–918 (2008).

[69] M.C. Blanco-López, M.J. Lobo-Castañón, A.J. Miranda-Ordieres, and P. Tuñón-Blanco, *Trends in Analytical Chemistry* **23**, 36-47 (2004).

[70] M. Avila, M. Zougagh, A. Rios, and A. Escarpa, *Trends in Analytical Chemistry* **27**, 54-65 (2008).

[71] S.A. Piletsky, E.V. Piletskaya, A.V. El'skaya, R. Levi, K; Yano, and I. Karube, *Analytical Letters* **30**, 445-455 (1997).

[72] Y.G. Tan, J. Yin, C.D. Liang, H. Peng, L.H. Nie, and S.Z. Yao, *Bioelectrochemistry* **53**, 141–148 (2001).

[73] P. van Gerwen, W. Laureyn, W. Laureys, G. Huyberechts, M. Op De Beeck, K. Baert, J. Suls, W. Sansen, P. Jacobs, L. Hermans, and R. Mertens, *Sens. and Act. B* **49**, 73-80 (1998).

[74] W. Laureyn, D. Nelis, P. Van Gerwen, K. Baert, L. Hermans, R. Mangée, J.-J. Pireaux, and G. Maes, *Sens. and Act. B* **68**, 360-370 (2000).

[75] F. Hooreman, J. Alenus, E. Bongaers, A. Weustenraed, R. Thoelen, J. Duchateau, L. Lutsen, D. Vanderzande, P. Wagner, and T.J. Cleij, *Biosensors &Bioelectronics,* submitted.

[76] F. Exl and J. Kindersberger, *Proceedings of the XIVth International Symposium on High Voltage Engineering.D* **47**,1 -5 (2005).

[77] G. Binning, C.F. Quate, and C. Gerber, *Phys. Rev. Lett*, **56**, 930-933 (1986).

[78] R. Howland and L. Benatar, A practical guide to scanning probe microscopy, Park Scientific Instruments (1997).

[79] P.P. Lehenkari, G.T. Charras, S.A. Nesbitt, and M.A. Horton, Expert *Reviews in Molecular Medicine* **2**, 1-19 (2000)

[80] J.R.MacDonald, Impedance Spectroscopy, John Wiley & Sons, New York, (1987).

[81] S. Grimnes and O. Martinsen, Bioimpedance and Bioelectricity Basics. 2000, London: Academic Press.

[82] E. Bongaers, J. Alenus, L. Grieten, P. Wagner, F. Troost, and R.-J. Brummer, *Physicalia Magazine* **29,** 123-131 (2007).

[83] S. Wenmackers, P. Christiaens, M. Daenen, W. Deferme, K. Haenen, M. Nesladek, P. Wagner, V. Vermeeren, L. Michiels, M. VandeVen, M. Ameloot, J. Wouters, L. Naelaerts, Z. Mekhalif, *Mater. Sci. Forum* **267**, 492-493 (2005).

[84] S Wenmackers, P. Christiaens, M. Daenen, K. Haenen, M. Nesládek, M. vandeVen, V. Vermeeren, L. Michiels, M. Ameloot, and P. Wagner, *Phys. Stat. Sol. (a)* **202**, 2212-2216 (2005).

[85] P Christiaens, V. Vermeeren, S. Wenmackers, M. Daenen, K. Haenen, M. Nesladek, M. vandeVen, M. Ameloot, L. Michiels, and P. Wagner, *Biosens. Bioelectron.* **22,** 170-177 (2006).

[86] D. Chevrier, J.-L. Guesdon, J.-C. Mazié, S. Avrameas, *J. of Immunol. Meth*. **94**, 119-125 (1986).

[87] E.J. Claret, J. Ouled-Diaf, and P. Seguin, *Comb. Chem. & High Throughput Screening* **6**, 789-794 (2003).

[88] W. Laureyn, F. Frederix, P. Van Gerwen, G. Maes, Transducers '99, *Digest of Technical Papers*, Sendai, Japan 1884-1885 (1999).

[89] R.J. Umpleby, M. Bode, and K.D. Shimizu, *Analyst* **125**, 1261–1265 (2000).

[90] D.A. Spivak, *Adv. Drug Deliv. Rev.* **57**, 1779–1794 (2005).

[91] H. Freundlich, *Z. Phys. Chem.* **57**, 385–470 (1906).

[92] K. Reimhult, K. Yoshimatsu, K. Risveden, S. Chen, L. Ye, and A. Krozer, *Biosens. Bioelectron.* **23**, 1908-1914 (2008).

[93] G. Sauerbrey, *Z. Phys.* **155**, 206-222 (1959).

[94] E. Bongaers, J. Alenus, F. Horemans, A. Weustenraed, L. Lutsen, D. Vanderzande, T. Cleij, F.J. Troost, R.-J. Brummer, and P. Wagner, *Phys. Stat. Sol (a),* submitted September 2009.

[95] T.B. Paiva, M. Tominaga, and A.C.M. Paiva, *Journal of Medicinal Chemistry* **13**, 689-692 (1970).

[96] H.A. De Abreu, W. B. De Almeida, and H.A. Duarte, *Chemical Physics Letters* **383**, 47-52 (2004).

[97] L. Alderighi, P. Gans, A. Ienco, D. Peters, A. Sabatini, and A. Vacca, *Coordination Chemistry Reviews* **184**, 311–318 (1999).

[98] V.A. Izumrudov, E. Kharlampieva, and S.A. Sukhishvili, *Biomacromolecules* **6**, 1782-1788 *(*2005).

Appendix 1 : Nomenclature

AIBN	Azobisisobutyronitrile
AFM	Atomic Force Microscopy
C	Capacitor
C_{dl}	double layer capacitance
CE	capillary electrophoresis
C_p	polymer capacitance
CPE	Constant Phase Element
Da	Dalton
DMSO	dimethylsulfoxide
EGDM	Ethylene glycol dimethacrylate
EIS	Electrochemical Impedance Spectroscopy
ELISA	Enzyme-Linked Immunosorbent Assay
HCG	human chorionic gonadotropin
HPLC	High-performance liquid chromatography
IBS	Irritable Bowel Syndrome
IDE	Interdigitated Electrodes
Ig	Immunoglobulin
IC-AFM	Intermittent Contact Atomic Force Microscopy

L	Inductance
MAA	Methacrylic acid
MIP	Molecularly Imprinted Polymer
NC-AFM	Non Contact Atomic Force Microscopy
NIP	Non-imprinted Polymer
PBS	Phosphate Buffered Saline solution
PDMS	polydimethylsiloxane
PMAA	Polymethacrylate
PPV	Polyphenylene vinylene
R	Resistance
R_{ct}	Charge transfer resistance
RIA	Radioimmunoassay
R_p	Polymer resistance
R_s	Solution resistance
W	Warburg element
wt%	Weight percentage

Appendix 2: List of figures

Appendix 3: List of tables

Appendix 4: Publications & Conference contributions

Publications

- **E. Bongaers**, J. Alenus, F. Horemans, J. Duchateau, L. Lutsen, D. Vanderzande, T. Cleij, F.J. Troost, R.-J. Brummer and P. Wagner, A MIP-based biomimetic sensor for the impedimetric detection of histamine in different pH environments, Phys Stat Sol (a), submitted.

- J. Alenus, R. Thoelen, **E. Bongaers**, J; Duchateau, F. Hooreman, L. Lutsen, D. Vanderzande, T.J. Cleij, and P. Wagner, Piezoelectric detection of Small Molecules sing synthetic MIP-based receptors, Physicalia Magazine 2010, in preparation.

- F. Horemans, J. Alenus, **E. Bongaers**, A. Weustenraed, R. Thoelen, J. Duchateau, L. Lutsen, D. Vanderzande, P. Wagner, and T.J. Cleij, MIP-based sensor platform for the detection of histamine in the nano and micro molar range in aqueous media, Biosensors & Bioelectronics, submitted.

- **E. Bongaers**, J. Alenus, L. Grieten, P. Wagner, F. Troost, R.-J. Brummer, Development of a Biosensor for the Detection of Histamine and Tryptase. Physicalia Magazine 29 (3), pp 123-131 (2007).

Oral contribution:

- **E. Bongaers**, J. Alenus, F. Horemans, J. Duchateau, L. Lutsen, D. Vanderzande, T. Cleij, F.J. Troost, R.-J. Brummer and P. Wagner, A MIP-based sensor for the impedimetric detection of histamine in an intestinal environment, Engineering of Functional Interfaces, ENFI 18-19 June 2009, Hasselt (Belgium)

Posters:

- **E. Bongaers**, J. Alenus, F. Horemans, J. Duchateau, L. Lutsen, D. Vanderzande, T. Cleij, F.J. Troost, R.-J. Brummer and P. Wagner, A MIP-based sensor for the impedimetric detection of histamine in an intestinal environment, Engineering of Functional Interfaces, 18-19 June 2009, Hasselt (Belgium).

- **E. Bongaers**, J. Alenus, F. Hooremans, P. Wagner, F. Troost, R.-J. Brummer, a MIP-based Biosensor for the Detection of Histamine , Joint General Scientific Meeting of the Belgian Physical Society and Belgian Biophysical Society, Hasselt, (Belgium) April 1st 2009.

- J. Alenus, R. Thoelen, **E. Bongaers**, J. Duchateau, F. Hooreman, L. Lutsen, D. Vanderzande, T.J. Cleij, P. Wagner, Piezoelectric detection of Small Molecules using synthetic MIP-based receptors. Joint General Scientific Meeting of the Belgian Physical Society and Belgian Biophysical Society, Hasselt, (Belgium) April 1st 2009.

- **E. Bongaers**, J. Alenus, L. Grieten, P. Wagner, F. Troost, R.-J. Brummer, Development of Impedimetric Immunosensors for the label-free detection of Histamine and tryptase in a direct assay, Tenth World Congress on Biosensors, Shanghai (China), 30th April 2008.

- **E. Bongaers**, L. Grieten, J. Alenus, P. Wagner, F. Troost, R.-J. Brummer, Development of a Biosensor for the Detection of Histamine and Tryptase, Joint General Scientific Meeting of the Belgian Physical Society and Belgian Biophysical Society, Antwerp, (Belgium), 30th May 2007.

A MIP-based sensor for the impedimetric detection of histamine for intestinal application

E. Bongaers[1], J. Alenus[1], F. Horemans[1], J. Duchateau[1], L. Lutsen[2], D. Vanderzande[1,2], T. Cleij[1], F. J. Troost[3], R.-J. Brummer[3] and P. Wagner[1]

1)Institute for Materials Research, Hasselt University, Wetenschapspark 1, 3590 Diepenbeek, Belgium
2) IMEC, Division IMOMEC, Wetenschapspark 1, B-3590 Diepenbeek, Belgium
3) Nutrition and Toxicology Research Institute Maastricht (NUTRIM), Maastricht University, Universiteitssingel 50, 6229 ER Maastricht, The Netherlands

Introduction

The Irritable Bowel Syndrome (IBS) is characterized by visceral hypersensitivity. The pathogenesis is poorly understood, but there is evidence that upon activation mast cells release histamine. The limited accessibility of the intestine makes it difficult to measure this mast cell activation. Therefore a miniaturized sensor for the detection of histamine in the intestine is developed using Molecularly Imprinted Polymers (MIPs). These polymers contain nanocavities with the exact shape, size and functional groups (hydrogen bridges) complementary to histamine. Upon presence of histamine it will be bound to the nanocavities thereby changing the dielectric properties of the MIP. These electrical changes are measured using impedance spectroscopy. For the envisaged intestinal applications the sensor is tested in both acid and basic environments.

A MIP-based sensor...

- **Target molecules:**
  - histamine
  - histidine

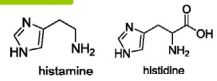

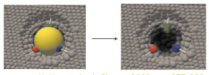

K. Haupt, Anal. Chem., 2003, pp. 377-383

Coplanar electrodes (200µm)

- **Sensor setup:**
  - Electrodes: 70nm Al coplanar electrodes
  - Transducer layer: coated with 100nm MDMO-PPV, a semiconducting polymer.
  - Recognition element: MIPS are immobilised via stamping and baking (10 min @ 120°C).
  - Integration in addition setup: four-channel cell for simultaneous reference measurements with Non-Imprinted Polymers (NIP).

Addition setup

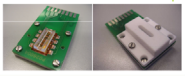

- **Electrochemical Impedance Spectroscopy:**
  - Impedance is measured as function of frequency from 1 Hz to 1 kHz.
  - electrical changes at the interface can be seen at low frequencies (@ 113 Hz)
  - An addition set-up is used @ 37°C

...for the impedimetric detection of histamine...

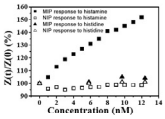

At low frequencies (113 Hz):

- **Sensitivity**: - Histamine MIP shows 30% response to 10 nM Histamine.
- Histamine NIP shows no significant response to Histamine
- **Specificity** confirmed by histidine : MIP and NIP show no significant response
- The **limit of detection** is 2 nM, below typical physiological conditions within mast cells around 200 nM.

...for intestinal application

Histamine can absorb protons from its solution at 2 different sites.

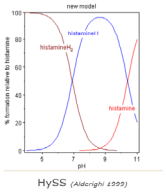

HySS (Alderighi 1999)

- Below pH 10.4 most of the present histamine will have absorbed one proton. It is now single protonated histamine.
- The MIP is made at neutral pH, meaning it is created towards the single protonated molecule.
- In an acidic buffer (pH 5) almost all histamine molecules are protonated and cannot be detected anymore illustrating the specificity of the MIP.
- In a basic environment (pH 9) neutral histamine is predominant improving the sensor sensitivity.

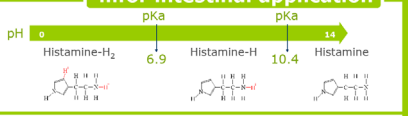

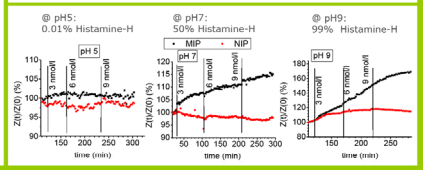

Conclusion

A sensor for the detection of histamine in the intestine is has been succesfully developed. Using Molecularly Imprinted Polymers (MIPs) the sensor can impedimetrically detect histamine with a detection limit of 2nM. In pH neutral environments the sensitivity is 30% to 10nM histamine and specificity is tested with respect to histidine, showing no significant sensor response. A dose response curve is measured in the 0-10 nM range. The histamine detection is strongly dependent on the pH of the environment due to protonation of histamine. In more basic environments (pH9) the sensitivity increases. In more acidic environments (pH5) approximately 100% of the histamine molecules are protonated to which the sensor shows no response, thereby confirming the specificity of the sensor.

Acknowledgements

This research is funded by the School for Life Sciences, part of the transnational University Limburg. The authors would like to thank L. Michiels for his help and advice and Peter Gans from Protonic Software for his assistance with HySS.

universiteit hasselt | transnationale UNIVERSITEIT LIMBURG | Universiteit Maastricht | nutrim

An Impedimetric MIP-based Sensor for the Detection of Histamine

E. Bongaers[1)], J. Alenus[1)], F. Horemans[1)], T. Cleij[1)], F. Troost [2)], R.-J. Brummer[2)] and P. Wagner [1)]

1)Institute for Materials Research, Hasselt University, Wetenschapspark 1, 3590 Diepenbeek, Belgium
2) Gastroenterology & Hepatology, dept. of Internal Medicine, Nutrition and Toxicology Research Institute Maastricht (NUTRIM), Maastricht University, Universiteitssingel 50, 6229 ER Maastricht, The Netherlands

Introduction

The Irritable Bowel Syndrome (IBS) is characterized by visceral hypersensitivity. The pathogenesis is poorly understood, but there is evidence that mast cells are involved in this process. Mast cells degranulate upon activation, and release histamine, tryptase and other compounds. The accessibility of the intestine makes it difficult to measure this intestinal mast cell activation *in vivo*. Therefore a sensor for the detection of histamine *in vivo* in the intestine is developed using Molecularly Imprinted Polymers (MIP). These polymers contain nanocavities in the exact shape of a histamine molecule. Upon presence of histamine it will be bound to the nanocavities thereby changing the dielectric properties of the MIP. These electrical changes are measured using impedance spectroscopy.

Materials & Methods

- Sensor preparation:
  - 4 coplanar aluminum electrodes
  - coated with the polymer MDMO-PPV
  - Immobilisation of MIP & NIP microparticles on the polymer : embedding (10 min @ 120°C)
  - A dilution series of histamine is made with phosphate buffered saline (PBS)

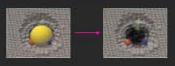

K. Haupt, Anal. Chem., 2003, pp. 377-383

Histamine

Coplanar electrodes (200mm)

- Sensor setup: The MIP-sensitized electrodes are integrated in an addition setup, which consists of a PCB with a 500 µL reservoir. allowing for simultaneous reference measurements with Non-Imprinted Polymers (NIP).

Addition setup

- Electrochemical Impedance Spectroscopy: For each sensing spot, spectra were measured sequentially at a low-frequency range from 1Hz to 1 kHz with zero bios voltage and an oscillating voltage of 50 mV, at 37°C

Biosensing

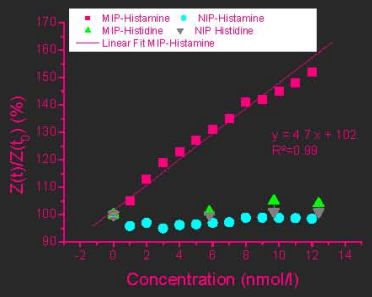

- Time-resolved analysis of the spectra occurred at a low frequency (213 Hz) where the sensor is more sensitive for surface interactions between the MIP binding sites and the target molecules.
- For a dose response curve the histamine concentrations were increased per 1 nM in a 0 to 12 nM range. The concentrations of histidine were increased in unequal steps of 5.8 nM, 9.7 nM and 12.4 nM.
- All impedance data are normalized relative to their initial impedance value, prior to addition of the target molecule.
- A response value is obtained 20 minutes after addition of the target molecule by averaging five data points. The error bars, which are thus a measure for the stability of the impedance signal, are smaller then the symbols utilized, indicating a low noise level.

Conclusion

The MIP sensor impedimetrically detects the low molecular weight molecule histamine. The limit of detection is 2 nM in agreement with physiological conditions around 200 nM. The sensitivity is 30% to 10nM histamine. A dose response curve is measured in the 0-10 nM range. Specificity was confirmed by tests with histidine, showing no significant change.

Acknowledgements

This research is funded by the School for Life Sciences , part of the transnational University Limburg. The authors would like to thank R. Thoelen and L. Michiels for their help and J. Bacchus for technical support.

Piezoelectric Detection of Small Molecules using Synthetic MIP-based Receptors

J. Alenus[a] , R. Thoelen[a], E. Bongaers[a], J. Duchateau[a], F. Horemans[a], L. Lutsen[b], D. Vanderzande[a], T.J. Cleij[a], P. Wagner[a].
a) Institute for Materials Research, Hasselt University, Diepenbeek, Belgium
b) IMEC, Division IMOMEC, Diepenbeek, Belgium

Introduction

Molecular Imprinted Polymers (MIPs) are becoming an important application in the world of biosensing. Especially non-covalent imprinting techniques are favorable because of the possibility of tailer-made, highly selective artificial receptors. They are synthesized by mixing the target molecule with an acrylic polymer. After UV hardening the monolith is crushed into micro-particles. After extraction of the analyte, nanocavities are left behind which can rebind the molecule by its size and functionality. In this recent work these synthetic receptors were implemented in a quartz crystal microbalance (QCM) sensing device for the detection of L-nicotine and histamine. The QCM showed a high selectivity for the target molecule in the micro-molar range. Recent work also showed the possibility of the QCM to monitor the binding characteristics of the MIPs.

QCM

Piëzo-electricity is a technique which is apprehended to investigate the binding of the target molecule to the MIP. In order to detect the target molecule, MIP micro-particles are stamped on a PVC layer, which is subsequently heated in order to sink the MIPs into the layer. When the transducer layers cools down, the MIPs are trapped. A 5 MHz quartz crystal coated with PVC and stamped with MIP micro particles is used for the detection of the L-nicotine and histamine. The resonance frequency is altered with the binding of the analyte to the MIP. Measurements are carried out with the aid of a flow system setup or a static setup. The flow system setup was used for detection of L-nicotine and histamine by exposing the sensor to an increasing concentration of the target molecule. The static setup was used for comparing different kind of L-nicotine MIPs.

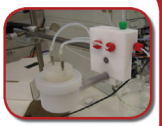

Results

L-Nicotine was measured with an increasing concentration from 50 to 300 µM. Binding of the L-nicotine to the MIP occurs in a linear fashion until the final concentration of 300 µM where the MIP is saturated with nicotine. Also a Non Imprinted Polymer (NIP) was exposed to the same concentrations. Here the small decrease in frequency can be attributed to aspecific binding of the L-nicotine to the NIP. This setup allows for detection of L-nicotine up to 250 µM and is insensitive for the resembling molecule L-cotinine.

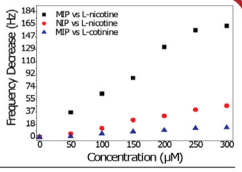

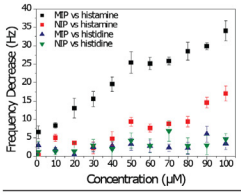

Histamine was measured with an increasing concentration from 1 to 100 µM. The frequency decrease is significantly greater for the MIP exposed to Histamine. Binding occurs in a linear fashion but doesn't go in saturation which suggests that the sensor could detect higher concentrations of histamine. The difference between the frequency decrease of the MIP and NIP at the concentration of 1 µM is slim, which means that lower concentrations cannot be measured with this setup. There is no difference between the binding of the resembling molecule histidine for the MIP or NIP but aspecific binding is higher for histamine to the NIP, especially at higher concentrations. The setup is able to detect histamine from 1 to 100 µM and is insensitive for histidine.

MIP comparison with the aid of the QCM is the next objective in this work. Different L-nicotine concentrations are measured with the new generation of L-nicotine MIPs. These measurements were performed in a static setup which allows more binding of the target molecule but as a drawback takes much longer to stabilize then the flow setup. As a reference the MIP (MIP17) used to collect the L-nicotine data above is also incorporated. It is obvious that the newer MIPs 121D and 121E can bind more L-nicotine. Not only do they bind more L-nicotine but it appears that they also bind the L-nicotine much faster. MIP195 on the other hand showed worse results then MIP17.

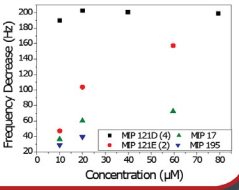

Conclusion

Using Piëzoelectric detection, it is possible to detect low-MW molecules by molecularly imprinted polymers on polymer carriers. This technique showed the possibility of detecting target molecules in the micro-molar range. The reference measurements with L-cotinine and histidine indicated a high specificity of the MIPs for L-nicotine and histamine respectively. Early tests with the new generation of L-nicotine MIPs show improved binding characteristics of the MIPs, which ultimatly will improve the sensitivity of the QCM sensor. As a new kind of sensor, the MIP-based QCM sensor could be useful for the detection of small molecules in the pharmaceutical, environmental, diagnostic and biotechnological sector.

In this project the work of J. Soogen, and J. Baccus is greatly acknowledged.

www.imo.uhasselt.be

Development of Impedimetric Immunosensors for the Label-Free Detection of Histamine and Tryptase in a Direct Assay

E. Bongaers[1)], J. Alenus[1)], L. Grieten[1)], P. Wagner[1)], F. Troost [2)] and R.-J. Brummer[2)]

1)Institute for Materials Research, Hasselt University, Wetenschapspark 1, 3590 Diepenbeek, Belgium
2) Gastroenterology & Hepatology, dept. of Internal Medicine, Nutrition and Toxicology Research Institute Maastricht (NUTRIM), Maastricht University, Universiteitssingel 50, 6229 ER Maastricht, The Netherlands

Introduction

Irritable Bowel Syndrome (IBS) is a gastrointestinal disorder which is associated with increased numbers of mast cells in the intestinal mucosa. These mast cells are involved in the pathogenesis of the disease, although the exact role of mast cell activation in IBS is still under investigation. There is ample evidence that mast cells degranulate upon activation, thereby releasing histamine, tryptase and other compounds. To verify the effectiveness of current therapies in vivo measurements need to be performed on the mucous membrane of the small intestine. The limited accessibility of the intestines however makes it difficult to measure this intestinal mast cell activation *in vivo*. Therefore an impedimetric immunosensor for the detection of histamine and tryptase *in vivo* is under development. For the low-molecular weight antigen histamine interdigital electrodes (IDE's) are used to increase sensitivity.

Materials & Methods

•Materials:
- Antigens: Tryptase (135 kDa) and histamine (111 Da)
- Antibodies IgG for tryptase and histamine.

•Sensor setup:
- Electrode material: - 50 nm TiN coplanar electrodes for tryptase
  - 100 nm Al interdigital electrodes (IDE) for histamine
- Coated with 100nm MDMO-PPV, a semiconducting polymer.
- Antibodies are immobilised using physical adsorption (1h @ 37°C). A 100pmol/ml solution is used for biosensor samples.

• Electrochemical Impedance Spectroscopy:
- Impedance is measured as function of frequency from 100 Hz to 1 MHz.
- An addition set-up is used at room temperature.

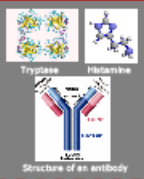

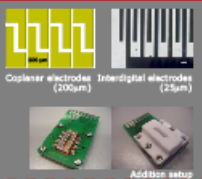

Characterisation

- **Contact angle**

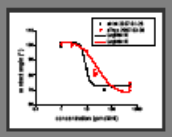

-PPV surface is hydrophobic (>90°).

-Incubating antibodies on PPV renders the film hydrophilic (<90°).

- This indicates the succesfull adsorption of Ab to polymer, according to the Vroman effect.

- The logistic fits show that at a concentration of 100pmol/ml the Ab adsorption is saturated.

- **AFM**

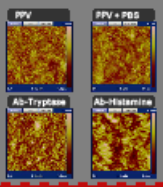

Incubation with PBS causes little swelling of the polymer. With AFM the receptor molecules can be visualised. The yellow structures are clusters of antibodies.

Physical adsorption profiles show that the antibodies for histamine and tryptase are succesfully immobilised on a polymer surface.

Biosensing

- **Impedance Spectroscopy**

Bodeplots before and after the addition of 50nmol/ml histamine are compared. The difference in amplitude signal is plotted for 3 electrodes (Al/PPV/ PPV functionalised with anti-histamine):

- The functionalised anti-histamine electrode shows a change in Z at low frequencies. This sensing effect is due to a change in surface capacity and charge transfer resistance when the antibodies are bound to their antigen.
- The PPV-electrode shows a change at low frequencies due to drift.
- The bare Al reference electrode stays constant.

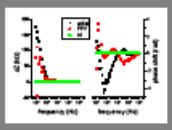

- **Time-resolved Impedance Spectroscopy**

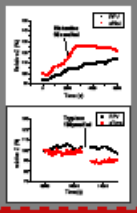

At low frequencies (212kHz):

- **Histamine**
  - IDE with anti-histamine shows 10% change in Z
  - apart from the signal drift, the polymer reference IDE remains constant after addition of histamine.

- **Tryptase**
  - -Electrode with anti-tryptase shows 10% change in Z
  - -polymer reference electrode remains constant

Conclusion

Antibodies for histamine & tryptase were succesfully immobilised on polymer-based electrodes. Upon detecting tryptase the immunosensor shows an impedimetric response of 10% at low frequencies. IDE's make it possible to detect smaller molecules. By using IDE's it was possible to detect the low-molecular weight histamine. Although a high concentration is required for the 10% increase in sensor signal, we were able to use a direct assay for the detection of such small molecules. IDE's are proven to be beneficial for use in both future histamine and tryptase experiments.

Acknowledgements

This research is funded by the School for Life Sciences , part of the transnational University Limburg. The authors would like to thank L. Michiels for his help and advice.

Development of a Biosensor for the Detection of Histamine and Tryptase

E. Bongaers[1)], L. Grieten[1)], J. Alenus[1)], P. Wagner[1)], F. Troost [2)] and R.-J. Brummer[2)]

1)Institute for Materials Research, Hasselt University, Wetenschapspark 1, 3590 Diepenbeek, Belgium
2) Gastroenterology & Hepatology, dept. of Internal Medicine, Nutrition and Toxicology Research Institute Maastricht (NUTRIM), Maastricht University, Universiteitssingel 50, 6229 ER Maastricht, The Netherlands

Introduction

Irritable Bowel Syndrome (IBS) is a gastrointestinal disorder which is associated with increased numbers of mast cells in the intestinal mucosa. These mast cells are involved in the pathogenesis of the disease, although the exact role of mast cell activation in IBS is still under investigation. There is ample evidence that mast cells degranulate upon activation, thereby releasing histamine, tryptase and other compounds. To verify the effectiveness of current therapies in vivo measurements need to be performed on the mucous membrane of the small intestine. The limited accessibility of the intestines however makes it difficult to measure this intestinal mast cell activation *in vivo*. Therefore an impedimetric immunosensor for the detection of histamine and tryptase *in vivo* is under development. For the low-molecular weight antigen histamine interdigital electrodes (IDE's) are used to increase sensitivity.

Materials & Methods

- **Materials:**
  - Antigens: Tryptase (135 kDa) and histamine (111 Da)
  - Antibodies IgG for tryptase and histamine.
- **Sensor setup:**
  - Electrode material: - 50 nm TiN coplanar electrodes for tryptase
    - 100 nm Al interdigital electrodes (IDE) for histamine
  - Coated with 100nm MDMO-PPV, a semiconducting polymer.
  - Antibodies are immobilised using physical adsorption (1h @ 37°C). A 100pmol/ml solution is used for biosensor samples.
- **Electrochemical Impedance Spectroscopy:**
  - Impedance is measured as function of frequency from 100 Hz to 1 MHz.
  - An addition set-up is used at room temperature.

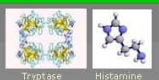

Coplanar electrodes (200µm) Interdigital electrodes (25µm)

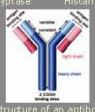
Structure of an antibody


Addition setup

Characterisation

- **Contact angle**

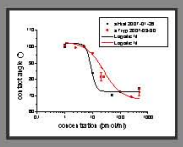

-PPV surface is hydrophobic (>90°).

-Incubating antibodies on PPV renders the film hydrophilic (<90°).

- This indicates the succesfull adsorption of Ab to polymer, according to the Vroman effect.

- The logistic fits show that at a concentration of 100pmol/ml the Ab adsorption is saturated.

- **AFM**

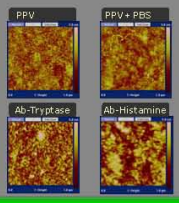

Incubation with PBS causes little swelling of the polymer. With AFM the receptor molecules can be visualised. The yellow structures are clusters of antibodies.

Physical adsorption profiles show that the antibodies for histamine and tryptase are succesfully immobilised on a polymer surface.

Biosensing

- **Impedance Spectroscopy**

Bodeplots before and after the addition of 50nmol/ml histamine are compared. The difference in amplitude signal is plotted for 3 electrodes (Al/PPV/ PPV functionalised with anti-histamine):

- The functionalised anti-histamine electrode shows a change in Z at low frequencies. This sensing effect is due to a change in surface capacity and charge transfer resistance when the antibodies are bound to their antigen.
- The PPV-electrode shows a change at low frequencies due to drift.
- The bare Al reference electrode stays constant.

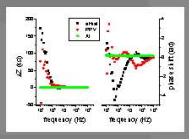

- **Time-resolved Impedance Spectroscopy**

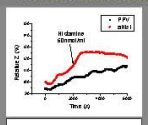

At low frequencies (212kHz):

- **Histamine**
  - IDE with anti-histamine shows 10% change in Z
  - apart from the signal drift, the polymer reference IDE remains constant after addition of histamine.

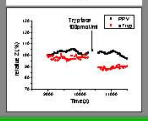

- **Tryptase**
  - Electrode with anti-tryptase shows 10% change in Z
  - polymer reference electrode remains constant

Conclusion

Antibodies for histamine & tryptase were succesfully immobilised on polymer-based electrodes. Upon detecting tryptase the immunosensor shows an impedimetric response of 10% at low frequencies. IDE's make it possible to detect smaller molecules. By using IDE's it was possible to detect the low-molecular weight histamine. Although a high concentration is required for the 10% increase in sensor signal, we were able to use a direct assay for the detection of such small molecules. IDE's are proven to be beneficial for use in both future histamine and tryptase experiments.

Acknowledgements

This research is funded by the School for Life Sciences , part of the transnational University Limburg. The authors would like to thank IMEC, R. Thoelen and W. Moons for supplying IDE's and L. Michiels for his help and advice.

universiteit hasselt | transnationale UNIVERSITEIT LIMBURG | Universiteit Maastricht | nutrim

Appendix 5: Scientific awards

European Physical Journal Poster contest, 30th May 2007, **2nd prize:**

> **E. Bongaers**, L. Grieten, J. Alenus, P. Wagner, F. Troost, R.-J. Brummer, *Development of a Biosensor for the Detection of Histamine and Tryptase,* Joint General Scientific Meeting of the Belgian Physical Society and Belgian Biophysical Society, Antwerpen, (Belgium).

European Physical Journal Poster contest, 1st April 2009, **3rd prize**:

> J. Alenus, R. Thoelen, **E. Bongaers**, J. Duchateau, F. Hooreman, L. Lutsen, D. Vanderzande, T.J. Cleij, P. Wagner, *Piezoelectric detection of Small Molecules using synthetic MIP-based receptors.* Joint General Scientific Meeting of the Belgian Physical Society and Belgian Biophysical Society, Hasselt, (Belgium).